Motion encoding in the salamander retina

DISSERTATION

for the award of the degree
'Doctor rerum naturalium'
of the Georg-August-Universität Göttingen

in the doctoral degree program
Sensory and Motor Neuroscience
of the Georg-August University School of Science (GAUSS)

Submitted by

Norma Krystyna Kühn

from Rostock, Germany

Göttingen 2016

Thesis Committee

Referee: Prof. Dr. Tim Gollisch
Sensory Processing in the Retina, Abteilung für Augenheilkunde,
Universitätsmedizin Göttingen

2nd Referee: Dr. Robert Gütig
Theoretische Neurowissenschaften,
Max-Planck-Institut für Experimentelle Medizin

Prof. Dr. Florentin Wörgötter
Biophysik, III. Physikalisches Institut,
Georg-August-Universität Göttingen

Further Members of the Examination Board

Prof. Dr. Alexander Gail
Sensorimotor Group,
Deutsches Primatenzentrum

Prof. Dr. Fred Wolf
Theoretische Neurophysik,
Max-Planck-Institut für Dynamik und Selbstorganisation

Prof. Dr. Andreas Stumpner
Abteilung Zelluläre Neurobiologie,
Schwann-Schleiden-Forschungszentrum

Date of the oral examination: June 22, 2016

Abstract

The detection and correct interpretation of motion in visual scenes is important in everyday tasks, e.g., for avoiding cars when crossing the street or for assessing the optic flow, induced by self-motion, when navigating through a room. The processing of visual motion starts in the retina where specialized neural circuits integrate the incoming signals and extract relevant features. Retinal ganglion cells, the output neurons of the retina, send the processed information to downstream brain areas.

Here, the retinal encoding of motion signals was studied in the salamander, a widely used model system for analyzing retinal function. Signals from up to 400 ganglion cells were recorded simultaneously from the *in-vitro* retina with multi-electrode arrays, allowing the classification of cell types and thorough population analyses. In the salamander retina, object-motion sensitive (OMS) ganglion cells have been identified which respond to the differential motion of an object on a moving background but are suppressed by global image motion. These cells might be relevant for detecting moving objects even during self-motion. Furthermore, many vertebrates possess direction-selective (DS) ganglion cells which preferably respond to a certain direction of drifting motion. They are thought to provide important information about the optic flow to higher brain areas. Yet, direction-selective ganglion cells have been absent in previous characterizations of the salamander retina.

Here, direction-selective ganglion cells could be identified in the retina of the axolotl salamander (*Ambystoma mexicanum*). Further, two distinct types of direction-selective ganglion cells could be discriminated. One might play a role in processing global image motion (standard DS cells), while the other is especially sensitive to object motion and may assist in detecting a moving object's direction (OMS-DS cells). Standard DS and OMS-DS cells differed in many fundamental properties, as their area of spatial integration and systems of preferred directions, and responded to different features of a composite motion stimulus. This suggests that the direction of global image shifts and of locally moving objects is processed in parallel via different pathways, reflected by the functional outputs of standard DS and OMS-DS cells, respectively.

The encoding of global motion direction by standard DS cells was additionally probed with more complex motion stimuli than traditional drifting gratings. This revealed that in complex visual scenes, standard DS cells simultaneously encode motion direction and strong local contrast changes caused by large translational movements independent of their direction. Populations of standard DS cells with different directional preferences could then partially compensate for the coding ambiguities of the individual cell, leading to a better readout of the motion trajectory than would be expected from single-cell responses. This synergy in the population readout illustrates that downstream brain areas could exploit combined inputs from standard DS cells with different preferred directions to decode global image motion more effectively.

Key words: retina, motion encoding, direction selectivity, object-motion sensitivity, population coding, linear decoding, salamander

Declaration

I hereby declare that this thesis is my own work and effort and that it has not been submitted anywhere for any award. Where other sources of information have been used, they have been acknowledged.

Göttingen, April 2016 Norma Kühn

Acknowledgments

First of all, I would like to thank my supervisor Tim Gollisch for giving me the opportunity to write my PhD thesis in his lab. I am grateful for all the support and the many things I learned from you during the past four years, thank you!
I also thank the members of my thesis advisory committee, Florentin Wörgötter and Robert Gütig, for the support throughout my PhD and the helpful discussions and criticism during meetings. The members of the extended examination board, Alexander Gail, Fred Wolf and Andreas Stumpner, I thank for dedicating their time to participate in my defense.
I thank all the present and former members of the Gollisch lab, Vidhyasankar Krishnamoorthy, Fernando Rozenblit, Michael Weick, Daisuke Takeshita, Jian Liu, Mohammed Khani, Helene Schreyer, Sebastian Bemme, Larissa Lauterbach and Christiane Westermann, for the enlightening discussions during and off lab meetings, the great whiskey tastings in the Irish pub, midnight pizza feasts and for the moral support during the last weeks of thesis writing.
I also would like to thank all the other amazing people that made my PhD time even more valuable: Leni Picher for her straightforward opinions and for being a very good friend; Rituparna Chakrabarti for her great and uplifting spirit; the Flamenco crew and especially Marivi for her inspiring classes; Leni Picher, Ursula Stalmann, Chao-Hua Huang and Tanvi Butola for crazy dance nights; Josephine Thomas aka Enigma Terrorista for brain-storm and jam sessions; Regina Schmälzle for her last-minute ideas; Manuel Schottdorf, Frank Stollmeier, Rainer Engelken and Cosima Mattner for the wonderful evenings full of interesting discussions and Ofenkäse.
Further, I thank my parents, Odett and Wolfgang, and my brother, Roland, for their enduring support and love. Reinhold and Ulla I thank for supporting me with their love and care for Alexander, and Eva and Anna for the light and sunny afternoons that we spent together. Special thanks go to Jonas and Alexander, you are my safe haven and source of inspiration.

To my son,
the moon and the stars.

Contents

1 — Introduction

The processing and perception of motion in visual scenes is of particular importance for exploring and navigating through our environment. For example, when crossing the street, the detection and avoidance of moving cars can be crucial for our survival. Likewise, during a ball game, the approaching ball has to be detected and the gaze has to follow its trajectory in order to catch it. These situations are complicated by self motion, introducing a global optic flow of our surroundings. But even the smallest eye movements will shift the image that is projected onto our retinas.

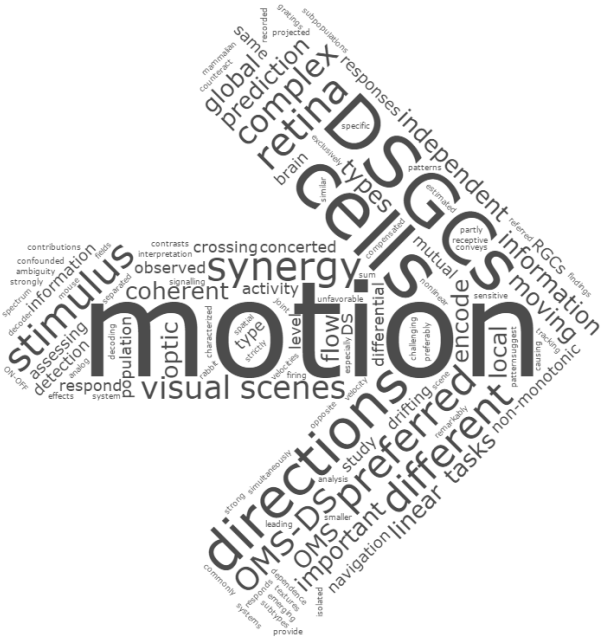

The processing of visual information starts in the retina where different features of a scene are processed in parallel (Gjorgjieva et al., 2014; Masland, 2012a; Wässle, 2004; Meister, 1996). This manifests in the diverse functional outputs of the retinal ganglion cells. They send the preprocessed information about the visual world to downstream brain areas.

I am interested in the retina's encoding of visual motion which can be of very complex nature. As mentioned above, motion in visual scenes does not only comprise *local motion* of objects within the scene but also *global shifts* of the image that is projected onto the retina. These shifts can be caused by body, head or eye movements.

When we fixate our gaze on a region of interest, our eyes are never still and perform tiny tremor-like eye movements, so-called *fixational eye movements*, to counteract adaptation to the static stimulation and prevent the image from fading (Martinez-Conde and Macknik, 2008). The induced retinal slip of the image is corrected for by microsaccades, stabilizing the position of the image on the retina (Engbert and Mergenthaler, 2006; Collewijn and Kowler, 2008; Ko et al., 2010). In order to perform these corrections, downstream brain regions which control the eye muscles have to receive information about the global image motion. This information is provided by visual feedback from retinal ganglion cells.
Also during head movements, when the vestibulo-ocular reflex is supposed to relocate the gaze, retinal input to the vestibulo-motor system is thought to fine-tune the correctional eye movements by providing additional information about the induced image shifts (Maekawa and Simpson, 1973; Simpson et al., 1988). Another type of involuntary corrective eye movements, as the ones mentioned above, is the optokinetic reflex. There, in contrast to the vestibulo-ocular reflex, the gaze is relocated in response to global image shifts that are caused by motion of the external world (Cochran et al., 1984). Also here, inputs from retinal ganglion cells are important to relocate the gaze to the region of interest.
But how can retinal output signals help to relocate our gaze? What kind of information do they send to downstream brain areas? Can retinal ganglion cells encode the direction or speed of the global image shifts induced by head and eye movements? In many species, there are types of retinal ganglion cells which respond selectively to certain angles of drifting motion and are silent for motion into the opposite direction. The asymmetric response of these so-called *direction-selective* retinal ganglion cells to drifting motion is thought to provide important information about motion direction to higher brain areas. Direction-selective ganglion cells have been found in the retina of frog (Lettvin et al., 1959; Maturana et al., 1960), turtle (Bowling, 1980; Jensen and DeVoe, 1983), mudpuppy (Werblin, 1970), fish (Maximov et al., 2005), pigeon (Maturana and Frenk, 1963), cat (Cleland and Levick, 1974a; Farmer and Rodieck, 1982), rabbit (Barlow and Hill, 1963) and mouse (Weng et al., 2005; Sun et al., 2006). Nevertheless, there is some controversy about their existence in the salamander retina (Pan and Slaughter, 1991; Segev et al., 2006).

A subtype of the direction-selective ganglion cells in the retina of mice and rabbits, the ON direction-selective cell (characterized by its strong response to flashes of light) (Oyster and Barlow, 1967; Sun et al., 2006), is thought to be involved into the correction of the retinal slip (Dhande et al., 2013). ON direction-selective cells send information to the accessory optic system in the midbrain which is connected to the vestibulo-motor system (Simpson, 1984). Their output is thought to fine-tune eye movements which correct for the retinal slip induced by head and body movements. Direction-selective ganglion cells are known to faithfully encode the motion direction of a drifting grating (Amthor et al., 2005; Fiscella et al., 2015) but eye and head movements are seldom continuous. Instead they often induce irregular global shifts of the image that is projected onto the retina. But can direction-selective ganglion cells provide detailed information about such a discontinuous motion trajectory? In fact, the ability of direction-selective retinal ganglion cells to encode the instantaneous direction and velocity of a discontinuously moving image has never been tested.

Apart from the corrections for global image shifts, our eyes often follow voluntarily the trajectory of a moving object. These pursuit eye movements keep the projection of the moving object centered on our retinas and are necessary for catching the object (Land and McLeod, 2000). Pursuit eye movements require information about the moving object's trajectory which could only be provided by the outputs of retinal ganglion cells (Lisberger et al., 1987). The underlying mechanisms how inputs from retinal ganglion cells to downstream brain areas are used to faithfully pursue and catch objects are still not well understood.
One problem for catching a moving object is that its motion trajectory always has to be anticipated since retinal processing and the subsequent motor response are delayed with respect to the current object position. Therefore, the encoding of the current position of an object is not enough for a faithful pursuit. It has been proposed, that the future position of the object could be extrapolated from retinal inputs by internal models in our brain. For a continuously moving object, the future position could simply be predicted from the object's past positions by extrapolating linearly and assuming a fixed delay in the visuomotor response. For example, a linear extrapolation model was able to explain the hit and miss trials of a salamander hunting prey where the salamander captured the prey when it moved in a continuous way but missed it when the prey suddenly changed direction during the capturing process (Borghuis and Leonardo, 2015).
But how could downstream brain areas interpret the output of retinal ganglion cells in order to anticipate the future object position? Many studies which focused on the encoding of object motion trajectories by retinal ganglion cells, pooled in-

formation from a large cell population. Several of these studies came to the conclusion that the population code by itself already provides a prediction of the future position of the object which simply has to be read out. For example, in the salamander retina, a continuously drifting bar was shown to drive a wave of spiking activity of the retinal ganglion cells (Berry II et al., 1999). This activity wave did not travel behind but actually preceded the current position of the bar which would allow a prediction of the future bar position by a simple linear readout of the location of the spiking activity. Similarly, it has been shown that the future position of a discontinuously moving spot could be estimated by taking the weighted average of the ganglion cells' receptive fields based on the current firing rate of each cell, as a *population vector* (Leonardo and Meister, 2013). A downstream neuron could thereby extrapolate a moving object's trajectory from the population responses.
Other studies have focused on the encoding of a sudden motion reversal (Schwartz et al., 2007; Chen et al., 2014). For a continuously moving object which suddenly reverses its motion direction, the linear extrapolation of its previous motion trajectory will incorrectly predict the object's future position. There, the synchronized firing of a large population of retinal ganglion cells is thought to act as an error signal to downstream brain regions for reporting the sudden change of direction. This would then allow to update the prediction.
Studies with more complex motion trajectories where the motion of the object was not just continuous or reversing, investigated the encoding of one-dimensional random bar motion with temporal correlations (Marre et al., 2015; Palmer et al., 2015). These studies focused on the predictability and reconstruction of the moving bar's position from the responses of a large population of retinal ganglion cells. It turned out that for a random motion trajectory, the population did not form a moving hill of ganglion cell activity, preceding the bars motion as seen for continuous motion (Marre et al., 2015). Instead, the jittering bar also evoked responses in cells far away from the bar location, similar to the population responses observed to motion reversal. The global activity of retinal ganglion cells led to a highly redundant reconstruction of the bar position. This disagrees with the assumption that correlations in the population code might carry additional information that is not present in the uncorrelated responses of individual neurons (Meister, 1996; Warland et al., 1997). But above studies did not investigate the population coding of cells with motion-specific responses, like the direction-selective cells.

Another important question to answer is how the motion of an object could be differentiated from the global shifts induced by eye and head movements?

Our attention is often driven to moving objects (Franconeri and Simons, 2003; Corbetta and Shulman, 2002), suggesting that object motion is detected very early in the visual processing pathway. Compared to the background, the object is only moving locally and usually with different speed and direction than the moving background. But even in computer vision, interpreting object and background motion correctly, is not trivial (Yu et al., 2007). More recently, retinal ganglion cells have been identified in salamander and rabbit which responded well to differentially moving objects but not to global background motion. These object-motion-sensitive (OMS) cells might provide information about the current position of a moving object (ÖLveczky et al., 2003; Baccus et al., 2008).
Though, there are retinal ganglion cell types which show intriguing motion-specific response properties, as the direction-selective and object-motion-sensitive cells, most of the previously mentioned population encoding studies focused on heterogeneous cell populations or on populations of cells characterized by their responses to flashed stimuli. A study of the motion encoding by populations of cells with motion-specific responses could therefore provide a different picture about the population encoding of motion patterns and their efficiency.

1.1 About this work

I investigated the motion encoding of retinal ganglion cells in the axolotl salamander on the single-cell and population level. I was interested how the functional outputs of retinal ganglion cells could assist in tracking moving objects or relocating the gaze during fixation. Therefore, I projected different moving visual stimuli onto the in-vitro retina and recorded the responses from up to four hundred retinal ganglion cells at the same time with multi-electrode arrays.
I systematically analyzed how individual retinal ganglion cells encoded different motion features and characterized the cells according to their responses to global coherent motion, differential motion and motion direction. I could identify three motion-specific response types in the salamander retina.
First, I found direction-selective (DS) cells, which preferably responded to certain angles of drifting motion but were silent for motion into the opposite direction. Second, I could identify object-motion-sensitive (OMS) cells which showed similar properties as the OMS cells identified in the tiger salamander (ÖLveczky et al., 2003). They responded well to differential motion but were suppressed by global coherent motion. Third, a subset of the identified direction-selective ganglion cells also showed strong object-motion-sensitivity. I called these cells OMS-DS cells to distinguish them from the standard DS cells. Standard DS cells responded equally

well to global coherent and differential motion while OMS-DS cells only responded well to local differential motion but not to global coherent motion.
I could show that standard DS and OMS-DS cells are presumably two distinct cell types, encoding different features of the visual world. They differ significantly in their organization of preferred directions, as well as their receptive field sizes, their areas of spatial integration. While standard DS cells integrate information over a large area, OMS-DS cells have very small receptive fields. I hypothesize that standard DS cells are important for the encoding of the motion direction of global background motion, while OMS-DS cells might play a role in detecting the motion direction of a locally moving object. This hypothesis was substantiated by the distinctive responses of standard DS and OMS-DS cells to more complex motion stimuli.
Furthermore, the receptive fields of retinal ganglion cells of a distinct functional type are thought to tile the retina like a mosaic, ensuring that the encoded feature can be captured across the entire visual field (Masland, 2012a). These mosaics occur because the dendritic trees of cells of the same genetic type usually avoid each other, thus, relating functional types to genetic ganglion cell types. The genetics of a retinal ganglion cell determines to which amacrine and bipolar cells it connects and to which downstream brain regions the ganglion cell projects. Thereby, the genetics of a cell type determines the ganglion cell's morphology and function. The directional subtypes of standard DS and OMS-DS cells showed independent receptive field mosaics but had strong receptive field overlaps between each other. This further indicates that standard DS and OMS-DS cells are distinct cell types.
What might be the function of standard DS and OMS-DS cells in visual processing? As standard DS cells have large receptive fields and respond well to global coherent motion, they might report the direction of global image shifts, as induced by fixational eye movements, to downstream brain areas. In terms of receptive field size and organization of preferred directions, standard DS cells showed strong analogies to the ON DS cells in the mammalian retina which project to brain areas related to vestibulomotor responses (Simpson, 1984; Dhande et al., 2013). Therefore, standard DS cells might also be involved in the correction of the retinal slip as induced by head and body movements.
On the other hand, OMS-DS cells encoded the motion direction of small moving objects and might provide important information for tracking these objects. Information about the motion direction of a moving object could be used to better extrapolate the motion trajectory of a moving object (Zelinsky et al., 2015; Kwon et al., 2015; Kalman, 1960). This information might be especially useful when the object is shortly occluded by another object (Kristan et al., 2009; Zago et al.,

2010).

Based on the prior classification of the motion-specific ganglion cell types in the axolotl salamander, I studied the responses of standard DS cells to jittering background motion. DS ganglion cells are known to respond selectively to certain directions of a drifting grating. Here, I hypothesized that they might provide information about global image shifts, induced by head and eye movements to downstream brain areas. Hence, I investigated whether they also respond in a direction-selective fashion to more complex motion patterns. I stimulated the cells with a moving background texture following a two-dimensional random walk, roughly resembling fixational eye movements. I could show that individual standard DS cells responded on average according to their directional preferences to this highly irregular motion trajectory.
To see what information a downstream neuron could extract from the standard DS cell responses, I reconstructed the motion trajectory from the single-cell responses assuming linear signal integration. The linear readout from the single-cell responses did only capture few low-frequency features of the random motion trajectory. Motion into the cell's preferred direction was especially well decoded.
From investigating the linear readout from a large population of standard DS cells, I found that the concerted firing of standard DS cells allowed a much better performance of the trajectory reconstruction than one would have estimated from the performance of a single cell. This kind of cooperative spiking of the DS ganglion cells where the population performs better than the sum of its individuals, is called *synergy*.
I found that this synergy arises from coding ambiguities on the single-cell level. It seems that standard DS cells do not only respond to motion into their preferred direction but are also driven by strong contrast changes. These contrast changes could also drive the cells when the image was moving into the cell's null direction. This diminishes the performance of the trajectory decoding from single-cell responses. But the concerted firing of standard DS cells with different preferred directions could partially resolve these ambiguities. I further showed that for standard DS cells with different preferred directions, important information is carried in the spike rate differences between cell pairs. Hence, the correlations in the population responses help to overcome the ambiguities in the individual DS cell responses to random motion and allow a better decoding of the random motion trajectory.

The different motion-specific outputs of individual retinal ganglion cells in the salamander retina emphasize the importance of visual motion processing. In-

formation about background and object motion from OMS, DS and OMS-DS cells might be crucial for the salamander's survival. First, the encoding of local motion by standard OMS cells might assist in the detection of moving prey. Second, information about the motion direction of moving prey from OMS-DS cell responses might improve the extrapolation of the prey's motion trajectory and assist in its tracking and final capture. Third, responses from standard DS cells might provide information about eye and self motion and thereby allow to decorrelate image information from the motion trajectory. Fourth, the simultaneous integration of object and background motion direction could correct the estimated object motion.
However, for highly irregular motion trajectories as induced by fixational eye movements, the motion direction can not be decoded very faithfully from the responses of individual standard DS cells. Instead, the concerted firing of populations of standard DS cells is necessary to get a better estimate of the image motion. It shows that highly specialized cells by itself are not sufficient for the proper encoding of complex motion stimuli but that downstream neurons might benefit from the response correlations within the standard DS cell population.
A single standard DS cell would encode motion direction but also spatial information of the shifted image. But the correlations in the population responses of standard DS cells allowed to decorrelate the motion trajectory from spatial image features which is the reason for the observed synergy.

1.2 Outline of the thesis

This work investigates the mechanisms of motion encoding in the salamander retina, expanding from the view of single motion processing units to the collective motion encoding of populations of certain subtypes of retinal ganglion cells.
For a better understanding of the motion encoding of retinal ganglion cells, chapter 2 introduces the circuitry of the vertebrate retina and motion-specific computational mechanisms. Since extensive research has been conducted in the mammalian retina, differences and similarities between the salamander and mammalian retinal circuitry are discussed. For linking ganglion cell output to function, important retinofugal projection areas of the early visual system and their function are illuminated. Furthermore, different approaches for understanding retinal population codes in response to visual motion are outlined.
Chapter 3 comprises a detailed description of the experimental procedures, as tissue preparation and recordings. Then, an overview of the applied stimuli and methods for single-cell and population analysis is given.

In chapter 4, I show the classification of motion-specific cell types in the salamander retina. It is based on the cells' responses to stimuli featuring either uniformly directed motion or jittering motion in a coherent or differential fashion. Then, the physiological and functional properties of the observed cell types and the underlying mechanisms for their response characteristics are discussed. The hypothesis that one of the observed cell types encodes the direction of moving objects while another might encode the motion direction of background motion is tested with more complex motion stimuli.
In chapter 5, the random motion encoding of populations of ganglion cells with directional preferences is studied. There, the cooperative coding of these cells leads to synergy in the linear readout. Possible reasons for the observed synergy and the structure of the correlated cell activity are examined.
Chapter 6 finally discusses the observed phenomena in a broader context. Follow up experiments and data analysis are suggested which could further substantiate my hypotheses.

2 — Early visual motion processing

2.1 The vertebrate retina

The retina is a delicate layer of nervous tissue in the back of our eyes. Its well-structured, yet complex circuitry is the starting point of visual information processing. Light which enters the pupil has to first pass through the vitreous humor and the five retinal layers until it reaches the photoreceptors. There, it triggers an electro-chemical signaling cascade which propagates through bipolar, horizontal and amacrine cells to the ganglion cells, the output neurons of the retinal circuitry (Fig. 2.1). They send the processed information in a bit-like code of action potentials or spikes through the optic nerve to downstream brain areas. The bipolar cells provide feed-forward excitation from the photoreceptors to amacrine and ganglion cells while horizontal and amacrine cells provide lateral inhibition within the circuitry.

When light hits the outer segments of the photoreceptors, it induces conformational changes of the photopigments which is called photo-isomerization. The signal which is caused by the photo-isomerization is strongly amplified by internal cell processes and leads to a hyperpolarization of the photoreceptor. Photoreceptors synapse onto horizontal and bipolar cells which in turn are hyperpolarized or depolarized depending on their dendritic glutamate receptors. Horizontal cells have *ionotropic* glutamate receptors which are *sign-conserving*. This means that horizontal cells also hyperpolarize when photoreceptors hyperpolarize with light. They mostly modulate the glutamate release of the photoreceptors by releasing the inhibitory neurotransmitter GABA.

There are two main types of bipolar cells which synapse onto the cone terminal (pedicle), the OFF and ON cone bipolar cells. ON bipolar cells have *metabotropic, sign-inverting* glutamate receptors and depolarize with hyperpolarizing cones while OFF cone bipolar cells have *ionotropic* glutamate receptors as the horizontal cells and are hyperpolarized (Haverkamp et al., 2001a,b; Vardi et al., 2000). In mice, the two cone bipolar cell types can be divided into at least nine subtypes, with characteristic depth of arborization and response kinetics (Euler et al., 2014). The

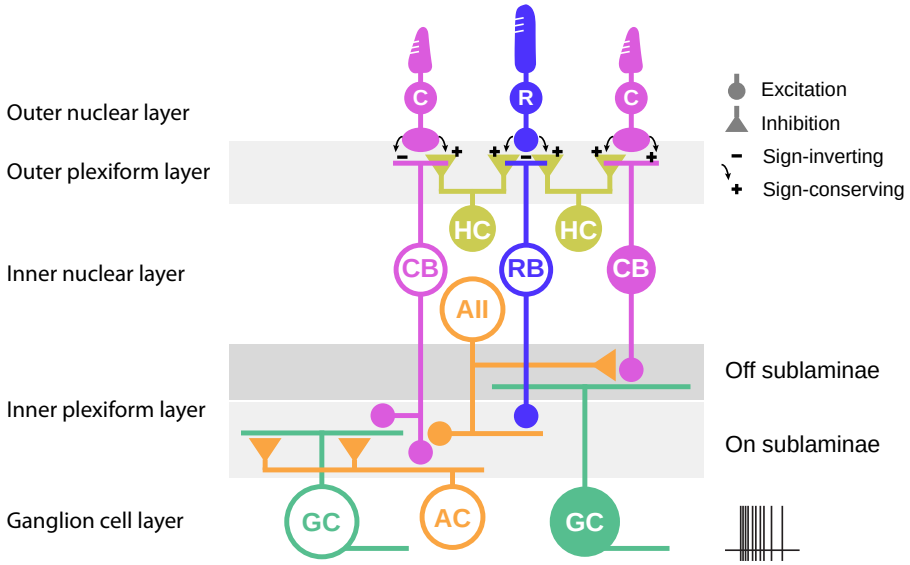

Figure 2.1 Schematics of the vertebrate retina consisting of three nuclear layers and two layers of cell processes. The outer nuclear layer (ONL) contains cell bodies of cone (C) and rod (R) photoreceptors. In the outer plexiform layer (OPL) they connect to horizontal (HC), rod bipolar (RB) and cone bipolar cells (CB) via sign-inverting (-) or sign-conserving (+) excitatory synapses. Cone bipolar cells with sign-inverting synapses are called ON cone bipolar cells (open circle) due to their depolarization in response to light flashes while OFF cone bipolar cells (filled circle) have sign-conserving synapses and respond to decrements of light. Horizontal cells are excited by light decrements as well and provide lateral inhibition to the photoreceptors. Horizontal and bipolar cells have their cell bodies in the inner nuclear layer (INL) together with amacrine cells (AC), another inhibitory cell class. Cell bodies of horizontal cells are closest to the outer plexiform layer while amacrine cells are furthest. Bipolar cells give excitatory input to amacrine and ganglion cells (GC) in the inner plexiform layer (IPL) which can be divided into ON and OFF sublaminae. ON cone bipolar cells and rod bipolar cells synapse in the ON sublaminae while OFF cone bipolar cells synapse in the OFF sublaminae. Rod bipolar cells do not synapse directly onto ganglion cells but onto AII amacrine cells (mouse nomenclature) which in turn excite ON cone bipolar cells via gap junctions. Amacrine cells mostly provide lateral inhibition to bipolar and ganglion cells. Some so-called displaced amacrine cells have their cell bodies in the ganglion cell layer together with the ganglion cells. Ganglion cells are the output neurons of the retina and send spikes via their axons through the optic nerve to downstream brain areas.

bipolar cells which synapse onto the rod terminal (spherule) have metabotropic glutamate receptors and depolarize when rods hyperpolarize with incoming light (Nomura et al., 1994). In the mammalian retina, there is only one type of rod bipolar cell. The rod pathway is important for night vision as rods are very sensitive to low light levels (mesopic and scotopic regimes, $10^{-6} - 10^{2}\,\mathrm{cd/m^2}$) but saturate at higher (photopic) light levels ($> 10^{2}\,\mathrm{cd/m^2}$). Cones are only sensitive to mesopic and photopic light levels ($> 10^{-3}\mathrm{cd/m^2}$) and are mainly used during daylight vision (Hood and Finkelstein, 1986; Stockman and Sharpe, 2006).
Bipolar, amacrine and ganglion cells form synapses in the inner plexiform layer (IPL). Bipolar cells provide glutamatergic excitatory input to amacrine and ganglion cells while amacrine cells provide mainly lateral inhibition to bipolar and ganglion cells by releasing neurotransmitter GABA or glycine (Masland, 2012b). Amacrine cells can also be modulatory via dopamine and serotonin release (Li et al., 1990; Contini and Raviola, 2003) or excitatory via gap junctions or the release of acetylcholine (Masland and Mills, 1979).
OFF cone bipolar cells synpase onto OFF ganglion cells in the outer part of the IPL (OFF sublaminae) while the synapses of the ON pathway are in the inner part of the IPL (ON sublaminae). Rod bipolar cells do not synapse onto ganglion cells directly but provide excitatory input to so-called AII amacrine cells (cf. Fig. 2.1). AII amacrine cells in turn provide excitatory input to ON cone bipolar cells via gap junctions (electrical synapses) and inhibitory input onto OFF cone bipolar cells.
The large variety of amacrine cells can be classified by their dendritic morphology, width of stratification and released neurotransmitters. In the mammalian retina, narrow to medium field amacrine cells are mostly glycinergic (Menger et al., 1998) while in the salamander they are mainly GABAergic (Yang et al., 1991). For wide field amacrine cells it is the other way around. In mammals, they are mainly GABAergic and in amphibians glycinergic. Well studied amacrine cell types in the mammalian retina are, apart from the AII amacrine cell which plays an important role in the rod pathway (Sharpe and Stockman, 1999), the starburst amacrine cell which integrates moving contrast along its dendrites (Euler et al., 2002; Kim et al., 2014) and the polyaxonal amacrine cell which is able to send spikes along its extended axons (Dacey, 1989; Stafford and Dacey, 1997; Davenport et al., 2007).
The complex wiring of bipolar, amacrine and ganglion cells leads to a great diversity of functional ganglion cell outputs (Wässle, 2004). Retinal ganglion cells integrate signals from several bipolar cells which in turn receive input from one or more photoreceptors. The converging connections of photoreceptors and bipolar cells form the receptive field of a ganglion cell which is the area of the visual field over which the ganglion cell integrates. A ganglion cell's receptive field is usu-

ally organized in an antagonistic center-surround structure (Kuffler, 1953; Barlow, 1953). For example, an ON ganglion cell strongly responds when a bright spot is flashed in the center of its receptive field but the response rate decreases when the bright spot extends to the surround of the cell's receptive field. Responses are strongest when the ON cell is stimulated with a bright spot in the center and a dark annulus in the surround. In contrast, OFF ganglion cells respond best to a dark spot in the center and a bright annulus in the surround. For distinguishing ON and OFF cells, usually only the center responses or responses to whole-field stimulation are determined.

Another important property of ganglion cells is their response kinetics. Retinal ganglion cells have often been classified by their response speeds and durations to flashed stimuli. For instance, a brisk transient ON cell would respond to an extended light pulse with a fast and short burst of spikes while a sluggish sustained cell would respond with a larger delay but with persistent spiking for the length of the pulse (Cleland and Levick, 1974b; Caldwell and Daw, 1978). In the salamander retina, usually only three ganglion cell types have been distinguished, ON cells, fast transient OFF cells and slow OFF cells which showed a weak ON response to higher contrasts (Meister et al., 1995).

In the following, I will focus on the response properties of retinal ganglion cells regarding the encoding of motion.

2.2 Motion encoding of retinal ganglion cells

Motion in visual scenes is of particular importance for navigating through our environment. The optic flow, induced by head and self motion, tells us which direction we are turning and where we are moving. Objects moving within the scene, move differentially to this moving background. The detection and correct interpretation of motion are not trivial. On the retinal level, direction-selective ganglion cells are known which strongly respond to certain motion directions and would be silent for motion into the opposite directions. Other ganglion cells preferably respond to the differential motion of an object on a moving background but not to the background motion alone which is why they are referred to as object-motion-sensitive cells. The properties and underlying circuitry of these cell types will be outlined below.

2.2.1 Direction-selective ganglion cells

The first time, direction-selectivity was observed in retinal ganglion cells was in single optic fiber recordings in the frog (*Rana pipiens*) (Lettvin et al., 1959).

There, a certain type of ganglion cell would fire action potentials along its axon when a dark spot or bar moved in a certain direction, the *preferred direction*, through the cell's receptive field but not for motion into the opposite direction, the cell's *null direction*. This response asymmetry is characteristic for direction-selective (DS) ganglion cells. Soon, similarly responding retinal ganglion cells were discovered in various mammalian and non-mammalian vertebrates (Barlow and Hill, 1963; Maturana and Frenk, 1963; Ariel and Adolph, 1985; Weng et al., 2005).

DS cells are best studied in mouse and rabbit where three types can be classified by their characteristic responses to increments and decrements of light into ON, ON-OFF and OFF DS cells (Borst and Euler, 2011). ON DS cells respond to the leading edge of an incoming bright object on a dark background while OFF DS cells would respond to the trailing edge. For a dark object on a bright background it would be the other way around. ON-OFF DS cells respond to both, leading and trailing edges (Vaney et al., 2001).

ON, ON-OFF and OFF DS cells exhibit different systems of preferred directions and receptive field characteristics (Oyster and Barlow, 1967; Kim et al., 2008). ON DS cells can be clustered into three subtypes according to their preferred directions which are separated by 120° angular difference. They usually have large receptive fields and respond well to slow speeds and a wide range of object sizes (Wyatt and Daw, 1975). In rabbit, ON DS cells could be divided into different subtypes by having either transient or sustained firing patterns (Kanjhan and Sivyer, 2010). Transient and sustained ON DS cells also showed different cell morphologies where the sustained cell had shorter and more numerous terminal dendrites than the transient cell. ON-OFF DS cells have four subtypes with preferred directions separated by 90° and pointing into the cardinal directions. Their receptive fields are smaller than those of ON DS cells and they are hence more numerous. In rabbit, 5% of the ganglion cells are ON DS cells and 20% are ON-OFF DS cells (Oyster, 1968).

OFF DS cells only occur with a preference for upward motion which corresponds to motion into the ventral direction of the image that is projected onto the retina (Kim et al., 2008). OFF DS cells have a highly asymmetric dendritic tree with ramifications ventrally directed. They are also called JAM-B cells due to the genetic marker, junctional adhesion molecule B, which was used to specifically label them in a transgenic mouse line. In the HoxD10-GFP mouse line, ON DS cells were labeled quite specifically along with some ON-OFF DS cells (Dhande et al., 2013). The molecular marker CART, cocaine- and amphetamine-regulated transcript, was shown to exclusively label ON-OFF DS cells (Kay et al., 2011). In

other mouse lines certain subtypes of ON and ON-OFF DS cells with a distinct preferred direction were labeled (Sanes and Masland, 2014). The genetic tools which are available in mouse, allow a more detailed investigation of the function and morphology of DS subtypes. Especially the coverage of the dendritic fields of all DS cells of a certain type and subtype-specific projections can be studied thoroughly.

Models and mechanisms Although DS cells are being investigated for decades now, there are still some uncertainties left about how the observed direction-selectivity is realized within the retinal circuitry. The first prominent models were the Hassenstein-Reichhardt and the Barlow-Levick model developed from the beetle and rabbit visual systems, respectively (Hassenstein and Reichardt, 1956; Barlow and Levick, 1965), see Fig. 2.2d-e for simplified versions. The Hassenstein-Reichardt detector only requires excitatory inputs from two cells with different spatial locations where the signal transmission from one cell is delayed by a certain amount of time τ. The inputs from the two cells are then multiplied and will only result in a response of the direction-selective cell if the cell with the response delay is activated first (Fig. 2.2d). The Barlow-Levick model is based on excitatory and inhibitory inputs. There, the inhibition is delayed and the summed inputs are rectified. Motion into the null direction will then lead to a canceling of the excitatory input with the inhibitory input (Fig. 2.2e).
In early experiments in rabbit, GABA antagonists picrotoxin and bicuculline could significantly reduce direction-selective responses of ON and ON-OFF DS cells (Wyatt and Daw, 1976; Caldwell et al., 1978). Nowadays it is known that so called starburst amacrine cells (SACs) give asymmetric inhibitory input to ON and ON-OFF DS cells (Dacheux et al., 2003). ON DS cells cofasciculate with displaced SACs in the ON sublamina of the IPL while ON-OFF DS cells ramify in the ON and OFF sublamina. In the OFF sublamina they receive input from SACs situated in the INL. To demonstrate the asymmetric input of SACs to ON and ON-OFF DS cells, the synaptic inputs to the OFF arbor of an ON-OFF DS cell are shown in figure 2.2a-b. SACs form inhibitory synapses with DS cells only on the null side of the DS cell (Lee et al., 2010; Briggman et al., 2011; Yonehara et al., 2013), i.e., the side from which the stimulus is coming when the cell is not responding (see Fig. 2.2b).
SACs have been first identified due to their release of acetylcholine, an excitatory neurotransmitter. SACs are the only acetylcholine releasing cells in the retina and their ramifications could be easily identified in choline-acetyl-transferase (ChAT) stainings where cofasciculation with DS cells has been studied. The role of acetyl-

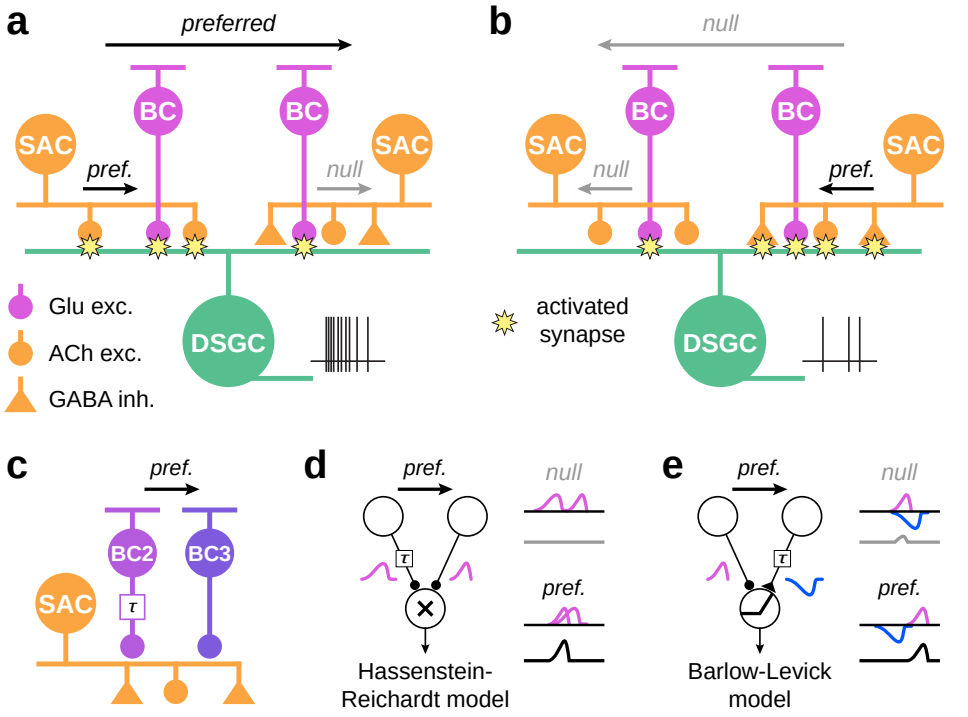

Figure 2.2 Circuitry generating direction-selectivity in ON and ON-OFF DS cells in mouse. **a-b** Circuitry and synaptic inputs to direction-selective ganglion cells (DSGC) during motion into the cell's *preferred* (a) and *null direction* (b). DSGCs receive excitatory inputs from bipolar cells (BCs) and starburst amacrine cells (SACs) marked by circular synapses. SACs also provide inhibitory, gabaergic input (triangular synapses). Activated synapses (when neurotransmitters are released) are marked by stars. **c** Possible mechanism for centrifugal direction-selectivity in SACs. At proximal dendrites, the SAC receives excitatory input from slow bipolar cell (B2), indicated by temporal delay τ. This input is amplified by excitatory input from fast bipolar cell (B3) when the stimulus is moving from the soma to the dendritic tip, similar to the Hassenstein-Reichardt model (d). **d-e** Simplified versions of the Hassenstein-Reichardt (d) and the Barlow-Levick model (e). Excitatory inputs are marked in magenta and inhibitory inputs in blue. The resulting post-synaptic potentials for the null and preferred directions are shown as gray and black curves, respectively. **d** Excitatory inputs from two different locations are multiplied. Direction-selectivity is realized by delayed input from one side. **e** Sum of excitatory and delayed inhibitory input is rectified.

choline in shaping the direction selectivity of ON and ON-OFF DS cells is still a matter of debate (Kittila and Massey, 1997; Lee et al., 2010; Briggman et al., 2011). It is mainly thought that the symmetric connections modulate the direction selectivity of DS cells.

Several models of passive and active signal integration along the SAC dendrites have been proposed which usually resulted in weak direction-selectivity. Passive conductance-based models produced centrifugal direction-selectivity in the dendritic tips (Tukker et al., 2004) where the output synapses are located but centripetal direction-selectivity at the soma (Borg-Graham and Grzywacz, 1992; Branco et al., 2010). This is not in accordance with experimental observations where a strong centrifugal direction-selectivity was observed across the entire SAC (Euler et al., 2002). Active conductance-based models of SAC dendrites where the Na^+ conductance is assumed nonlinear from experimental observations showed a centrifugal direction-selectivity across the entire SAC (Hausselt et al., 2007). Evidence was found that slow and fast responding bipolar cells which synapse onto proximal and distal dendrites, respectively, would shape the observed centrifugal direction-selectivity (Kim et al., 2014), similar to a Hassenstein-Reichardt detector (Fig. 2.2d, (Hassenstein and Reichardt, 1956)). In a more recent work, the GABA release sites of SACs have been found to be only located at the distal dendrites while excitatory input is received at the more proximal dendrites (Vlasits et al., 2016). This observed skewed distribution of input and release sites leads to strong centrifugal direction-selectivity in a physiological SAC model.

Cholinergic amacrine cells have also been reported in the salamander retina (Zhang and Wu, 2001; Cimini et al., 2008), hence, similar mechanisms for computing direction selectivity might be present. Nevertheless, the existence of direction-selective ganglion cells is still disputed (Segev et al., 2006).

In contrast to ON and ON-DS cells, the OFF DS cells, known as JAM-B cells in the mouse retina, have a different mechanism of direction-selectivity. Their asymmetric dendritic tree does not require a direction-selective input (Kim et al., 2008). According to the Barlow-Levick model, a combination of excitatory input from bipolar cells at the proximal dendrites and slower inhibition from amacrine cells at the distal dendrites would already generate a strong direction selectivity towards the dendritic tips. Evidence for this is the highly asymmetric center-surround structure of the OFF DS cell receptive field (Kim et al., 2008). However, these cells are only direction-selective at mesopic light levels due to the rod-cone antagonistic center-surround structure of their receptive fields with the surround inhibition being driven exclusively by rod inputs (Joesch and Meister, 2016).

2.2.2 Object-motion-sensitive ganglion cells

Object-motion sensitivity of retinal ganglion cells has been first characterized in tiger salamander and rabbit (ÖLveczky et al., 2003). These cells did not respond to a full-field jittering grating but to a jittering grating confined to a small region, similar to a moving object. The response was even stronger when the full-field grating was jittering in the back of the confined region but with a different trajectory (Fig. 2.3b, left) (Baccus et al., 2008; Krishnaswamy et al., 2015). This can be considered as the differential motion of an object in front of a moving background. Therefore, cells showing this property are called object-motion-sensitive (OMS) cells.

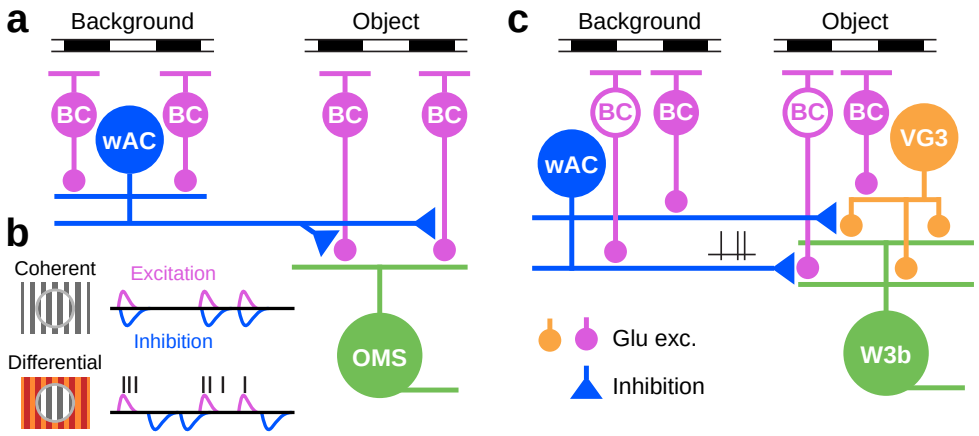

Figure 2.3 Circuitry for object-motion-sensitivity in salamander (a) and mouse (c). **a** Object-motion-sensitive (OMS) cells in tiger salamander receive excitatory input from bipolar cells in the object region (RF center) and glycinergic inhibitory input from wide-field amacrine cells (wACs) in the background region (RF far surround) (ÖLveczky et al., 2003; Baccus et al., 2008). **b** Interplay between excitation and inhibition in a coherent (upper) and differential motion scenario (lower). For coherent motion, inhibition from the far surround (background region) of the OMS cell is synchronous with excitation in the center (object region) and spiking is suppressed. For differential motion, inhibition and excitation are asynchronous and the OMS cell can respond to the object motion. **c** Unconventional circuitry of the object-motion-sensitive W3B cell in the mouse retina. Spiking wide-field amacrine cells (wACs) give inhibitory input to a vesicular-glutamate-transporter-3 amacrine cells (VG3s) which give glutamatergic excitatory input to the W3B cells (Kim et al., 2015; Krishnaswamy et al., 2015). Output of VG3s is object-motion-sensitive, modulated in a similar fashion as in (b) by far surround inhibition from wACs and center excitation from bipolar cells. The wAC, VG3 and W3B cells stratify in the on- and off-laminae of the inner plexiform layer and receive input from on- (open circles) and off-bipolar cells (solid circles).

In salamander, the mechanisms allowing the observed object-motion-sensitivity include inhibition from polyaxonal wide-field amacrine cells (wACs) (Baccus et al., 2008). The wACs integrate background motion across their receptive fields in

the far surround region of the OMS cell and are the counterpart to the excitatory inputs to OMS cells within the object region (Fig. 2.3a). When the object and background move coherently, excitatory and inhibitory inputs are synchronized and the OMS cell does not respond. When the object moves differentially from the background, excitation and inhibition are desynchronized and the cell can fire (Fig. 2.3b).
In mouse, a cell type with similar response properties has been identified, called the W3B cell due to its bright labeling in the TYW3 mouse line (Kim et al., 2010; Zhang et al., 2012). W3B cells receive excitatory input from narrow-field amacrine cells expressing vesicular-glutamate-transporter-3, so-called VG3s (Kim et al., 2015; Krishnaswamy et al., 2015; Lee et al., 2014). The output of VG3s is already object-motion-sensitive realized by mechanisms which could be similar to the OMS ganglion cells in salamander (Fig. 2.3c). Spiking wide-field amacrine cells are suspected to provide lateral inhibition to the unconventional circuitry (Kim et al., 2015).
OMS cells in salamander and W3B cells in mouse have in common that they do not respond to global coherent motion but to differential motion within a small area. Furthermore, they have small receptive fields (Baccus et al., 2008; Zhang et al., 2012). Interestingly, the OMS cells observed by Ölveczky et al. (2003) in the tiger salamander are fast-responding OFF cells while the W3b cell responds rather slowly due to the interposed VG3 cells (Zhang et al., 2012; Krishnaswamy et al., 2015).
In rabbit, ON brisk transient and ON-OFF DS cells were found to have strong object motion sensitivity (ÖLveczky et al., 2003).

2.3 Central projections of retinal ganglion cells

The encoded information of retinal ganglion cells is sent via the optic nerve to downstream brain areas. At the optic chiasma, the optic nerves of the left and right eye meet and their optical fibers are rearranged into the optic tracts of the left and right hemisphere with *ipsi*- and *contra*lateral projections from each eye, e.g., the right eye makes ipsilateral and the left eye contralateral projections to the right hemisphere.
In order to understand how the motion-specific responses of retinal ganglion cells could be used for behavioral computations in downstream brain areas one has to observe the areas and nodes where retinal ganglion cells project. Although lower vertebrates as salamanders lack a cortex for more complex visual processing, there are striking similarities in the retinofugal projection areas of mammals and am-

phibians. Amphibians share central projection areas in hypothalamus, thalamus, pretectum and tectum with mice and rabbits (Herrick, 1925; Fritzsch, 1980). These projection areas are related to different functions as object recognition, control of sleep-wake cycle and motor control depending on their downstream connections. Amphibians even have an accessory optic system (AOS) which is associated to the vestibulo-motor system. The AOS was first discovered in rabbit and is important for correcting the retinal slip caused by eye and head movements (Simpson, 1984).

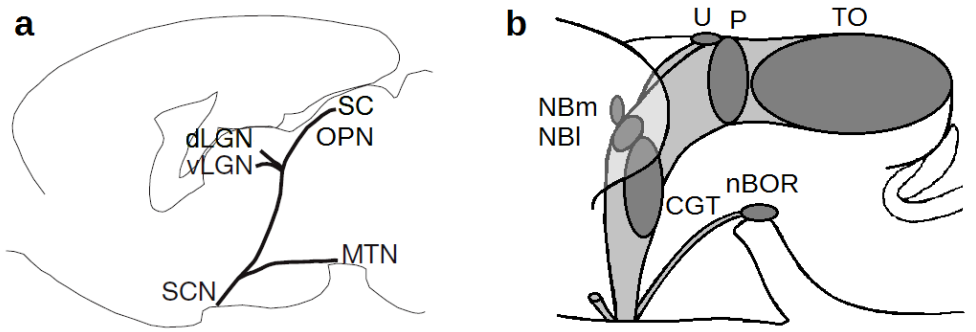

Figure 2.4 **Central retinofugal projections of mouse (a) and salamander (b).** Retinal ganglion cells project to hypothalamus, thalamus, pretectum, tectum and accessory optic system (AOS). **a** In mouse, prominent nuclei of these areas are the suprachiasmatic nucleus (SCN), the dorsal lateral geniculate nucleus (dLGN), the olivary pretectal nucleus (OPN), the superior colliculus (SC) and the medial terminal nucleus (MTN), respectively. Illustration adapted from Kim et al. (2008). **b** In salamanders, thalamic projection sites are the lateral and medial neuropil Bellonci (NBl/m), the corpus geniculatum thalamicum (CGT), the uncinate field (U) and the pretectal area (P). Other important projections go to the nucleus of the basal optic root (nBOR) of the AOS and the optic tectum (TO), adapted from Fritzsch (1980). NBl seems to be the analogue of dLGN while TO and BON correspond to SC and MTN, respectively.

A comparison between mammalian and amphibian systems is important since many genetic tools have been developed in mouse over the past years. For instance, cell type-specific genetic markers allow not only to classify different ganglion cell types more accurately but are also useful to identify cell type-specific projection areas (Sanes and Masland, 2014).

In mouse and rabbit, three retinofugal projection areas are of particular importance for visual motion processing, the dorsal lateral geniculate nucleus (dLGN) in thalamus, the superior colliculus (SC) in tectum (May, 2005) and the nuclei of the accessory optic system (AOS) with the medial terminal nucleus (MTN) as the most important one (Fig. 2.4a). The dLGN relays retinal inputs to the cortex for higher visual processing (V1/4) and maybe even conscious perception of motion (area MT in monkeys). The SC is an important node of the oculomotor system for directing eye and head movements to a point of interest within

the visual scene. These movements are often triggered by the visual detection of moving objects. The object-motion-sensitive W3 cells in the mouse retina were found to project to SC and dLGN and might therefore be important for making voluntary eye movements towards moving objects. The AOS is involved in the optokinetic reflex which corrects for image shifts caused by head and involuntary eye movements and which stabilizes the image that is projected onto our retinas (Simpson, 1984).
In the amphibian brain, the lateral neuropil Bellonci (NBI) and the optic tectum (TO) are the analogs of dLGN and SC, respectively (Fig. 2.4b, (Herrick, 1925; Ebbesson, 1972; Fritzsch, 1980)). The amphibian AOS has only one terminal node, the nucleus of the basal optic root (nBOR) which seems to be the analog of the medial terminal nucleus (MTN) (Simpson, 1984).
Other retinal projection sites in mammals which are not related to motion processing are the suprachiasmatic nucleus (SCN) and the preoptic area (PO) in hypothalamus which are important for regulating the circadian rhythm (Klein et al., 1991) and the olivary pretectal nucleus (OPN) for the pupillary light reflex. These areas receive input from intrinsically light sensitive retinal ganglion cells (Hattar et al., 2002, 2006).

Projections of DS cells ON, ON-OFF and OFF DS cells in mouse have been found to project to different downstream brain areas. Most ON-OFF and OFF DS cells project to the dLGN for higher visual processing and the SC which is important for involuntary motor responses to motion in visual scenes (Kim et al., 2010; Rivlin-Etzion et al., 2011). ON DS cells project to several nodes of the AOS (Oyster et al., 1980; Simpson, 1984; Dhande et al., 2013). The projections to the AOS provide visual input to the vestibulo-motor system which also controls eye movements to correct for head and body movements (Maekawa and Simpson, 1973). The detection of the motion direction from visual inputs is thought to work as a fine tuning of the rough inputs from the vestibular system. Most neurons of the three terminal nuclei of the AOS in rabbits (lateral, dorsal and medial terminal nucleus: LTN, DTN and MTN) and the nucleus of the optic tract (NOT) are directionally tuned. They show similar preferred directions as ON DS cells (Collewijn, 1975; Soodak and Simpson, 1988). DTN and NOT neurons prefer anterior motion while LTN and MTN neurons prefer up- or downward motion. In mouse, only DTN, MTN and NOT were found. ON DS cells with preference for anterior motion projected to DTN and NOT while ON DS cells preferring upward or downward motion projected to the dorsal or ventral MTN, respectively (Dhande et al., 2013). In rabbits, only the sustained ON DS cells seem to project to the

MTN but not the transient ON DS cells (Yonehara et al., 2008; Kanjhan and Sivyer, 2010). A subtype of ON-OFF DS cells preferring anterior motion also projected to the NOT apart from the usual projections to SC. Note here that upward, downward, posterior and anterior direction with respect to the animal refer to ventral, dorsal, nasal and temporal direction of the projected image on the retina, respectively. In frogs, extracellular recordings nBOR projecting axons revealed that DS retinal ganglion cells responding to image darkening are projecting to the AOS (Bastakov et al., 2015). Retrograde labeling showed that the nBOR-projecting retinal ganglion cells were OFF-type with large to medium sized receptive fields. Some of them were displaced to the inner nuclear layer (Montgomery et al., 1981; Cook and Podugolnikova, 2001).

2.4 Population motion encoding

For salamanders there is only a limited amount of genetic tools available. Nevertheless, the salamander retina has become considerably popular for investigating motion encoding on the population level, in particular for the encoding of motion onset (Chen et al., 2013), motion reversal (Schwartz et al., 2007; Chen et al., 2014) and the encoding of object motion trajectories (Leonardo and Meister, 2013; Palmer et al., 2015). The salamander retina is especially suitable for stable long-term recordings from large populations of retinal ganglion cells in-vitro. With multi-electrode arrays, signals from hundreds of cells can be captured at the same time with a high spatial resolution. This allows to investigate population encoding with single-spike resolution and to obtain spiking statistics over long time intervals.

2.4.1 Effect of noise correlations

The responses of two retinal ganglion cells can be strongly correlated either because they respond similarly to a given stimulus, leading to *stimulus correlations*, or because they share the same inputs from upstream neurons. Noise in the signal of upstream neurons will propagate to the downstream ganglion cells and will lead to so-called *noise correlations* in the downstream population. There is an ongoing debate whether noise correlations are important for the encoding of visual stimuli in the retina. The amount of information that the retina can send to downstream brain areas is confined by the number of optic fibers and the maximum firing rate of the ganglion cells. Therefore, some studies suggest that noise correlations between close-by ganglion cells could contain information that is not present in the uncorrelated responses of individual neurons (Meister, 1996; Warland et al.,

1997). Others found that noise correlations in the neural code of retinal ganglion cell populations did not carry a significant amount of information (Nirenberg et al., 2001; Panzeri et al., 1999).
More recently, it could be shown that noise correlations are important for the encoding of the direction of a drifting grating by a population of ON-OFF DS cells (Cafaro and Rieke, 2010; Fiscella et al., 2015; Zylberberg et al., 2016). There, the strength of the noise correlations strongly depended on the direction of the drifting grating which led to a better estimate of the actual direction of the grating than would be expected without noise correlations. On the other hand, if the strength of the noise correlations would have been constant for all directions, the encoding of the motion direction would have been less faithful than without noise correlations.

2.4.2 Synchronized activity

A special case of response correlations is the synchronized activity of retinal ganglion cells, i. e., when the cells fire together within a narrow time window. The degree of synchrony of a cell pair can be determined from the cross-correlograms of the *spontaneous activity* of the cells (Meister, 1996). The width of the central peak of the cross-correlogram then indicates the time window of the synchronized pair activity. The time window in which ganglion cells show synchronized activity will strongly depend on the source of shared upstream noise. For synchrony within $10 - 50\,\mathrm{ms}$, the cell pair might share input from the same amacrine cell, coupled via gap junctions. For synchrony in a $40 - 100\,\mathrm{ms}$ time window, noise correlations between ganglion cells probably originate from shared bipolar cell or photoreceptor inputs (Brivanlou et al., 1998). Synchrony below a millisecond, arises from the direct coupling between ganglion cells through gap-junctions.
Synchrony between retinal ganglion cells is often induced by certain visual stimulus features. In order to separate the stimulus-driven correlations from the correlations induced by upstream noise, a shuffle or shift predictor correction is usually applied where the cross-correlogram from the responses of shuffled trials is subtracted from the original cross-correlogram (Perkel et al., 1967). It has been found that a sudden reversal of drifting motion as well as the onset of motion elicit bursts of synchronized activity among retinal ganglion cells (Chen et al., 2013; Schwartz et al., 2007). The synchronized activity is thought to signal the onset or change of motion direction to downstream neurons. Downstream neurons could then use this information to better interpret the following inputs. For a grating that was shifted with a high frequency forth and back, the induced synchronized activity in the ganglion cell population, was proposed to work as an internal timer for down-

stream neurons signaling the input of new spatial information (Greschner et al., 2002). The knowledge about the timing of a shift would thereby improve the estimation of the spatial frequency of the grating. Other studies showed that the synchronized spikes of certain ganglion cell pairs had sharp orientation or direction tunings in response to drifting gratings (Stanley et al., 2012). The orientation tunings of the synchronized pair spikes were much sharper than orientation tunings observed in the individual cells.

These studies indicate that the correlated population activity can provide valuable information about important stimulus features. For example, the decoding of motion features by downstream neurons might strongly profit from the additional information that is carried by the response correlations, as information about motion reversal and improved directional estimates. Whether synchronized activity or other response correlations could improve the estimation of motion direction and speed in more complex motion scenarios with random motion trajectories, remains to be investigated.

3 — Experimental procedures & data analysis

3.1 Multi-electrode recordings in the vertebrate retina

The vertebrate retina has a layered structure, with photoreceptors in the outer plexiform layer, horizontal, bipolar and amacrine cells in the inner plexiform layer and ganglion cells in the innermost layer, located close to the vitreous humor. They are the only spiking neurons in the salamander retina, except for some types of amacrine cells (Heflin and Cook, 2007). The spikes of the retinal ganglion cells can be recorded extracellularly with planar multi-electrode arrays from the in-vitro retina.

3.1.1 Setup

The setup for recording the ganglion cell responses consisted of a USB-MEA256-System with multielectrode arrays (MEAs) with 256 electrodes (Multi Channel Systems MCS GmbH, Reutlingen, Germany). Extra-cellular recordings were performed with two different MEAs. Both had 252 TiN electrodes, one with $10\,\mu\mathrm{m}$ electrode diameter and $60\,\mu\mathrm{m}$ spacing (256MEA60/10iR-ITO) and the other with $30\,\mu\mathrm{m}$ diameter and $100\,\mu\mathrm{m}$ spacing (256MEA100/30iR-ITO). The signals were sampled with $10\,\mathrm{kHz}$.
The retinas were visually stimulated by a monochromatic white eMagin OLED microdisplay (SVGA+ OLED-XL) with 800 x 600 square pixels of $15\,\mu\mathrm{m}$ length and an update rate of $60\,\mathrm{Hz}$. The stimuli were directly projected onto the photoreceptor layer through a 2.0x telecentric measuring lense (Edmund Optics, Karlsruhe, Germany), such that the effective pixel length was $7.5\,\mu\mathrm{m}$. The mean irradiance of the projected stimuli was at $6.33\,\mathrm{mW/m^2}$ which corresponds to a low photopic range (Farrow et al., 2013). The mean irradiance was obtained by first measuring the photocurrent of a photodiode which was placed at the usual distance of

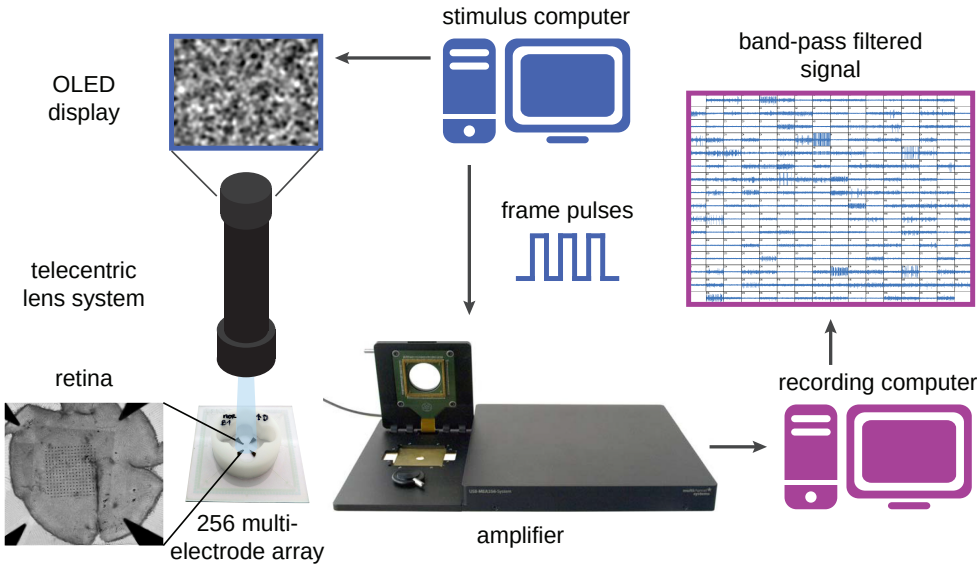

Figure 3.1 **Schematics of the recording setup.** The visual stimulus is created in the **stimulus computer**. It sends the stimulus frames to the **oLED display**. The **frame pulses** are sent to one of the analog inputs of the **amplifier** and mark the timing of each stimulus frame. The stimulus is projected via a **telecentric lens system** onto the **retina** and the extracellular electrical activity of the retinal ganglion cells is picked up by the **multielectrode array**. From the amplifier, cell signals and frame pulses are read out by the **recording computer** where the cell signals are high-pass filtered.

the retina from the display, projecting a confined region of mean luminance on a dark background. Then, the spectrum of the OLED display was measured with a compact CCD spectrometer (CCS200, Thorlabs Inc, Newton, NJ, USA) and the spectral density for each wavelength interval multiplied with the corresponding spectral sensitivity of the photodiode and summed over all wavelength intervals from $360 - 1100\mathrm{nm}$. The mean irradiance is then the measured photocurrent divided by the area of the mean luminance region and the factor of OLED spectral density and photodiode sensitivity.

The timing of each stimulus frame was recorded simultaneously with the cell responses to be able to reversely correlate stimulus and response in the later analysis. Every time a new stimulus frame was presented, the stimulus computer would send a signal to a NI USB-6501 digital I/O device (National Instruments, Australia) which in turn would send an analog square pulse of $25\mathrm{mV}$ and $33\mathrm{ms}$ length to one of the analog inputs of the amplifier. The frame timings can then be retrieved by obtaining the time points when the measured voltage crossed a certain threshold (here: $10\,\mathrm{mV}$).

3.1.2 Tissue preparation

I used retinas from adult axolotl salamanders (*Ambystoma mexicanum*, pigmented wild type) of either sex. Before tissue preparation, the animals were dark-adapted for half an hour. Then, the animals were decapitated and pithed under low red light levels. Before enucleating the eye, the ventral region of the anterior eye segment was marked with a soldering iron to keep track of the eye's orientation. The dissection of the eye was performed under infrared illumination with help of a night vision goggles equipped microscope. The eyes were hemisected along the cornea and the dorsal region marked with a vertical cut through the sclera. The vitreous humor was removed and the retina was separated from the posterior eye cup and remaining pigment epithelium was removed. The retina was mounted onto a semipermeable membrane with the photoreceptors facing the membrane. The membrane was positioned on a multi-electrode array (MEA) oriented along the ventral-dorsal axis and RGCs facing the electrodes.
During the dissection and recording, the retina was superfused with oxygenated amphibian Ringer's solution containing $110\,\mathrm{mM}$ NaCl, $2.5\,\mathrm{mM}$ KCl, $1\,\mathrm{mM}$ $\mathrm{CaCl_2}\bullet 2\mathrm{H_2O}$, $1.6\,\mathrm{mM}$ $\mathrm{MgCl_2}$, $22\,\mathrm{mM}$ $\mathrm{NaHCO_3}$ and $10\,\mathrm{mM}$ D-Glucose.

3.1.3 Pharmacology

In some experiments, I blocked inhibitory pathways by switching from a pure Ringer's solution (see above) to another Ringer's solution containing either $20\,\mu\mathrm{M}$ strychnine, $130\ \mu\mathrm{M}$ picrotoxin or $10\ \mu\mathrm{M}$ gabazine (SR-95531). Strychnine is a competitive glycine receptor antagonist while picrotoxin and gabazine are a non-competitive GABAa/c and competitive GABAa receptor antagonist, respectively. I used the very specific GABAa antagonist gabazine as a control to picrotoxin since picrotoxin is also known to block several ion channels. The strychnine solution was prepared from a $50\,\mathrm{mM}$ strychnine DMSO-stock solution. The picrotoxin and gabazine solutions were prepared from $13\ \mathrm{mM}$ picrotoxin and $10\ \mathrm{mM}$ gabazine aqueous stock solution, respectively.
I always did a control recording before drug application and another one 20 minutes after switching back to pure Ringer's solution. The recordings during drug superfusion started 10 minutes after switching to the drug Ringer's solution.
The effect of the drugs on the cells' direction-selectivity and object-motion-sensitivity was tested by a Wilcoxon signed-rank test and a two-sample Kolmogorov-Smirnov test comparing the DSI and OMSI values, respectively, between the control and during drug application. Data from three retinas per drug was used.

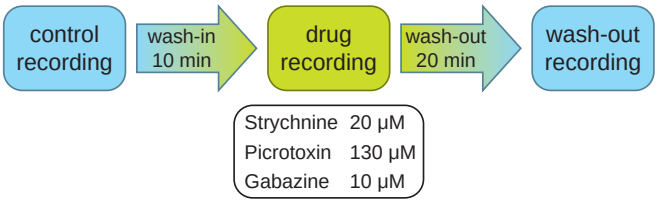

Figure 3.2 Protocol for pharmacological experiments. During control spatio-temporal white noise, drifting gratings, patches with jittering gratings and a temporal white noise stimulus were shown. Then, the Ringer's solution was switched to a drug containing Ringer's solution and drug recordings were started after $10\mathrm{min}$. A wash-out with normal Ringer's solution lasted $20\mathrm{min}$ before the wash-out recordings started. Except for the spatio-temporal white noise, same stimuli were used during control, drug application and wash-out.

3.1.4 Spike sorting

The binary files of each channel of the recorded data were loaded and sorted in a custom-made program in Igor Pro 6.32A 64-bit (WaveMetrics, Lake Oswego, USA) originally developed by Dr. Ofer Mazor (Harvard University, Cambridge, USA) (Pouzat et al., 2002). The program first grouped the channels into tetrodes (containing four channels or less) based on the cross-correlations between voltage traces of each channel. Then, events with amplitudes above 4 standard deviations of the noise level were detected in each channel. These putative spikes were then clustered within the channel groups according to their shape of their voltage trace in the time interval from $0.6\mathrm{ms}$ before and $1.4\mathrm{ms}$ after the peak time and assigned to units.

These units were assumed to be single neurons if the spikes in at least one channel were large enough (amplitude larger than two standard deviations above threshold) and were properly clustered (shortest distance between clusters larger than ten standard deviations). Another important criterion was that the spikes of one unit had to respect the refractory period of at least $2\,\mathrm{ms}$ which is the lower limit of inter-spike-intervals at which retinal ganglion cells can fire. Only these units were used during the later analysis.

For pharmacological experiments, spike sorting was performed for each condition (control, drug, wash-out) separately to account for noise and the possible mutability of the spike shapes due to drug application. The sorted units from each condition were matched to each other by comparing the spike amplitudes and shapes in each channel of a group. Usually, only half of the cells could be identified during all three conditions.

3.2 Receptive field analysis

I used spatio-temporal white noise for estimating the area of spatial integration, the receptive field, and the temporal dynamics of each cell. This stimulus consisted of 80x60 squares of $75\,\mu\mathrm{m}$ length independently switching to black or white with a frequency of $30\,\mathrm{Hz}$.

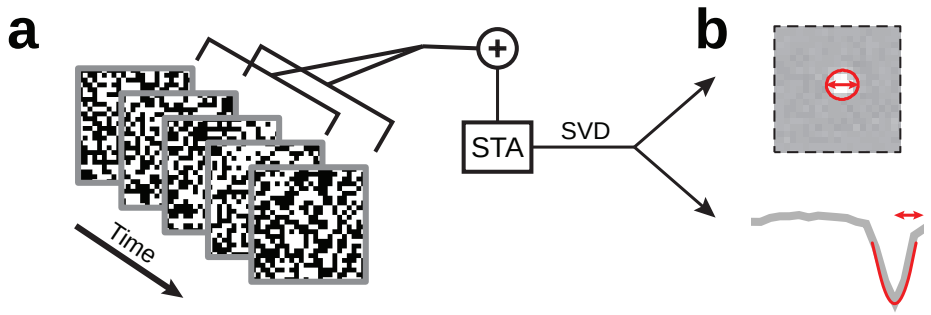

Figure 3.3 Schematics of temporal filter and spatial receptive field derivation from a spatio-temporal white noise stimulus. a The spike-triggered average (STA) is calculated from frames of spatio-temporal white noise which follow a spike. **b** The singular-value-decomposition (SVD) splits the spatio-temporal STA into its spatial (upper) and temporal components (lower). The spatial receptive field (upper) is fitted by a 2D Gaussian. Contours at 1.5 standard deviations (red circle) are used to estimate the receptive field diameter (double-headed arrow). First peak of the temporal filter (lower) is fitted by a parabola (red curve) to estimate the first peak latency (double-headed arrow).

First, I obtained the spatio-temporal filters of each cell by calculating the spike-triggered average (STA) (Chichilnisky, 2001) from the responses to the spatio-temporal white noise stimulus. Then, I used singular-value-decomposition (SVD) to separate the spatial and temporal components of the STA (Fig. 3.3a). The singular value decomposition turns the spatio-temporal filter into two sets of orthonormal bases in space and time. The singular vectors belonging to the largest singular value, constitute the least square fits of the filter in space and time. The SVD can be thought of as decomposing a matrix into a weighted, ordered sum of separable matrices. Separable models often arise in biological systems, and the SVD factorization is useful to analyze such systems. For example, some visual area V1 simple cells' receptive fields can be well described by a Gabor filter in the space domain multiplied by a modulation function in the time domain (De Valois et al., 2000).

The spatial receptive field of each cell was obtained by fitting a two-dimensional Gaussian to the first spatial component of the SVD (Fig. 3.3b, upper). The contours at 1.5 standard deviations of the Gaussian fit then marked the receptive field

of each cell. From these ellipses, the receptive field diameters $d = \sqrt{a \cdot b}$ were obtained from the lengths of the major and minor axis of the ellipse, a and b, respectively.
To estimate the temporal dynamics of the cells, I determined the first peak latencies from the first temporal component of the SVD (Fig. 3.3b, lower). Therefore, a parabola was fitted to the highest peak and the first peak latency determined from its peak time. It provides an estimate of how fast a cell responds to a visual stimulation.

3.3 Direction-selectivity and object-motion-sensitivity measures

Drifting square wave gratings of $600\,\mu\mathrm{m}$ period and a speed of $450\,\mu\mathrm{m/s}$ were used to determine the directional preference of each cell (Fig. 3.4a). The gratings were presented in a sequence of eight equidistant directions $\theta \in \{0°, 45°, \ldots, 315°\}$ with every direction being presented for $6.67\mathrm{s}$ with $1.67\mathrm{s}$ gray screen (mean display intensity) in between. This sequence was repeated five times.
I determined the degree of direction-selectivity and the preferred direction of each cell by first calculating the vector sum of the mean firing rates f_θ in direction θ. The first second of each trial was not included into the average to cut the stimulus onset response. The angle of this direction vector then provided the preferred direction of a cell while its strength, normalized by the sum of the mean firing rates yielded the direction-selectivity index

$$\mathrm{DSI} = \frac{|\sum_\theta f_\theta e^{i\theta}|}{\sum_\theta f_\theta}. \tag{3.1}$$

A DSI close to zero indicates low direction-selectivity and a DSI close to one a high direction-selectivity with narrow tuning width. This measure of direction selectivity is more robust than simply comparing the response rates for the preferred and null direction (Mazurek et al., 2014). I considered all cells with a DSI above 0.3 as direction-selective cells. Cells with a low response rate to drifting gratings ($< 1\ \mathrm{Hz}$) were considered as non-direction-selective but were not included into the distribution diagrams of the DSI.
I assessed the object-motion-sensitivity of each cell by using patches of jittering gratings in either a coherently or differentially moving fashion (Fig. 3.4b). The circular patches of $750\,\mu\mathrm{m}$ diameter were arranged in a honeycomb pattern. Each patch contained square wave gratings of $300\ \mu\mathrm{m}$ period, jittering with a random

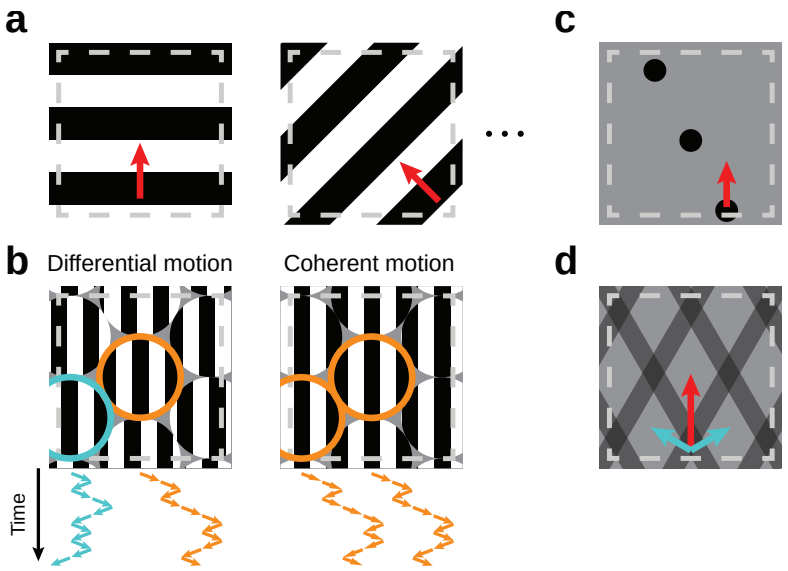

Figure 3.4 Stimuli for classifying standard DS, standard OMS and OMS-DS cells. **a** Drifting square wave gratings are applied in 8 equidistant directions (red arrows) in sequential order. **b** Patches of jittering gratings are running in two modes, differential and coherent motion. For differential motion (upper), gratings jitter independently with different trajectories (examples in cyan and orange). For coherent motion (lower), all gratings jitter coherently with the same trajectory (orange). The trajectory of the central patch (orange) is the same in both modes. **c d** Gray dashed lines indicate borders of the MEA.

trajectory of $15\ \mu\mathrm{m}$ steps to the left or right, every $0.33\mathrm{s}$. The surrounding area was at mean display intensity. The center patch was aligned with the center of the multi-electrode array.
The stimulus was displayed in two modes. In the first mode, all gratings moved independently with a different trajectory, resembling differential motion (Fig. 3.4b, left). In the second mode, all gratings moved coherently with the same trajectory (Fig. 3.4b, right). This simulated coherent global motion. The trajectory of the center patch was the same in both modes. The two modes were presented for $23.33\mathrm{s}$ each in an alternating sequence of six repetitions, separated by $1.67\mathrm{s}$ of mean luminance background.
I calculated an object-motion-sensitivity index (OMSI) from the difference between the mean firing rates in response to differential and coherent motion of the jittering patches, f_d and f_c, respectively, normalized by their sum:

$$\mathrm{OMSI} = \frac{f_\mathrm{d} - f_\mathrm{c}}{f_\mathrm{d} + f_\mathrm{c}}. \tag{3.2}$$

This resulted in a OMSI ranging from -1 to 1 which was negative for cells which prefer coherent motion and positive for differential or object-motion-sensitive cells. Due to the bimodal distribution of the experimentally obtained OMSI (Fig. 4.1e), I considered cells with an OMSI above 0.7 as object-motion-sensitive cells.

In some experiments, the object-motion specific responses of direction-selective cells were tested with more complex motion stimuli. One stimulus consisted of drifting dark spots which had a diameter of $180\ \mu\mathrm{m}$ and covered the whole width of the MEA (Fig. 3.4c). The spots drifted with a velocity of $450\ \mu\mathrm{m/s}$ across the retina into the same eight directions as the drifting gratings. Each direction is presented once for $40\ \mathrm{s}$. During this time, each spot drifts three times across the retina. The distances between the centers of nearest spots are $900\ \mu\mathrm{m}$ in the direction of motion and $288\ \mu\mathrm{m}$ in the direction perpendicular to the motion direction.
The second stimulus consisted of two crossed half-transparent square wave gratings which drifted into different directions (Fig. 3.4d). The analysis of the cell responses to this stimulus are outlined in the following.

3.4 Component and pattern selectivity

I used a plaid stimulus known from psychophysics and physiology (Adelson and Movshon, 1982; Castelo-Branco et al., 2002; Movshon et al., 1985) to test whether standard DS and OMS-DS cells responded differently to more complex motion

scenarios containing local and global motion features. The stimulus consisted of individual components which moved locally into different directions than the pattern of the fused components.
The components of the stimulus were semitransparent black bars in two orientations, rotated by $\alpha = 120°$, on a mean luminance background (Fig. 3.4d). The bars were $180\,\mu\mathrm{m}$ thick and spanned the whole screen. Bars of the same orientation were equally spaced every $600\,\mu\mathrm{m}$. The contrast was 50% for each individual bar and 75% where the bars crossed. The bars drifted with a velocity of $v_c = 450\,\mu\mathrm{m/s}$ perpendicular to their orientation. The velocity of the plaid pattern is given by the velocity of the components v_c and their separation angle α by $v_p = v_c \cdot \cos(\alpha/2) = 900\,\mu\mathrm{m/s}$.
The drift directions of the components were chosen thus that the plaid pattern was moving into the same directions as the usual drifting gratings stimulus. The stimulus was presented five times for $6.67\,\mathrm{s}$ for each direction. Tuning and DSI for this stimulus were calculated based on the motion direction of the pattern.
To obtain whether the cells were more strongly driven by the motion of the individual components or by the motion of the pattern, I calculated the tuning predictions for pattern- and component-selective cells based on the tunings to the drifting gratings. The pattern prediction was the same as the drifting gratings tuning while the component prediction was the sum of the drifting gratings tunings turned by $\pm 60°$. To obtain whether the plaid tuning of each cell was more driven by the pattern or the component motion, I calculated the partial correlations

$$R_p = \frac{r_p - r_c r_{pc}}{\sqrt{(1 - r_c^2)(1 - r_{pc}^2)}} \tag{3.3}$$

$$R_c = \frac{r_c - r_p r_{pc}}{\sqrt{(1 - r_p^2)(1 - r_{pc}^2)}} \tag{3.4}$$

from the Pearson correlation coefficients r_p of the pattern prediction with the plaid tuning, r_c of the component prediction with the plaid tuning and r_{pc} of the pattern prediction with the component prediction (Movshon et al., 1985). Whether a cell was significantly pattern or component selective was determined from the 95% confidence interval of the Fisher transformed partial correlations $Z_{p/c} = 3 \tanh^{-1}(R_{p/c})$ (Fisher, 1915).

3.5 Linear decoding of random motion trajectories

I used three different stimuli which I usually ran for $40\,\mathrm{min}$ to investigate the independent encoding of random background and object motion trajectories (Fig. 3.5).

First, I used a correlated noise background (Fig. 3.5a) which I generated from a spatial white noise pattern with 30x30 μm^2 pixel size where I applied a Gaussian smoothing of $60\,\mu m$ standard deviation. The pattern was shifted in a 2-dimensional random walk with independently, Gaussian-distributed motion steps in x- and y-direction with $22.5\,\mu m$ standard deviation and a frequency of $30\,Hz$.

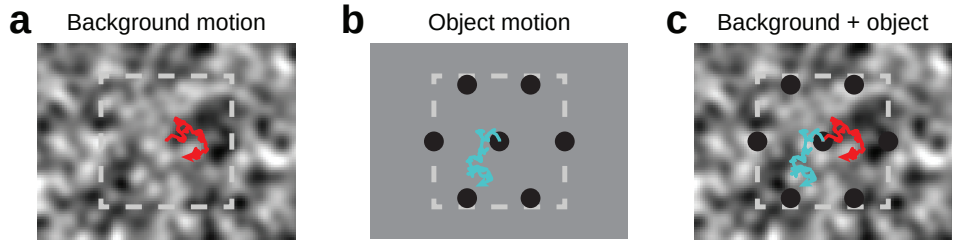

Figure 3.5 **Jittering textures used for trajectory decoding.** **a** Correlated noise texture moving in a 2-dimensional random walk (red trajectory). **b** Object texture consisting of 7 dark spots moving on a mean luminance background with different trajectory than correlated noise texture (cyan trajectory). **c** Object texture on top of correlated noise texture, both moving independently of each other with the same trajectories as in (b) and (a), respectively. Gray dashed lines indicate borders of the MEA.

Second, I used a jittering object on a mean luminance background, consisting of seven dark spots of $240\,\mu m$ diameter, arranged in a hexagonal pattern with spots separated by $750\,\mu m$ (Fig. 3.5b). This object-like texture was shifted according to Ornstein-Uhlenbeck processes (Uhlenbeck and Ornstein, 1930) in x- and y-direction with a reset force to keep the object within range of the recording area. Each motion step Δx_t was calculated by

$$\begin{aligned} \Delta x_t &= -F x_t \Delta t + \sigma \Delta W_t \\ &= -F x_t \Delta t + \underbrace{\sigma\sqrt{\Delta t}}_{G}\, \xi_t \end{aligned} \tag{3.5}$$

where $\Delta t = 0.033\,s$ was the time interval between frames and $G = 22.5\,\mu m$ the standard deviation of the independently, normally-distributed motion steps ξ_t, same as for the background motion. The magnitude of the reset force $F = 0.05\,Hz$ was chosen in such a way that it would only mildly change the distribution of the motion steps and at the same time not allow too far explorations from the recording area. Then, the x- and y-positions of the object-like texture would be Gaussian-distributed with $x_t, y_t \sim \mathcal{N}\left(0, \frac{\sigma^2}{2R}\right) \sim \mathcal{N}\left(0, (391.7\,\mu m)^2\right)$, centered on the recording area.

Also, I used a stimulus where the object-like texture was superimposed on the correlated noise texture and both were moving with independent trajectories (Fig. 3.5c)

to investigate the simultaneous encoding of object and background motion trajectories.

3.5.1 The LN-model

The linear-nonlinear model is a simple model for estimating neural firing rates in response to a given stimulus. For retinal ganglion cells, the response rate $f(t)$ at time t is put into a linear relationship to the visual stimulus immediately before the response $s(I_{t-T,t})$ similar to the STA (Sect. 3.2) but normalized to have a standard deviation of unity, where T corresponds to the length of the resulting linear filter (Fig. 3.6). Ideally, the stimulus should have a Gaussian white noise statistics for an unbiased estimate of the linear filter. If the frequency of the stimulus is fast enough so that the integration time of the cell is much larger than the interval between stimulus frames, a binary white noise is usually sufficient since the distribution of the integrated stimulus will approach a Gaussian according to the central limit theorem. The stimulus can be a temporal flicker of the screen intensity, a spatio-temporal white noise or a trajectory with independently chosen random motion-steps, as I used for the background motion.

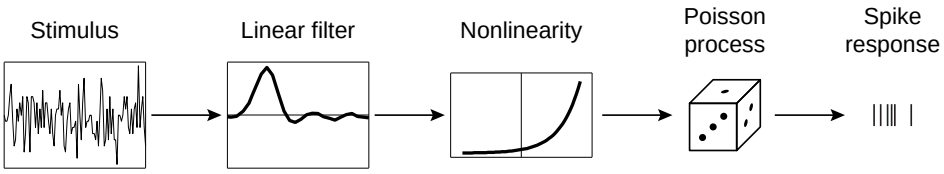

Figure 3.6 Schematics of the linear-nonlinear model with Poissonian spike generation. First, the spike-triggered average of a stimulus with independently, randomly changing values is determined as the linear relationship between stimulus and response (*linear filter*). Then, the *nonlinearity* is determined from value pairs of the filtered stimulus and mean response. A *Poisson process* then generates the *spike output* from the mean responses estimated by the stimulus which is passed through the linear filter and nonlinearity relation.

For a temporal Gaussian flicker stimulus, the linear filter $a(t)$ is only time-dependent. For estimating the nonlinearity, the stimulus is first projected into filter space by convolving the stimulus with the filter, to obtain the *generator signal* $g(t) = \sum_{\tau=0}^{T} a(\tau) \cdot s(t-\tau)$. The generator signal is then set in relation to the actual response rate $f(t)$ to estimate the nonlinearity $N(g)$. Therefore, I subdivided the space of the generator signal into bins containing equal amount of data points and calculated the average generator signal and mean response rate in each bin. If stimulus and filter are normalized to standard deviation of one, the generator signal is usually normal-distributed with positive values corresponding to preferred

stimuli and negative values to unfavored stimuli. Nonlinearities are usually rectifying since there can be no negative spike rates.
To now generate the response to a new stimulus, the experimentally obtained nonlinear relation between generator signal and response rate should be approximated by a continuous function. Often, a sigmoidal is fitted to the data which is able to capture the spontaneous activity (for $g \ll -1$) and spike rate saturation (for $g \gg 1$) of the cell. For nonlinearities were no saturation is observed, the curve can usually be described by a simple exponential (cf. Fig. 3.6, nonlinearity).
Responses to a new stimulus can now be generated by passing it through the linear filter and estimating the mean firing rates $m(t) = N(g(t))$ at time t from the nonlinear relation between generator signal g and response. Spike rates are then generated according to a Poisson process with mean and standard deviation corresponding to the estimated mean firing rates $m(t)$.

Motion nonlinearities The motion trajectory of the background motion is a two-dimensional uncorrelated random walk and the two-dimensional linear filter consists of two independent filters in x- and y-direction. Instead of obtaining a one-dimensional generator signal by integrating over time and direction, I calculated two independent generator signals in x- and y-direction, $g_x(t)$ and $g_y(t)$, respectively, from the corresponding filters.
The quasi-independent nonlinearities in x and y direction can then be estimated by calculating the conditional nonlinearities $N_x(g_x|g_y \approx 0)$ and $N_y(g_y|g_x \approx 0)$. For example, for the conditional nonlinearity in x-direction, the response rate was measured for each time bin where the filtered stimulus in y-direction was close to zero, i.e., where the motion in y-direction had least influence on the encoding in x-direction. Then, the measured pairs of filtered stimulus and response were divided into bins with equal number of data points and averaged which yielded non-monotonic nonlinearities.
For estimating the influence of different nonlinearity models to the random motion encoding of DS cells, I fitted the conditional nonlinearities of the DS cells either with a simple exponential function $N(x) = A \exp(x/B)$ or with a non-monotonic function of a quadratic function combined with an exponential $N(x) = A\, x^2 \exp(x/B)$. The two different nonlinearities were then used to generate the independent responses of DS cell pairs to the random motion.

3.5.2 Linear multi-cell decoder

I used a linear multi-cell decoder (Warland et al., 1997) to investigate how well a random motion trajectory can be decoded from the responses of a population

of ν DS cells. A linear readout is the simplest way to decode information from a population of spiking neurons and a valid assumption for the integration of input signals by hypothetical downstream neurons.
From the first $28\,\mathrm{min}$ of a recording with random background or object motion, the independent linear filters of the responses to motion into x- and y-direction, $\mathbf{a}_x$ and $\mathbf{a}_y$, respectively, were calculated. Therefore, the stimulus was convolved with the from the response matrix $\mathbf{F}$ and the stimulus $\mathbf{s}$ (Fig. 3.7a)

$$\mathbf{F} = \begin{pmatrix} f_0^1 & f_1^1 & \cdots & f_{L-1}^1 & \cdots & f_0^\nu & \cdots & f_{L-1}^\nu \\ f_1^1 & f_2^1 & \cdots & f_L^1 & \cdots & f_1^\nu & \cdots & f_L^\nu \\ \vdots & \vdots & & \vdots & & \vdots & & \vdots \\ f_{M-1}^1 & f_M^1 & \cdots & f_{L+M-2}^1 & \cdots & f_{M-1}^\nu & \cdots & f_{L+M-2}^\nu \end{pmatrix}, \; \mathbf{s} = \begin{pmatrix} s_{x0} & s_{y0} \\ s_{x1} & s_{y1} \\ \vdots & \vdots \\ s_{x(M-1)} & s_{y(M-1)} \end{pmatrix} \tag{3.6}$$

$$\mathbf{b} = (\mathbf{F}^\mathrm{T}\mathbf{F})^{-1} \cdot (\mathbf{F}^\mathrm{T}\mathbf{s}) = \begin{pmatrix} b_{x0}^1 & b_{x1}^1 & \cdots & b_{x(L-1)}^1 & \cdots & b_{x0}^\nu & \cdots & b_{x(L-1)}^\nu \\ b_{y0}^1 & b_{y1}^1 & \cdots & b_{y(L-1)}^1 & \cdots & b_{y0}^\nu & \cdots & b_{y(L-1)}^\nu \end{pmatrix}^\mathrm{T} \tag{3.7}$$

where the f_j^i were the firing rates of DS cell i during time interval j and the s_{xj} and s_{yj} the motion steps in x- and y-direction at time j, respectively. The time intervals were of length $\Delta t \approx 33\,\mathrm{ms}$ and corresponded to the interval between stimulus frames. $M\Delta t = 28\,\mathrm{min}$ was the duration of the first stimulus fragment for the training of the decoder and $L\Delta t = 800\,\mathrm{ms}$ the time interval during which the neural responses to a new stimulus frame was measured. The linear filters $\mathbf{b}$ contained two important terms, the stimulus-weighted averages of the cell responses $\mathbf{F}^\mathrm{T}\mathbf{s}$ and the normalization term $\mathbf{F}^\mathrm{T}\mathbf{F}$ containing the first order correlations between cell pairs within time interval $L\Delta t$.
The linear reconstruction of the motion in x- and y-direction, $\mathbf{u} = \mathbf{F} \cdot \mathbf{b}$, I then derived from the responses to the last $12\,\mathrm{min}$ of the stimulus for cross-validation (Fig. 3.7b).

3.5.3 Mutual information between stimulus and reconstruction

For estimating how much information the linear readout of the DS cell responses provided about the stimulus, I calculated a lower bound of the *mutual information* between stimulus $\mathbf{s}$ and reconstruction segments $\mathbf{u}$ of length $L\Delta t$ similar to Warland et al. (1997). The mutual information between stimulus and reconstruction in x- and y-direction, $I_{\mathbf{s},\mathbf{u}}^x$ and $I_{\mathbf{s},\mathbf{u}}^y$, respectively, were calculated independently of each other from the motion steps $\mathbf{s}_{x/y}$ and reconstructions $\mathbf{u}_{x/y}$ in x- and y-

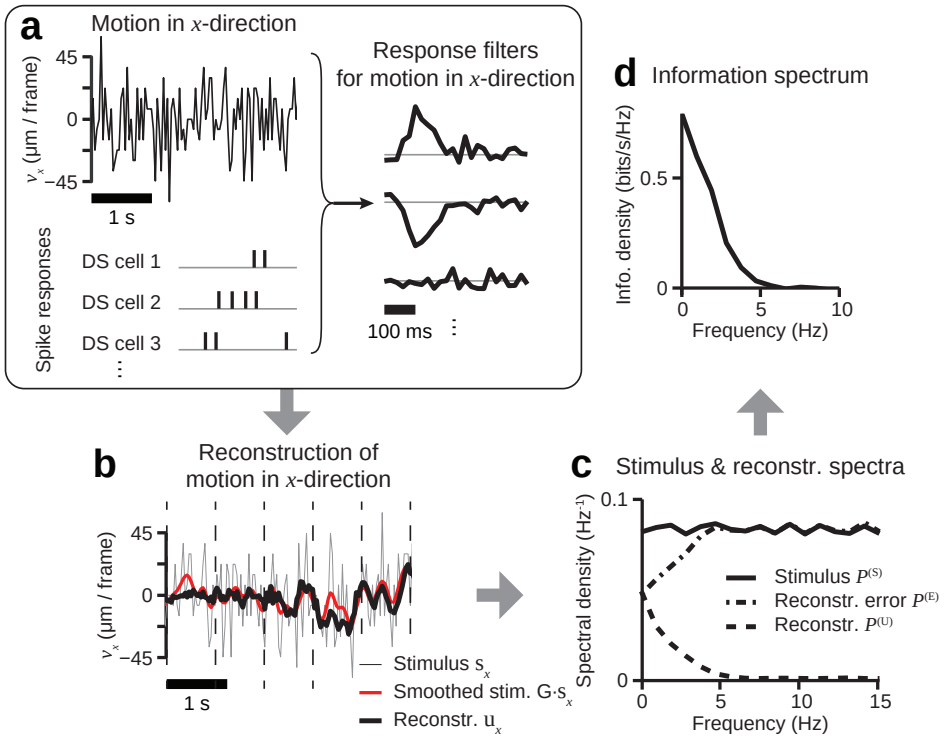

Figure 3.7 Schematics of linear multi-cell decoder and determination of information spectrum. **a** Motion filters of x-direction are derived from motion steps in x-direction and cell responses. **b** Multiplication of response matrix with filter vector gives motion reconstruction in x-direction (thick black line). Prediction is close to smoothed stimulus (red line). Stimulus $\mathbf{s}$ and reconstruction $\mathbf{u}$ are divided into blocks of the length of the filter (dashed lines). **c** Stimulus $\{s\}_i$ and reconstruction blocks $\{u\}_i$ are Fourier transformed and the ensemble average over all blocks is taken to obtain the power spectra $P^{(\mathrm{S})}$ and $P^{(\mathrm{U})}$, respectively. Power spectrum of the reconstruction error $P^{(\mathrm{E})}$ is obtained in the same way from $e_i = s_i - u_i$. **d** Information spectrum is obtained from the power spectra of stimulus and reconstruction error.

direction. The information for either direction $I_{\mathbf{s},\mathbf{u}} = H_\mathbf{s} - H_{\mathbf{s}|\mathbf{u}}$ is derived from the Shannon entropy of the stimulus $H_\mathbf{s} = -\sum_\mathbf{s} p(\mathbf{s}) \log_2 p(\mathbf{s})$ (Shannon, 1948) and the conditional entropy of the stimulus motion given the information from $\mathbf{u}$, $H_{\mathbf{s}|\mathbf{u}} = -\sum_\mathbf{u} p(\mathbf{u}) \sum_\mathbf{s} p(\mathbf{s}|\mathbf{u}) \log_2 p(\mathbf{s}|\mathbf{u})$. The motion steps are independently Gaussian-distributed with standard deviation $\sigma = 22.5\,\mu\mathrm{m}$ leading to a probability distribution of the stimulus segments $\mathbf{s}$

$$p(\mathbf{s}) = \frac{1}{\sqrt{(2\pi)^L \det \mathbf{S}}} \exp\left(-\frac{1}{2}\mathbf{s}^\mathrm{T}\mathbf{S}^{-1}\mathbf{s}\right) \tag{3.8}$$

where $\mathbf{S} = \langle \mathbf{s}\mathbf{s}^\mathrm{T} \rangle = \sigma^2 \cdot \mathbb{1}^{L\times L}$ is the covariance matrix of the stimulus. The probability distribution of the stimulus given the reconstruction, $p(\mathbf{s}|\mathbf{u})$, can be approximated by a Gaussian distribution

$$p(\mathbf{s}|\mathbf{u}) = p(\mathbf{s}-\mathbf{u}) = \frac{1}{\sqrt{(2\pi)^L \det \mathbf{E}}} \exp\left(-\frac{1}{2}\mathbf{e}^\mathrm{T}\mathbf{E}^{-1}\mathbf{e}\right) \tag{3.9}$$

where $\mathbf{e} = \mathbf{s} - \mathbf{u}$ is the reconstruction error and $\mathbf{E} = \langle \mathbf{e}\mathbf{e}^\mathrm{T} \rangle$ its covariance matrix. The Gaussian approximation provides an upper boundary for the conditional entropy $H_{\mathrm{s}|\mathrm{u}}$ (Cover and Thomas, 1991). Then, the mutual information can be approximated by the lower bound

$$I_{\mathbf{s},\mathbf{u}} = -\sum_\mathbf{s} p(\mathbf{s}) \log_2 p(\mathbf{s}) + \sum_\mathrm{u} p(\mathbf{u}) \sum_\mathbf{s} p(\mathbf{s}|\mathbf{u}) \log_2 p(\mathbf{s}|\mathbf{u}) \tag{3.10}$$

$$> -\sum_\mathbf{s} p(\mathbf{s}) \log_2 p(\mathbf{s}) + \sum_\mathrm{u} p(\mathbf{u}) \sum_\mathbf{s} p(\mathbf{s}-\mathbf{u}) \log_2 p(\mathbf{s}-\mathbf{u}). \tag{3.11}$$

Now, let $\mathbf{e} = \mathbf{s} - \mathbf{u}$

$$\begin{aligned} I_{\mathbf{s},\mathbf{u}} > & \underbrace{-\underbrace{\sum_\mathbf{s} \frac{\exp(-\frac{1}{2}\mathbf{s}^\mathrm{T}\mathbf{S}^{-1}\mathbf{s})}{\sqrt{(2\pi)^L \det \mathbf{S}}}}_{=1} \left(\left(-\frac{\mathbf{s}^\mathrm{T}\mathbf{S}^{-1}\mathbf{s}}{2\ln 2}\right) - \underbrace{\log_2 \sqrt{(2\pi)^L \det \mathbf{S}}}_{\text{const.}}\right)}_{=\frac{1}{2\ln 2}} \\ & + \sum_\mathbf{u} p(\mathbf{u}) \underbrace{\sum_\mathbf{e} \frac{\exp(-\frac{1}{2}\mathbf{e}^\mathrm{T}\mathbf{E}^{-1}\mathbf{e})}{\sqrt{(2\pi)^L \det \mathbf{E}}} \left(\left(-\frac{\mathbf{e}^\mathrm{T}\mathbf{E}^{-1}\mathbf{e}}{2\ln 2}\right) - \underbrace{\log_2 \sqrt{(2\pi)^L \det \mathbf{E}}}_{\text{const.}}\right)}_{=-\frac{1}{2\ln 2}} \\ & > \log_2 \sqrt{(2\pi)^L \det \mathbf{S}} - \underbrace{\sum_\mathbf{u} p(\mathbf{u})}_{=1} \log_2 \sqrt{(2\pi)^L \det \mathbf{E}} \end{aligned} \tag{3.12}$$

$$> \log_2 \sqrt{\det(\mathbf{S}\mathbf{E}^{-1})}. \tag{3.13}$$

Since $\mathbf{S}$ and $\mathbf{E}$ are diagonal due to time translation invariance, the information estimate can easily be converted into frequency space to observe the frequency dependence of the mutual information between stimulus and reconstruction

$$I_{\mathbf{s},\mathbf{u}} > \sum_{j=0}^{L/2} I_j = \sum_{j=0}^{L/2} \log_2 \left(P_j^{(S)} / P_j^{(E)} \right) \tag{3.14}$$

where $P_j^{(S)} = \langle 2 \, |\tilde{s}_j|^2 \rangle_{\text{blocks}}$ and $P_j^{(E)} = \langle 2 \, |\tilde{e}_j|^2 \rangle_{\text{blocks}}$ are the power spectra of the stimulus $\mathbf{s}$ and the reconstruction error $\mathbf{e}$, respectively, at frequency $j/(L\Delta t)$. To determine the power spectra, stimulus, reconstruction and reconstruction error were divided into non-overlapping blocks of the length of the filter interval $L\Delta t$ and the Fourier transforms of each block $\tilde{s}_j$, $\tilde{u}_j$ and $\tilde{e}_j$, respectively, were calculated. The power density spectra were then averaged over all blocks (Fig. 3.7c) and the information density derived (Fig. 3.7d). The lower boundary of the total mutual information would then be the sum of the information density over all frequencies. For estimating the effect of noise correlations on the encoding performance of the cell population, I repeated a $15\,\text{min}$ trajectory 10 times and calculated the mutual information with cell responses from shuffled trials I_{shuffle}. This way correlations induced by shared input noise from upstream neurons were destroyed and only the correlations induced by the stimulus itself persisted (Schneidman et al., 2003).

3.5.4 Canonical correlation analysis

I used canonical correlation analysis to gain insight into the population activity in response to different motion components. Canonical correlation analysis (CCA) is a reverse correlation method where singular value decomposition (SVD) is used to find the stimulus components to which a cell assembly responds most strongly. At the same time it provides the activity of the assembly that is maximally correlated to the stimulus components (Zeck et al., 2008). The stimulus filter $\mathbf{a}_1$ and the correlated response filter $\mathbf{b}_1$ which maximize the correlation coefficient

$$\rho_1 = \frac{cov(\mathbf{a}_1^{\mathrm{T}} S, \mathbf{b}_1^{\mathrm{T}} F)}{\sqrt{var(\mathbf{a}_1^{\mathrm{T}} S) var(\mathbf{b}_1^{\mathrm{T}} F)}} \tag{3.15}$$

can be found by applying an SVD to the whitened cross-covariance matrix derived from the covariance matrices of stimulus and response Σ_s and Σ_r, respectively,

and Σ_{sr} the cross-covariance between stimulus and response

$$C = \Sigma_s^{-1/2}\Sigma_{sr}\Sigma_r^{-1/2} \quad (3.16)$$

$$= UDV^{\mathrm{T}}\,(\mathrm{SVD}) \quad (3.17)$$

The whitened cross-covariance matrix is decomposed into the unitary matrices U and V and the diagonal matrix D containing the correlation coefficients. The preferred stimuli within this framework can then be derived from the column vectors in U and the covariance matrix of the stimulus with $\mathbf{a}_k = \Sigma_s^{-1/2}\mathbf{u}_k$. The correlated neuronal activity is then $\mathbf{b}_k = \Sigma_r^{-1/2}\mathbf{v}_k$. The correlation-coefficients ρ_k of the k-th component in D are in a decreasing order. The stimulus filters $\mathbf{a}_k$ and the correlated response $\mathbf{b}_k$ form orthonormal bases spanning the stimulus and response space, respectively.

4 — Characterization of motion-specific cell responses

Salamander is a common model for studying retinal motion encoding (Chen et al., 2014; Leonardo and Meister, 2013; Marre et al., 2015; Schwartz et al., 2007) but its retinal ganglion cell types have been mostly defined by responses to flash stimulation and temporal white noise flicker (Marre et al., 2012; Segev et al., 2006; Warland et al., 1997). In the first part of this thesis, I characterized retinal ganglion cells in the axolotl retina (*Ambystoma mexicanum*) according to their responses to simple visual motion stimuli. I obtained the functional properties of the motion-classified cell types and analyzed their responses to more complex motion stimuli. Using multielectrode arrays, I could extracellularly record the responses from more than 300 ganglion cells at a time which further allowed me to determine correlations within a population of cells of the same response type.

4.1 Direction-selectivity and object-motion-sensitivity

I characterized retinal ganglion cells by their responses to two moving stimuli. First, I used drifting square wave gratings (inset Fig. 4.1a, details in Sect. 3.3) to observe how the axolotl retinal ganglion cells responded to different directions of uniform motion and to identify directional preferences. The second stimulus consisted of circular patches arranged in a honeycomb pattern with jittering square wave gratings (inset Fig. 4.1c). The gratings in each patch were moving in two different modes. Either all gratings would jitter with the same trajectory, simulating global coherent motion of tremor-like eye movements, or each grating would jitter with a different trajectory, resembling the local differential motion of independently moving objects. Only the trajectory of the central patch would be identical during both conditions. This stimulus aimed at uncovering preferences

for one of the two conditions, local differential or global coherent motion, i. e., if the cells responded better to an object, moving differentially to its surrounding area, or to a globally moving background, respectively.
The responses to the drifting gratings revealed that some cells had a strong directional preference (Fig. 4.1a-b, left). These so-called direction-selective (DS) cells (Lettvin et al., 1959; Barlow and Hill, 1963) strongly responded to a certain direction of the drifting gratings, their *preferred direction* (indicated by the arrow in Fig. 4.1b, left), but did barely respond to the opposite direction, their *null direction*. For the patches of jittering gratings, these cells responded equally well to the differential and coherent motion conditions (Fig. 4.1c, left).
Other cells did not have a directional tuning but showed a strong asymmetry in their responses to the patches of jittering gratings (Fig. 4.1c, middle). They responded well to differential motion but not to the coherent motion condition. Although the receptive field of the OMS cell was within the central patch (inset Fig. 4.1c), it was still influenced by motion in its remote surround. This type of cell has been discovered more recently in rabbit and tiger salamander by using a similar stimulus with a single central patch and a jittering background grating (ÖLveczky et al., 2003). They are called object-motion-sensitive (OMS) cells due to their preferences for local differential motion as induced by moving objects on a moving or static background.
Furthermore, I found a subgroup of DS cells with a strong preference for differential motion (Fig. 4.1, right). These cells were robustly directionally tuned to drifting gratings but had a much lower firing rate than the direction-selective cells discussed before (Fig. 4.1a-b). Due to their object-motion-sensitivity, I named them OMS-DS cells. To distinguish DS cells which were not object-motion-sensitive and OMS cells which were not direction-selective from the OMS-DS cells, I will in the following refer to them as standard DS and standard OMS cells, respectively. Standard DS, standard OMS and OMS-DS cells had in common that they responded only to the dark bars of the drifting gratings (Fig. 4.1, top) and therefore might be OFF cells, i.e., cell which respond to a darkening within their receptive field center.
To investigate the properties of the three motion-specific response types, I determined direction-selective and object-motion-sensitive cells by using relative rate measures, the direction-selectivity index (DSI) and the object-motion-sensitivity index (OMSI), respectively (Fig. 4.2). For the DSI, I calculated the absolute vector sum of the directional tuning from the drifting gratings (Fig. 4.1b) and normalized by the sum of the mean firing rates (Eq. 3.1). This direction-selectivity measure considered the entire directional tuning curve of a cell, hence, it is more robust

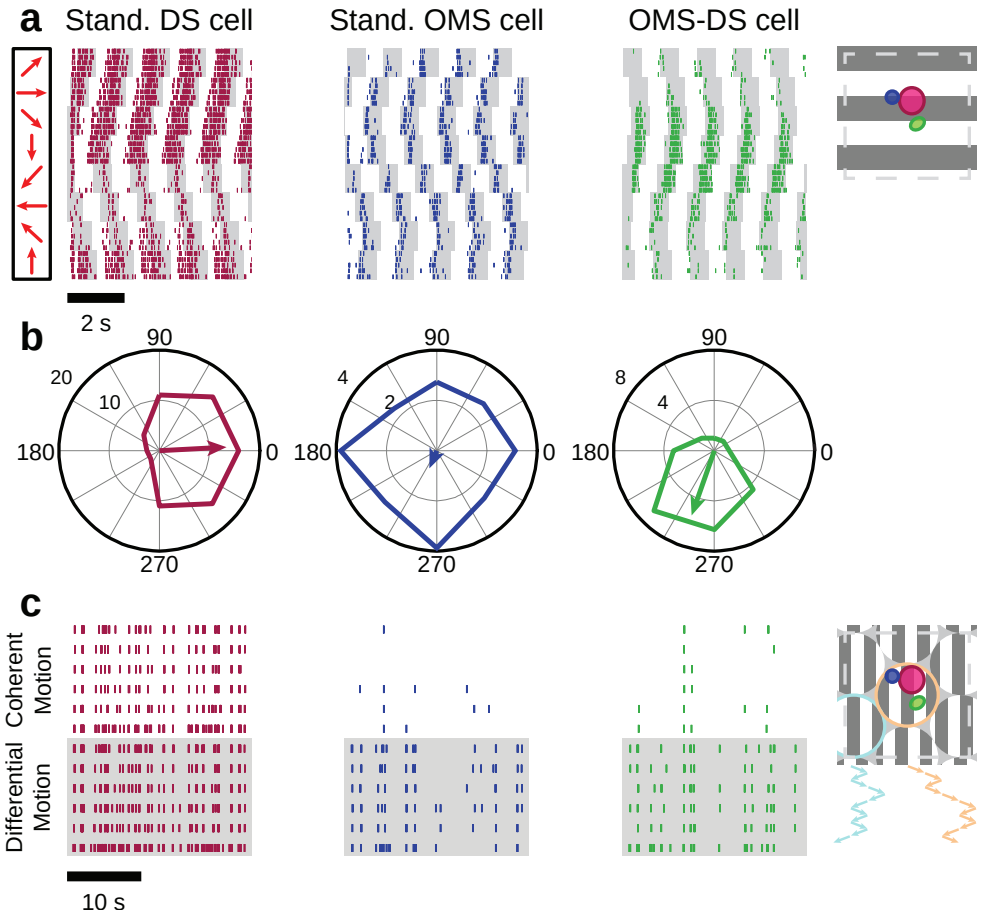

Figure 4.1 **Responses of a standard DS (left), a standard OMS (middle) and an OMS-DS cell (right) to drifting gratings and patches of jittering gratings. a** Raster plots of elicited spikes during five trials of a drifting gratings sequence with eight directions (red arrows). Gray bars indicate when a dark region covered the receptive field center of the cell. Inset: illustration of stimulus with receptive fields of standard DS (magenta), standard OMS (blue) and OMS-DS cell (green). **b** Polar plots of the mean firing rates (in Hz) in response to the eight drift directions. Arrow indicates preferred direction according to the vector sum of the eight mean firing rate vectors, length was divided by 2 for better display. Standard DS (left) and OMS-DS cell (right) show a clear directional preference. **c** Raster plots of elicited spikes during seven identical trials of patches of jittering gratings alternating between differential and coherent motion mode, stimulus shown in inset. Standard OMS (middle) and OMS-DS cell (right) responded with much fewer spikes to coherent motion than to differential motion while the standard DS cell responded equally well to both motion conditions.

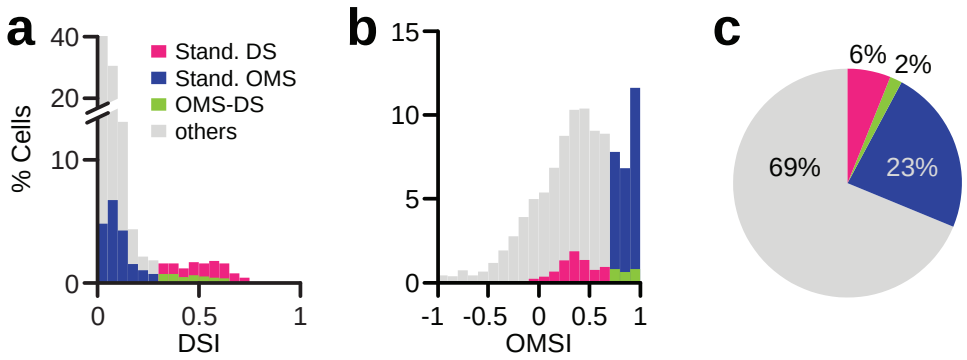

Figure 4.2 **Classification of standard DS (magenta), standard OMS (blue) and OMS-DS cells (green). a** Distribution of the direction-selectivity index (DSI) (Eq. 3.1). Cells with a DSI above 0.3 are classified as direction-selective (DS) cells. **b** Bimodal distribution of the object-motion-sensitivity index (OMSI) (Eq. 3.2). Cells with a positive OMSI respond better to differential motion while cells with a negative OMSI respond better to coherent motion. Cells with an OMSI above 0.7 are classified as object-motion-sensitive (OMS) cells. The OMSI threshold splits the distribution of DS cells into two groups, the standard DS cells and the OMS-DS cells. **c** Proportion of standard DS, standard OMS and OMS-DS from 30 retinas and 4126 recorded cells. Unspecified cells are marked in gray.

against firing rate fluctuations along the preferred-null direction axis and better suitable for slightly skewed tuning curves. Cells with a DSI close to zero responded equally well to each direction and did not show any directional preferences while cells with a DSI close to 1 would show almost perfect direction-selectivity where the cell would mainly respond to one of the eight directions. Most of the ganglion cells in the salamander retina were not direction-selective (Fig. 4.2a). Only cells with a DSI above 0.3 and a mean firing rate above $1\,\mathrm{Hz}$, to exclude poorly responding cells, were considered as direction-selective cells. They showed strong and robust directional preferences.

For the OMSI, the mean firing rate in response to the coherent motion of the jittering patches was subtracted from the mean response rate to the differential motion and then normalized by their sum (Eq. 3.2). A positive OMSI close to 1 signifies strong sensitivity to differential or object motion and a negative OMSI close to -1 signifies a strong sensitivity to coherent global motion. The obtained distribution of the OMSI from 30 experiments is visibly right-shifted with a median markedly above zero (Fig. 4.2b). This signifies that the average cell had a preference for differential motion. The two peaks of the bimodal distribution strongly overlap which makes a clear separation of OMS and non-OMS cells difficult. By applying a 2-component Gaussian mixture model, a threshold around 0.8 could be estimated above which cells would be considered as OMS cells. However, I

decided on a rather low threshold of 0.7 to include as many putative OMS cells as possible for later analysis and accepting the chance of false positives. Nevertheless, above this threshold all cells showed strong object-motion-sensitivity by visual inspection.
The intersection of the thus identified OMS and DS cells were the OMS-DS cells. They showed direction selectivity with a DSI larger than 0.3 and object-motion-sensitivity with an OMSI larger than 0.7. They made up only 2% of the recorded cell population, while there were 6% of standard DS and 23% of standard OMS cells (Fig. 4.2c).
One could ask now if standard DS and OMS-DS cells actually belong to the same group of cells with small variations in their responses to coherent global motion or if they could belong to distinct cell types, with different morphology and function, encoding specific features of a visual scene.

4.2 Receptive field properties

Different cell types often show distinctive spatio-temporal dynamics. With a spatio-temporal white noise stimulus a cell's area of spatial integration, the *receptive field* (RF), and dynamics of temporal integration can be determined by reversely correlating stimulus and response (see Sect. 3.2 for details). These properties can be indicators of the cells' morphology and function. For example, the receptive field size is usually strongly correlated with the size of the cell's dendritic field (Yang and Masland, 1994). Furthermore, the temporal dynamics indicate the characteristic temporal frequency range that a cell can encode. Cells with fast temporal dynamics can encode higher temporal frequencies.
The example in figure 4.3a shows the receptive field contours of standard DS (magenta), standard OMS (blue) and OMS-DS cells (green) within a small retinal patch where standard DS cells had much larger receptive fields than standard OMS and OMS-DS cells. The contours were obtained from a two-dimensional Gaussian fit of the spatial component of the spatio-temporal STA at 1.5 standard deviations (Sect. 3.2). In the pooled data from 16 retinas (Fig. 4.3c), standard OMS and OMS-DS cells were among the smallest, with receptive field diameters around $290 \pm 80\,\mu\mathrm{m}$. Standard DS cells had very large receptive fields ($390 \pm 90\,\mu\mathrm{m}$) which would allow them to integrate motion within a large area and might be useful for capturing information about global background motion. Small receptive fields, as of the standard OMS and OMS-DS cells observed here, usually result in a higher density of cells of the same type which would provide a higher spatial resolution and might be important for detecting small moving objects.

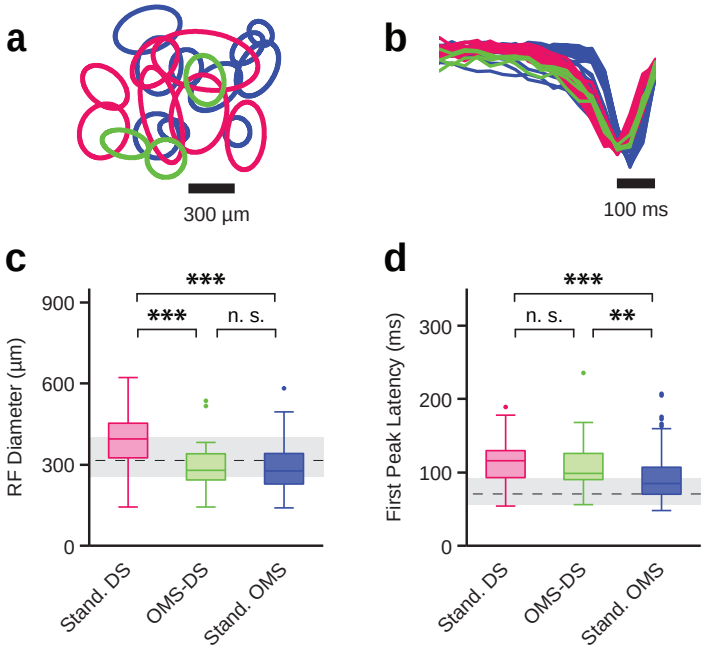

Figure 4.3 **OMS-DS cells have small receptive fields like OMS cells and long response latencies as standard DS cells. a-b** Receptive field contours (**a**) and temporal filters (**b**) of standard DS (magenta), OMS (blue) and OMS-DS cells (green) from a single retina. A negative deflection of the temporal filter signifies an average darkening of the screen before spiking. **c-d** Box plots of receptive field diameters (**c**) and first peak latencies (**d**) of 134 standard DS (magenta), 186 OMS (blue), 18 OMS-DS (green) and 852 unspecified cells (gray) from 16 experiments. Upper and lower box edges indicate interquartile range (IQR) between the 25th and 75th percentiles, respectively. Central box line indicates the median. Whiskers are extended to the most extreme values which are within $1.5 \cdot$ IQR from the edges of the box, outliers are marked with bullets. Gray bar in the background indicates population IQR with population median (dashed line). **c** RF diameters of standard OMS and OMS-DS cells were not significantly different from each other (n.s.) but significantly different from RF diameters of standard DS cells ($p < 0.005$). **d** First peak latencies of standard DS and OMS-DS cells were significantly slower than latencies of OMS cells ($p < 0.01$). Standard DS and OMS-DS cells had similar first peak latencies (n.s.).

To characterize the temporal integration of the cells, one usually considers the timing of the first peak of the temporal filters (Fig. 4.3b), the *first peak latency*. This measure provides an estimate for how fast the cells respond to contrast changes. Standard DS and OMS-DS cells were significantly slower with first peak latencies of $114 \pm 27\,\mathrm{ms}$ and $112 \pm 41\,\mathrm{ms}$, respectively, than standard OMS cells ($87 \pm 27\,\mathrm{ms}$). Though, all three cell types were significantly slower than the population average (Fig. 4.3d). The sign of the filter peaks (Fig. 4.3b) suggests that all three cell types responded to changes from bright to dark contrast within their receptive field center and could therefore be OFF types as indicated in the responses to the drifting gratings before (Sect. 4.1a).

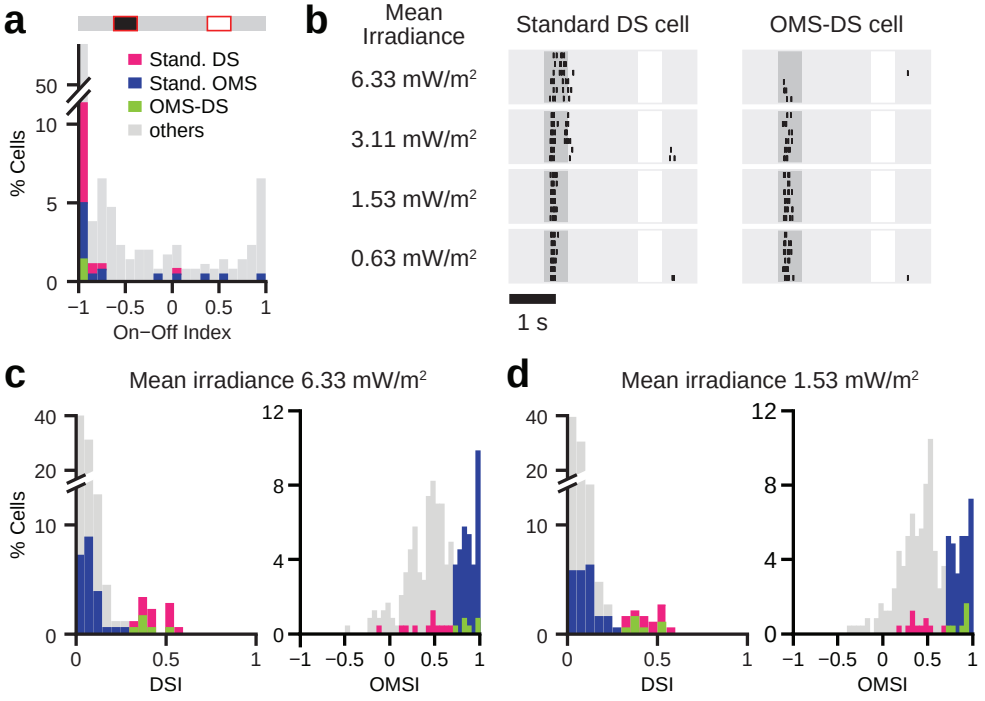

Figure 4.4 **Standard DS and OMS-DS cells are OFF-cells throughout photopic and high mesopic light levels, DS and OMS properties did not change.** **a** Distribution of the On-off index at $6.33\mathrm{mW/m^2}$ mean irradiance. **b** Responses of a standard DS and an OMS-DS cell to 40% contrast steps from a mean luminance background at different light levels (mean irradiance $0.63\mathrm{mW/m^2} - 6.33\mathrm{mW/m^2}$). **c-d** Distributions of DSI and OMSI do not change significantly between low photopic (c) and high mesopic light levels (d).

As the direction-selective cells observed in mammals were usually ON or ON-OFF type, I tested if standard DS and OMS-DS cells were true OFF cells by examining their responses to flash stimuli. I used alternating flashes of half a second of 40% bright or dark contrast with $1.5\,\mathrm{s}$ periods of mean background illumination in between (Fig. 4.4a-b). I calculated an on-off index by subtracting the

responses to dark contrast from the responses to the bright contrast flashes and normalizing by the total spike count. A negative index signified an OFF preference while a positive index showed an ON preference. By this measure, standard DS and OMS-DS cells were clearly OFF-cells as most cells in the salamander retina (Fig. 4.4a). But responses to the bright contrast might also be suppressed at high light levels. Therefore, I tested the flash responses for several lower light levels, starting from the usual low photopic range and going down to the high mesopic range (Fig. 4.4b). Throughout light levels standard DS and OMS-DS cells only responded to the dark contrast but with slightly changing spike patterns.
The distributions of the DSI and OMSI were also stable across different light levels (Fig. 4.4c-d). This demonstrates that direction-selectivity and object-motion-sensitivity seem to be fairly robust properties of retinal ganglion cells in the salamander, not depending on ambient light levels.
Standard OMS cells were more diverse in their responses to contrast flashes (Fig. 4.4a). Although most of them were OFF cells, the distribution of the on-off index indicated that they also comprised ON and ON-OFF types. Whether these ON and ON-OFF types were subtypes of the standard OMS cells or whether they were non-OMS cells which were erroneously classified as standard OMS cells by their high OMS index, still needs to be illuminated but will not be objective of this work. In the following, I will focus on the properties of standard DS and OMS-DS cells and will provide evidence that standard DS and OMS-DS cells could be different cell types.

4.3 Different systems of preferred directions

Standard DS and OMS-DS cells, both responded selectively to certain angles of drifting motion but differed remarkably in other properties, as their responses to global jittering motion and their receptive field sizes. Hence, they might encode the motion direction of different features within a visual scene as background motion or moving objects, respectively. This might also be reflected in the arrangement of their preferred directions.
The preferred directions of standard DS and OMS-DS cells were not evenly distributed but formed discrete clusters (Fig. 4.5a). For standard DS cells, I found three subtypes with distinctive preferred directions (Fig. 4.5a, upper). The preferred directions of different subtypes were separated by $120°$, as indicated by the distribution of the angular differences between pairs of standard DS cells (Fig. 4.5b, upper). I also analyzed the distribution of the absolute preferred directions in relation to the eye's position in the head by keeping track of the orientation of

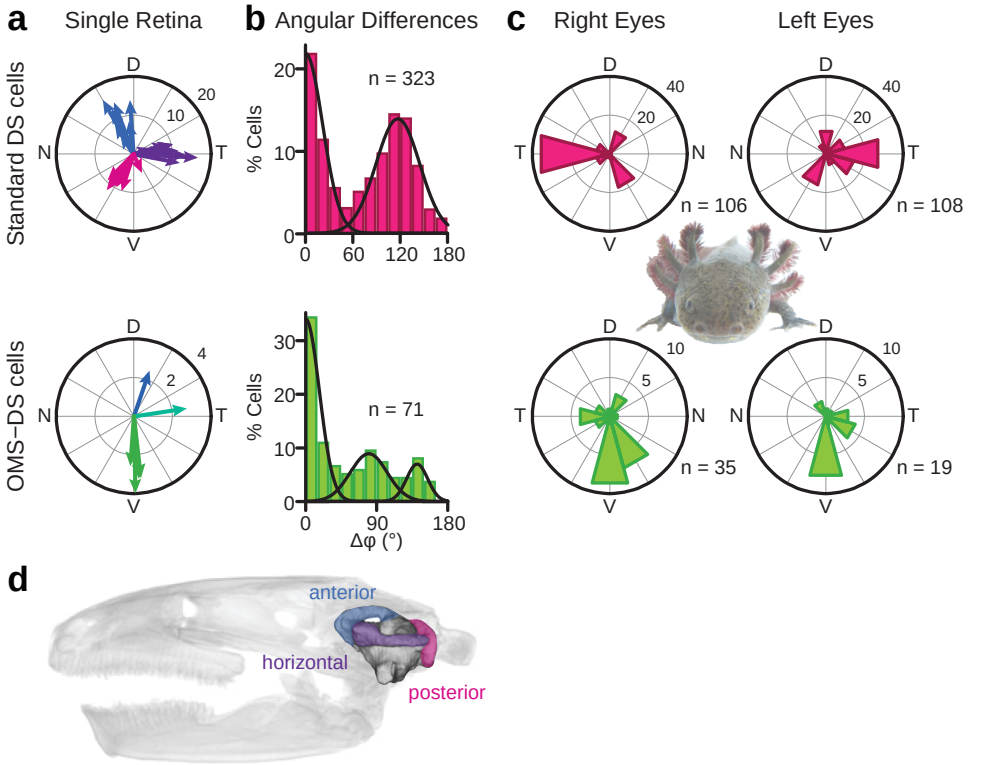

Figure 4.5 Standard DS and OMS-DS cells show different systems of preferred directions. **a** Preferred directions of standard DS (upper) and OMS-DS cells (lower) of a left eye retina. Different colors signify different subgroups. Dorsal (D), temporal (T), ventral (V) and nasal direction (N) correspond to the projection onto the retina. **b** Histograms of angular differences ($\Delta\phi = |\phi_1 - \phi_2|$) between pairs of standard DS (upper) and OMS-DS cells (lower) from same experiments. Gaussian-mixture models are fitted to the mirrored distributions and peak at 0° and 120° and at 0°, 90° and 145° for standard DS and OMS-DS cells, respectively. Data from 24 retinas with a total of 323 standard DS and 71 OMS-DS cells. **c** Polar distributions of preferred directions from aligned retinas of 6 right and 5 left eyes. Standard DS cells (upper) show three subtypes with temporal, nasal-dorsal and nasal-ventral preferred direction. The temporal direction is most frequent. OMS-DS cells (lower) show at least two preferred directions, ventral and temporal, separated by 90°. Most recorded OMS-DS cells preferred ventral direction. **d** Lateral view of otic endocast of the left inner ear of *Ambystoma mexicanum* from Maddin and Sherratt (2014), anterior (blue), horizontal (violet) and posterior (magenta) canals highlighted.

the retina during preparation (see Sect. 3.1.2). The distribution of the preferred directions from the properly aligned retinas showed that standard DS cells preferred motion into the temporal, nasal-dorsal or nasal-ventral direction with a bias for cells encoding the temporal direction (Fig. 4.5c, upper). Note that motion into the dorsal, ventral, temporal and nasal direction on the retina correspond to downward, upward, anterior and posterior motion, respectively, of an object in front of the eye. The observed preferred directions of standard DS cells co-align with the three semi-circular canals of the vestibular system (Fig. 4.5d) which is well-developed in most amphibians (Maddin and Sherratt, 2014).
OMS-DS cells clustered into at least three subtypes (Fig. 4.5a, lower). In distinction from standard DS cells, the preferred directions of OMS-DS cells were separated by 90° and were aligned with the cardinal body axes (Fig. 4.5b-c, lower). These directions correspond to the horizontal and vertical rotation axes, controlled by the four extraocular recti eye muscles (Hilton, 1956). Many recorded OMS-DS cells had a preference for the ventral direction and only some were found with directional preferences for motion into the temporal or dorsal direction. The lack of OMS-DS cells which preferred motion into the nasal direction might be caused by the generally low number of OMS-DS cells in my recordings.
However, standard DS and OMS-DS cells showed clear differences in their systems of preferred directions, indicating that they could be different cell types.

4.3.1 Receptive field tiling

The receptive fields of cells of the same cell type usually tile the visual field like a mosaic since the cells' dendritic arbors usually avoid each other (Masland, 2012a). For direction-selective cells in the mammalian retina, each directional subtype showed an independent tiling, leading to strong overlaps between cells of different preferred direction (Amthor and Oyster, 1995; Vaney et al., 2012).
In the salamander retina, the receptive fields of the entire standard DS and OMS-DS cell population were overlapping severely (Fig. 4.6a). Only when clustering the cells by object-motion-sensitivity and their preferred directions, one could observe that each subtype was reasonably tiling the recording area (Fig. 4.6b). For most subtypes, the number of recorded cells was not sufficient to observe a complete tiling but the clustering resolved crucial receptive field overlaps between cells of different subtypes (see color-coding in Fig. 4.6a). The population of standard DS cells with preference for motion into the temporal direction seemed to be especially complete.

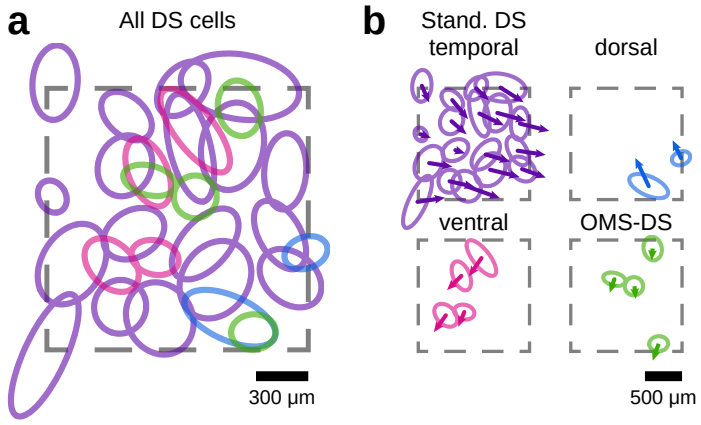

Figure 4.6 **Receptive fields of DS subtypes tile the retina.** **a** Receptive fields of DS cells from a left eye retina clustered by preferred direction and object-motion-sensitivity. Arrows indicate the preferred direction of each cell. Gray dashed lines mark the borders of the MEA. Standard DS cells are clustered by their preferred direction: temporal (violet), dorsal (blue), ventral (magenta). OMS-DS cells (green) show only one preferred direction here. Within clusters are only minor overlaps. **b** Receptive fields of all DS cells (see colors above). Note the strong overlaps between receptive fields of different colors.

4.4 Looking behind the scenes

What is the underlying retinal circuitry leading to direction-selectivity and object-motion-sensitivity in the salamander retina? And how could a retinal ganglion cell be direction-selective and object-motion-sensitive at the same time? In mammals, the direction-selectivity of ON and ON-OFF DS cells is mediated by direct gabaergic inhibition from so-called starburst amacrine cells (Euler et al., 2002; Yonehara et al., 2013). For object-motion-sensitivity, glycinergic inhibitory input from wide-field amacrine cells has been proposed to mediate the object-motion-sensitvity of OMS cells in the tiger salamander (ÖLveczky et al., 2003; Baccus et al., 2008) (Sect. 2.1). Here, I investigated if similar inhibitory mechanisms might be present in the axolotl retina.

I blocked specific inhibitory pathways by applying bath solutions with different GABA and glycine receptor antagonists and compared the responses of the cells to drifting gratings and patches of jittering gratings with the responses of the control experiments (before applying the antagonists) (Sect. 3.1.3).

A $20\,\mu\mathrm{M}$ strychnine solution aimed at blocking glycine receptors. In the salamander retina, the neurotransmitter glycine is usually released from wide-field amacrine cells (Yang et al., 1991). When observing the responses of a standard DS cell to drifting gratings (Fig. 4.7a), the application of strychnine had no effect on the direction-selectivity of the cell. Only the overall firing rates were lower. On

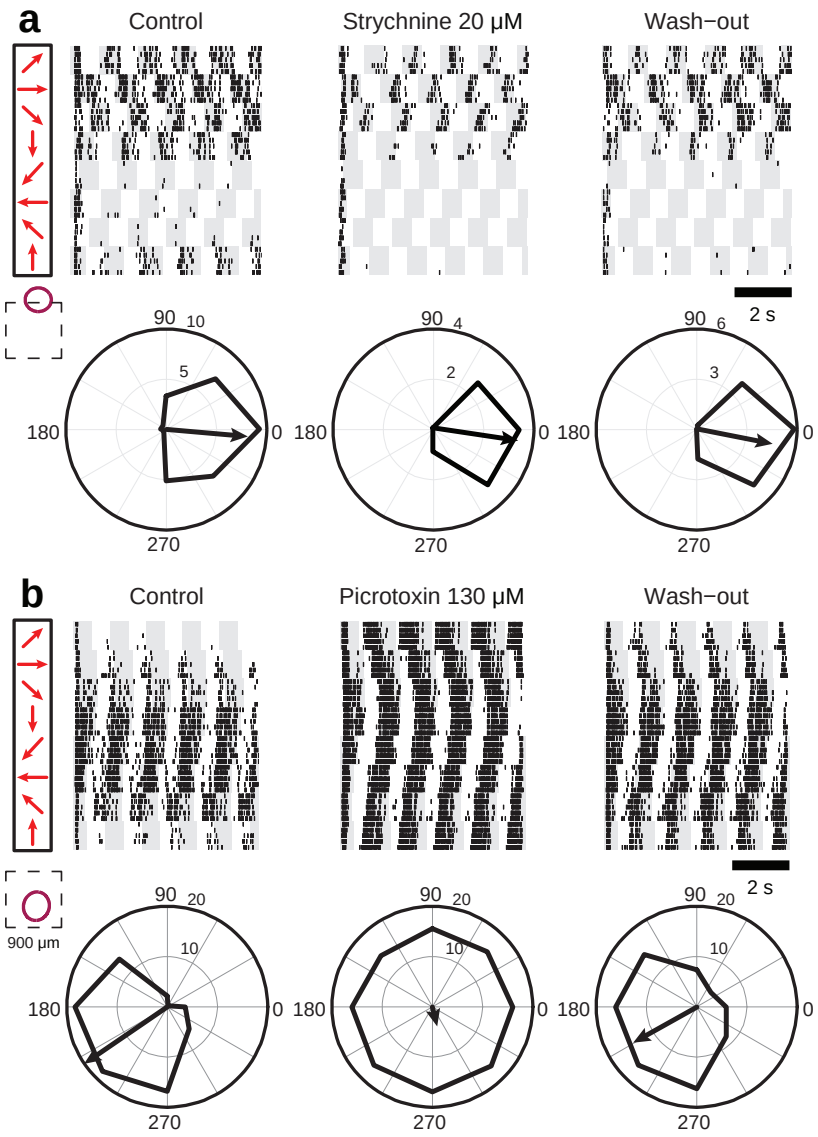

Figure 4.7 GABAa/c antagonist picrotoxin suppressed direction-selectivity of DS cells while glycine antagonist strychnine did not. a-b Responses of two standard DS cells from different experiments to drifting gratings before (left), during (middle) and after (right) application of a $20\,\mu\mathrm{M}$ strychnine (a) and a $130\,\mu\mathrm{M}$ picrotoxin bath (b), respectively. Red arrows indicate the eight directions of the drifting gratings. Corresponding polar plots of the mean firing rates are shown below each raster plot. Insets show receptive fields of the standard DS cells (red ellipses) in relation to the multielectrode array (dashed lines). **a** Strychnine did not affect directional tuning of a standard DS cell, only the overall firing rate was reduced (central polar plot). **b** Directional tuning of a standard DS cell (left) was lost during application of picrotoxin (middle). After wash-out (right), directional tuning slightly recovered (polar plot).

the other hand, the application of a solution with $130\,\mu\mathrm{M}$ picrotoxin, a GABAa/c receptor antagonist, led to a high response rate to all the directions of the drifting gratings, corresponding to a loss of the cell's direction-selectivity (Fig. 4.7b).
To study the inhibitory mechanisms involved in the computation of object-motion-sensitivity, I first reproduced the paradigm of a former pharmacological study in tiger salamander (ÖLveczky et al., 2003) to test if my stimulus with patches of jittering gratings would allow the same conclusions. I used a single patch with a jittering grating on a jittering background grating (inset Fig. 4.8a). The trajectories of patch and background were independent of each other and the radius of the patch was altered. For a standard OMS cell with receptive field located in the patch center, the firing rate in the control experiment drastically decreased with increasing patch radius (Fig. 4.8a). When applying the strychnine solution, the firing rate decreased less strongly and saturated at half of the maximum firing rate. This is equivalent to what has been observed in the previous study (ÖLveczky et al., 2003).
When now observing the responses of the same standard OMS cell to the patches of differentially or coherently jittering gratings which I normally use for classifying the retinal ganglion cells, the effect of strychnine was more apparent (Fig. 4.8b). Here, the strong response to the coherently jittering gratings when strychnine was applied, can be observed easily. The response rates of the differential and coherent motion regimes resembled the peak and minimum firing rates in response to the single patch of increasing size, respectively. Using several patches with jittering gratings had the advantage that the whole population of recorded cells could be taken into account and not only the cells in the center of the single patch. Therefore, I proceeded with the patches of differentially or coherently jittering gratings to study the effects of GABAa and GABAa/c receptor blockers, gabazine and picrotoxin, respectively.
The contribution of GABA-mediated inhibition to the computation of object-motion-sensitivity has not been studied before. Here, I found that both GABA antagonists had a strong effect on the object-motion-sensitivity of the standard OMS cells (Fig. 4.8c-d). It should be mentioned that for either of the three antagonists not only the responses to coherent motion increased but also the responses to differential motion were stronger during drug application.
The effect of glycine and GABA antagonists on the direction-selectivity and object-motion-sensitivity of the whole population can be best observed by comparing the cells' DS and OMS index, respectively, before and during drug application (Fig. 4.9). The direction-selectivity of both, standard DS and OMS-DS cells, was not affected by strychnine, as their DS indexes did not decrease (Fig. 4.9a,

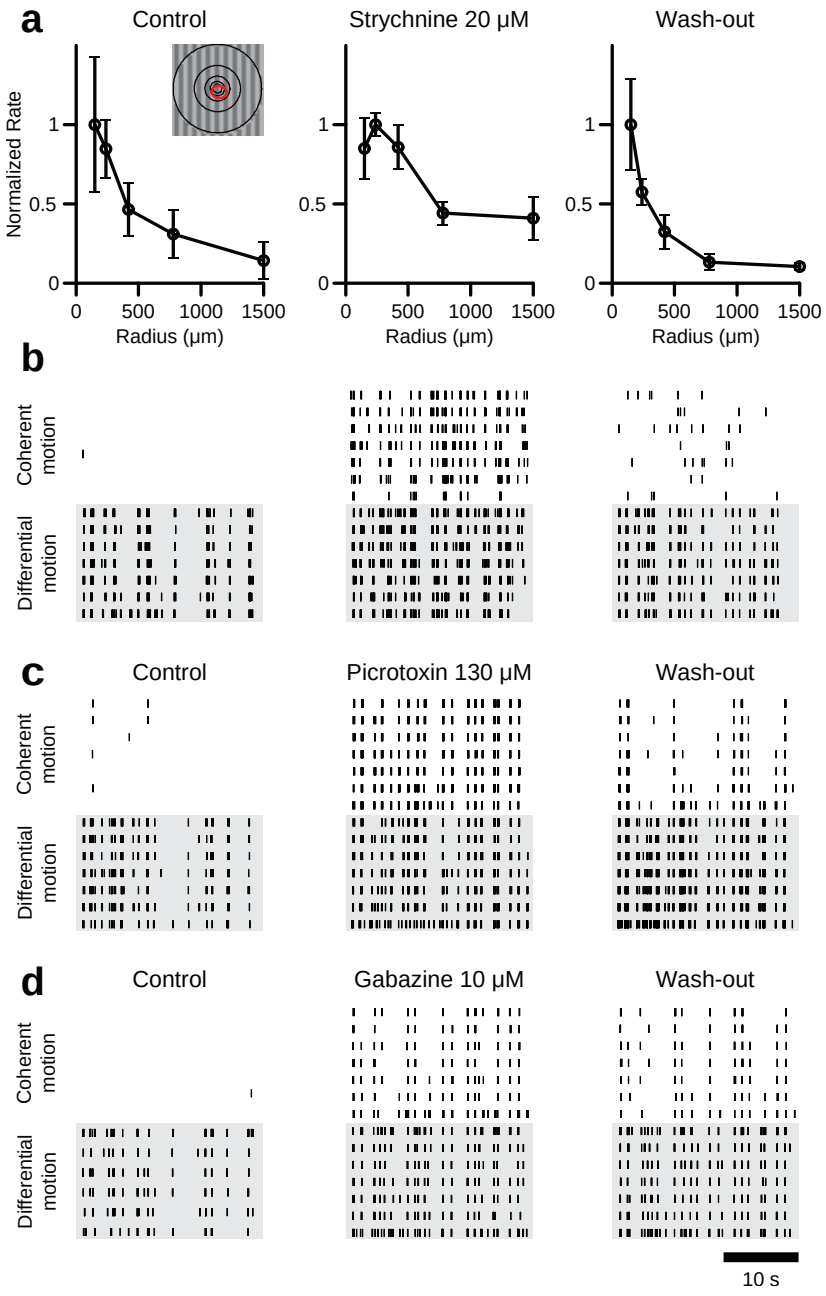

Figure 4.8 **Glycine and GABAa/c antagonists reduced object-motion-sensitivity of standard OMS cells. a** Normalized firing rates of an OMS cell in response to a circular patch of varying size with jittering gratings (inset) before (left), during (middle) and after application of a $20\,\mu\mathrm{M}$ strychnine bath solution (right). A background grating jittered with a different trajectory, similar to Ölveczky et al. The red circle marks the cell's position. Mean firing rates from three identical trials were normalized by the maximum firing rate and plotted against the patch radius, error bars show the standard deviation. Control shows rapidly decreasing firing rates with increasing size of the patch. During strychnine application, the firing rate saturated at half of the maximum firing rate. After wash-out, the firing rate decreased fast again. **b-d** Responses of three OMS cells to patches of jittering gratings before (left), during (middle) and after (right) application of a $20\,\mu\mathrm{M}$ strychnine (b), $130\,\mu\mathrm{M}$ picrotoxin (c) and a $10\,\mu\mathrm{M}$ gabazine bath solution (d), respectively. In the control, the cells barely responded to the coherent motion but during drug application they responded equally well to coherent and differential motion for either drug. After wash-out, the object-motion-sensitivity recovered. Cell in (b) was the same as in (a).

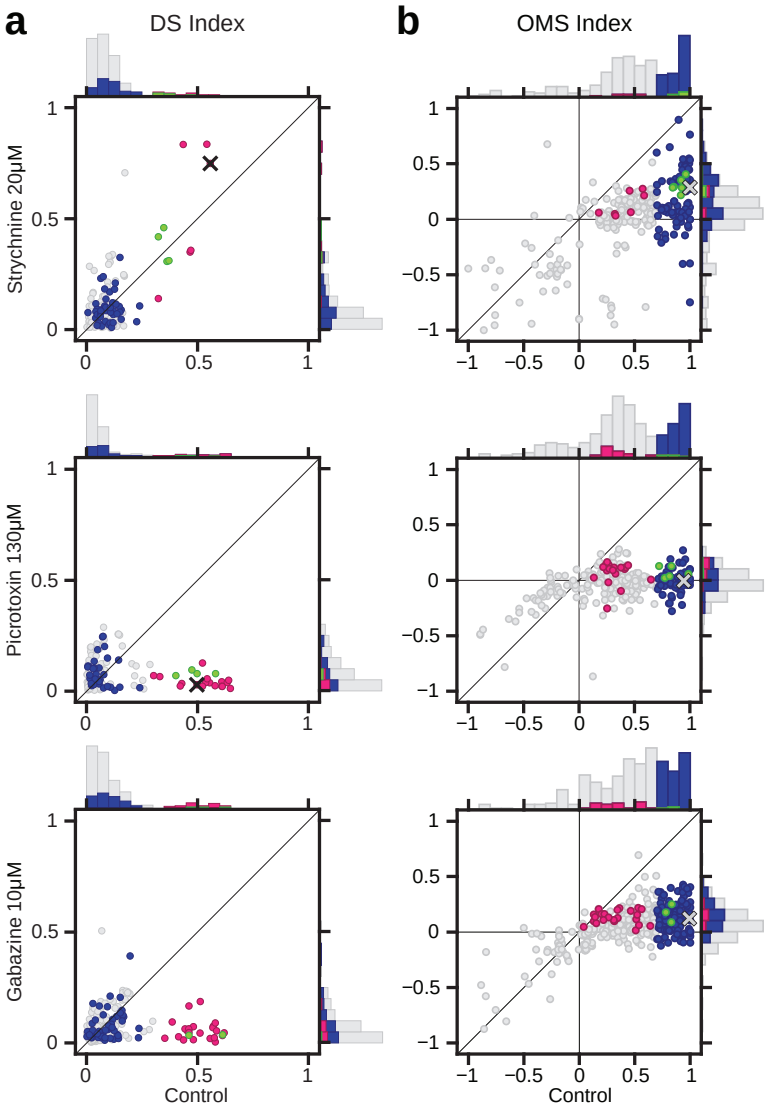

Figure 4.9 **Drug-induced changes of the DS and OMS index. a** Scatter plots and histograms of the DS index of standard DS (magenta), OMS (blue), OMS-DS (green) and unspecified cells (gray). DS indices during drug application were plotted against the control. Strychnine (upper) did not affect direction-selectivity. Picrotoxin (middle) and gabazine (lower) diminished direction-selectivity of standard DS and OMS-DS cells significantly. Black crosses in top and middle panel mark the standard DS cells in figure 4.7. **b** Scatter plots and histograms of the OMS index. OMS indices during drug application were plotted against the control. For strychnine, picrotoxin and gabazine, the object-motion-sensitivity decreased significantly during drug application (Wilcoxon signed-rank: $p < 0.001$, Kolmogorov-Smirnov: $p < 0.001$). Gray crosses mark the OMS cells from figure 4.8. Data from three retinas per drug.

top). On the other hand, the application of either GABA antagonist reduced the DS index of standard DS and OMS-DS cells significantly (Fig. 4.9a, middle and bottom). The reduction of direction-selectivity by GABA antagonists has also been observed in the mammalian retina (Wyatt and Daw, 1976; Caldwell et al., 1978). There, the cholinergic starburst amacrine cells mediate direction-selectivity via gabaergic inhibition (Briggman et al., 2011; Vaney et al., 2012). Cholinergic amacrine cells were also found in the salamander retina (Zhang and Wu, 2001; Cimini et al., 2008) and might therefore be part of the mechanisms leading to direction-selectivity in the salamander retina.
From the effect of glycine and GABA antagonists on the OMS index of the whole population one can observe that all applied antagonists significantly diminished the object-motion-sensitivity of standard OMS and OMS-DS cells (Fig. 4.9b). But also cells with weak preference for object motion got reduced in their object-motion-sensitivity. The effect of GABA antagonists was even more pronounced than of the glycine antagonist. This observation raises the question how gabaergic inhibition could be involved into the computation of object-motion-sensitivity. Hitherto, only glycinergic wide-field amacrine cells have been considered to contribute to the underlying circuitry (ÖLveczky et al., 2003; Baccus et al., 2008). Here, I have shown that OMS cells might also receive direct or indirect inhibition from gabaergic amacrine cells. An asymmetric gabaergic input could thereby result in the observed direction-selectivity of OMS-DS cells.

4.5 Responses to more complex motion stimuli

The previous observations suggest that standard DS and OMS-DS cells might be different cell types. They showed distinct responses to coherent global motion, significantly different receptive field sizes and systems of preferred directions. The receptive fields of standard DS cells showed strong overlaps with the receptive fields of OMS-DS cells while within clusters of similar preferred directions, the receptive fields of standard DS and OMS-DS cells showed independent tilings of the visual field.
Standard DS cells might be important for encoding the direction of global background motion, since they responded well to coherent global motion and had large receptive fields. On the other hand, OMS-DS cells preferentially responded to differential motion but not to coherent global motion and had small receptive fields. They might play a role in encoding the direction of small moving objects.
I tested this hypothesis by using more complex motion scenarios with stimuli featuring either small moving objects or local and global motion components. Drifting

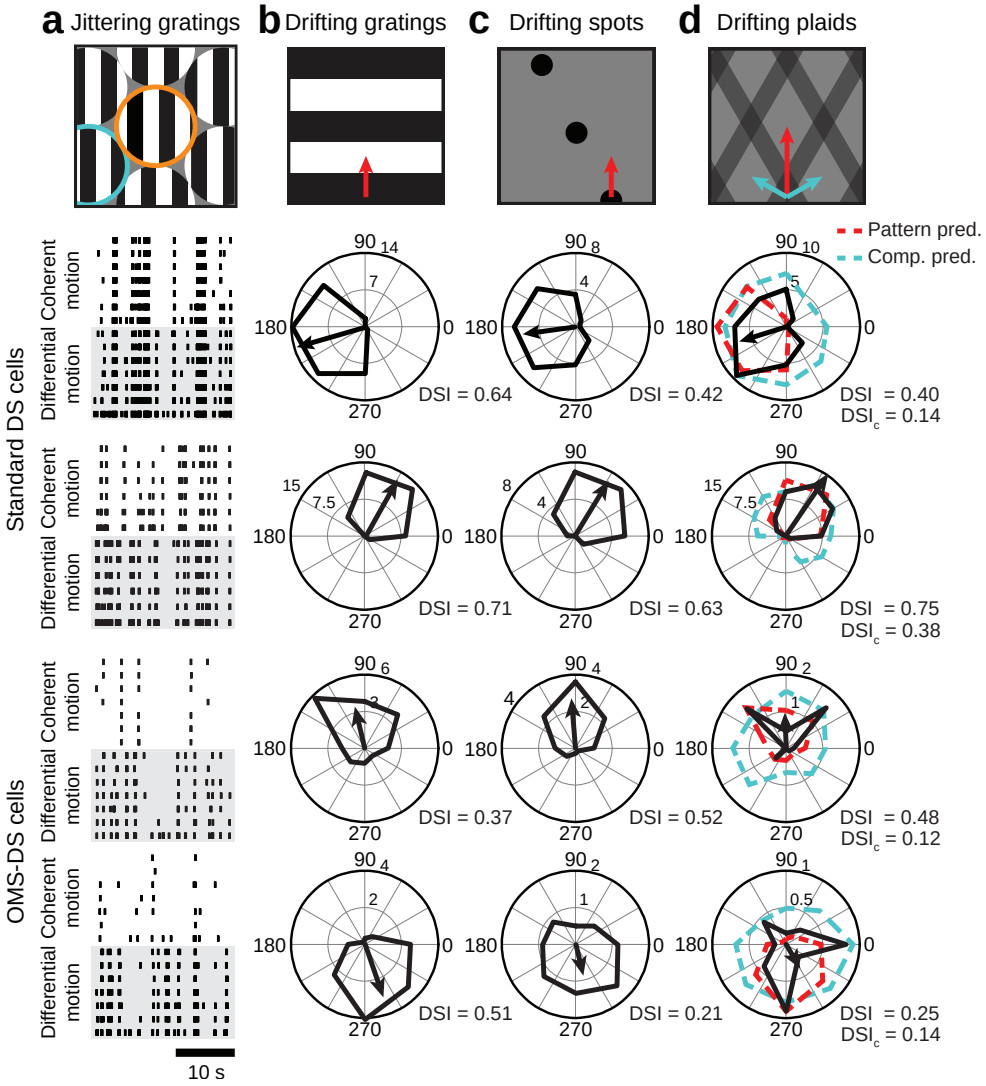

Figure 4.10 Standard DS and OMS-DS cells respond differently to stimuli with global and local motion features. a Responses of two standard DS cells (middle) and two OMS-DS cells (bottom) to patches of differentially and coherently jittering gratings to show degree of object-motion-sensitivity. **b-d** Polar plots of mean firing rates of same cells in response to drifting gratings (b), drifting spots (c) and drifting plaids (d) in eight directions. Arrows point into the respective preferred directions. DSI values indicate the degree of direction-selectivity for each stimulus. **b** In response to drifting spots, standard DS and OMS-DS cells kept their preferred directions compared to drifting gratings. **d top** Drifting plaids with individual bars moving in a $\pm 60°$ angle of the pattern direction. Cyan arrows indicate direction and velocity of the bars, red arrow of the pattern. **below** Mean firing rates in response to drifting plaids were plotted against motion direction of the pattern. Cyan and red dashed lines indicate tuning predictions for a cell with a drifting gratings tuning as in (b) that would exclusively respond to either the component or pattern motion direction, respectively. $\mathrm{DSI_c}$ is the DSI of the component prediction. DSI of pattern prediction corresponds to DSI in (b).

spots (Fig. 4.10c, top) aimed at testing the direction-selectivity of standard DS and OMS-DS cells for small moving objects. Especially OMS-DS cells should be well directionally tuned to the drifting spots if they are important for encoding of the direction of small moving objects. In figure 4.10c, one can observe that standard DS and OMS-DS cells were both well directionally tuned for the drifting spots. Both kept their preferred directions and tuning strengths compared to the drifting gratings (Fig. 4.10b). Only the overall firing rates were reduced due to the lower density of dark regions in the drifting spots stimulus compared to the drifting gratings. Since standard DS and OMS-DS cells are both OFF-type cells, their responses are triggered by regions of dark contrast.

Drifting plaids, known from psychophysics experiments and physiology in the visual cortex (Movshon et al., 1985; Stoner and Albright, 1993; Castelo-Branco et al., 2002), feature local differential motion of the individual components and global motion of the plaid pattern, resulting from the overlaid components (Fig. 4.10d, top). The components were dark bars drifting into two different directions, separated by 120° (cyan arrows). The motion directions of the individual components were then chosen in a way that the motion direction of the overlaid pattern would be aligned with the motion directions of the drifting gratings stimulus (Fig. 4.10b, d, red arrows).

For this stimulus, most standard DS cells showed a directional tuning which was similar to their drifting gratings tunings (Fig. 4.10b). Two example cells are shown in figure 4.10, middle. There, the tuning shapes were only slightly affected by the motion of the individual components.

On the contrary, I found several OMS-DS cells which showed a directional tuning with two peaks in response to the drifting plaids (Fig. 4.10d, bottom). Those OMS-DS cells responded better to plaid motion into directions that were $\pm 45^\circ$ shifted from their preferred directions. For plaid motion into these directions, one of the components would approximately move into the preferred direction of the cell. This probably indicates that the cells were stronger driven by the local motion of the bar sections.

In order to estimate, whether standard DS and OMS-DS cells were stronger driven by the motion direction of the global pattern or the local bar sections, I calculated tuning predictions from the assumption that cells would exclusively respond to either the pattern motion direction (*pattern prediction*) or the motion direction of the bars (*component prediction*) (Movshon et al., 1985). The pattern prediction was equal to the tuning obtained from the drifting gratings (Fig. 4.10d, red dashed lines). The component prediction was the sum of the $\pm 60^\circ$ shifted drifting gratings tunings, with the baseline firing rate subtracted (Fig. 4.10d, cyan dashed

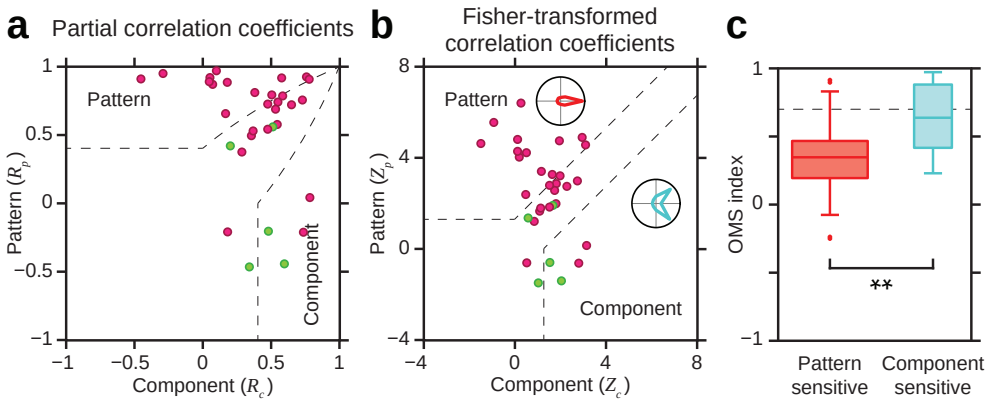

Figure 4.11 Component-sensitive cells were significantly more object-motion-sensitive than pattern-sensitive cells. **a-b** Scatter plots of partial correlation coefficients (a), R_p and R_c, of standard DS (magenta) and OMS-DS cells (green) and their Fisher-transformations (b), Z_p and Z_c, respectively. Dashed lines mark the 95% confidence intervals of the Fisher-transformed correlation coefficients which defined significantly component- and significantly pattern-sensitive cells. **c** Box plots of the OMS index of 15 significantly component- and 30 significantly pattern-sensitive DS cells. Data from 6 retinas with 115 DS cells. Dashed line marks the threshold above which cells were considered OMS.

lines).

Then, I determined whether the plaid tunings were closer to the pattern or component predictions by calculating the *partial correlation coefficients* between plaid tuning and pattern prediction R_p, and plaid tuning and component prediction R_c (Movshon et al., 1985). The partial correlation coefficients, R_p and R_c, were independent of each other by removing the correlations between pattern and component prediction. The Fisher transformation of the correlation coefficients provided a normal-like distribution of the data points (see Sect. 3.4 for details). This allowed to determine confidence intervals above which cells were considered significantly pattern- or component-sensitive (dashed lines in Fig. 4.11a-b).

In a typical data set, the partial correlation coefficients of standard DS and OMS-DS cells were widely scattered (Fig. 4.11a). There, standard DS cells did not clearly fall into one group of pattern- or component-sensitive cells. Instead, some of them were significantly pattern-sensitive while others were significantly component-sensitive. Also OMS-DS cells were not clearly object-motion-sensitive (Fig. 4.11a-b). Many standard DS and OMS-DS cells fell into the group of neither significantly pattern- nor component-sensitive cells. This might be caused by the broad directional tunings of standard DS and OMS-DS cells for the drifting gratings stimulus (Fig. 4.10b). It would lead to a diffuse component prediction where the two firing rate peaks that were observed in the tunings of OMS-DS

cells would become washed out (Fig. 4.10d, cyan dashed lines).
Therefore, I only took significantly pattern- and component-sensitive cells for population analysis and compared the distributions of their OMS indices (Fig. 4.11c). It turned out that the OMS indices of component-sensitive cells were significantly higher than the OMS indices of pattern-sensitive cells, though, the median OMS index of the component-sensitive cells was below the threshold above which cells were considered OMS. Nevertheless, object-motion-sensitivity and component-sensitivity seem to be positively correlated.

5 — Trajectory encoding by populations of direction-selective cells

Direction-selective ganglion cells are known to preferably respond to certain angles of drifting motion and to be suppressed for motion into the opposite direction. This response asymmetry to uniform motion has been extensively studied with drifting gratings stimuli during the past decades (Lettvin et al., 1959; Barlow and Hill, 1963; Vaney et al., 2001; Fiscella et al., 2015; Franke et al., 2016). But motion is seldom uniform under natural viewing conditions. Head and eye movements cause irregular shifts of the image that is projected onto our retinas. This apparent motion of the image on our retinas is known as retinal slip. In mammals, it is widely suspected that direction-selective ganglion cells with large receptive fields, namely the ON DS cells, contribute information about the retinal slip to downstream brain areas (Vaney et al., 2001; Engbert and Mergenthaler, 2006; Martinez-Conde and Macknik, 2008; Dhande et al., 2013). Here, I investigated how direction-selective ganglion cells in the salamander encoded motion direction in a spatio-temporally rich stimulus with highly irregular motion trajectories. Thereby, I focused on the linear readout of single DS cell responses and population responses of different subpopulations of DS cells and how well a random motion trajectory could be reconstructed from this readout.

5.1 Direction-selective responses to random motion

I used a correlated noise texture following a 2-dimensional random walk (Fig. 5.1a, inset, for details see Sect. 3.5) to stimulate the retinal ganglion cells. The texture was shifted with a frequency of $30\,\mathrm{Hz}$ with independently Gaussian-distributed motion steps. This allowed to calculate a spike-triggered average (STA) from a cell's response to the motion steps (Chichilnisky, 2001). Motion in x- and y-direction was independent of each other and STAs could be calculated independently for

either direction.

For the classified standard DS cells, the STAs of the motion in x- and y-direction showed pronounced peaks (Fig. 5.1b). For example, the standard DS cell in figure 5.1b showed a negative peak of the filter in x-direction. This represents an average stimulus motion to the left before the cell spiked. The positive peak of the filter in y-direction corresponds to an average upward motion right before spiking. Hence, the STA which was obtained from the random motion stimulus captured the directional preferences of the standard DS cell (Fig. 5.1b, inset). This means that standard DS cells responded in a direction-selective fashion to the random motion with similar directional preferences as for uniform image motion.

OMS-DS cells did not respond well to the global motion of the texture and had very noisy STAs with low peaks (data not shown).

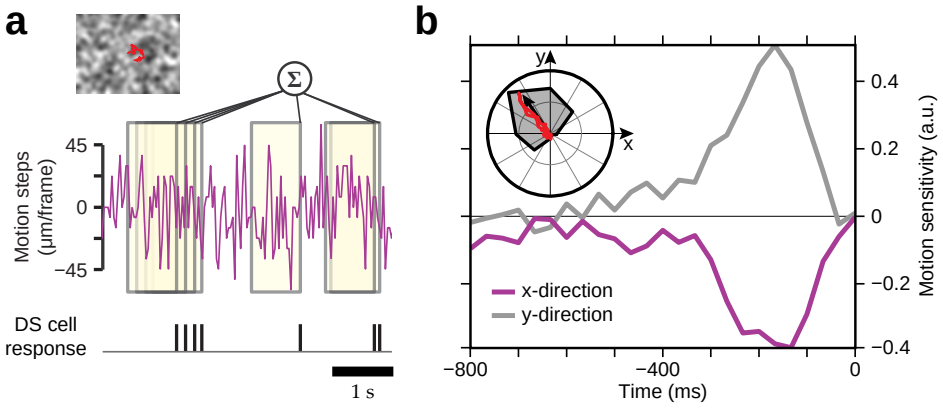

Figure 5.1 **Background trajectory encoding of a direction-selective cell.** **a** Schematics of the calculation of the spike-triggered average of motion into the x-direction. Motion steps into x- and y-direction are independent and Gaussian-distributed. **b** Spike-triggered averages of motion into the x- and y-direction of a standard DS cell. Inset: Directional tuning from drifting gratings, black arrow indicates preferred direction of the cell, red trace shows the filters of x- and y-direction in phase space.

5.2 Linear decoding of random motion trajectories

Individual standard DS cells responded in a direction-selective fashion to the random motion. But when trying to reconstruct the motion trajectory from the responses of the standard DS cell in figure 5.1b by using the linear motion filters (STAs), the performance was very poor (Fig. 5.2a). The linear readout of the cell responses could capture some low-frequency features of the random motion trajectory (compare solid red and black lines). Especially, upward motion was well captured in the reconstruction of the y-direction. This corresponds to the directional preference of the observed standard DS cell (cf. Fig 5.1b). The recon-

struction of the motion trajectory was flat when the cell did not respond to the stimulus for an extended time period.

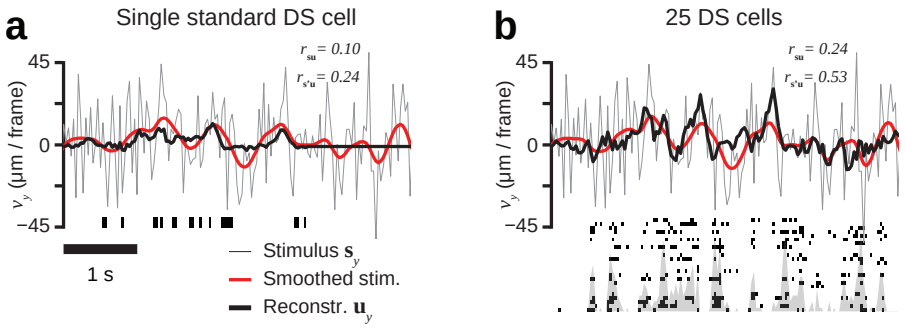

Figure 5.2 Comparison of random motion reconstructions from single cell and population responses. a-b Reconstruction of motion trajectory in y-direction from the responses of the standard DS cell in figure 5.1b (a) and the correlated responses of 25 standard DS cells (b). Stimulus is shown in time-bin discretized motion steps (gray thin line). Stimulus was smoothed with Gaussian kernel (red thick line) to optimize correlations between stimulus and reconstruction (black thick line). Correlation coefficients between stimulus and reconstruction, and smoothed stimulus and reconstruction are given by $r_{\mathbf{su}}$ and $r_{\mathbf{s'u}}$, respectively. Vertical bars indicate cell responses to the stimulation. Summed firing rates of the population in (b) are shown in gray.

To overcome the deficiencies of a single-cell's encoding, like poor encoding of the DS cell's null direction or extended periods where the cell did not respond, downstream neurons might pool from several direction-selective ganglion cells. The decoding of a random motion trajectory from the responses of a population of DS ganglion cells would provide a more accurate picture of the motion trajectory. I assumed the downstream neuron to be a simple linear decoder, integrating the multiple neural inputs in a linear fashion. Therefore, I used a linear multi-cell decoder as introduced by Warland et al. (1997) to calculate reconstructions of the motion trajectory from the population responses (Sect. 3.5.2).

In a first step, the reverse correlations of stimulus and population responses were calculated from the first $28\,\mathrm{min}$ of a $40\,\mathrm{min}$ stimulation, where pair response correlations within a time window of $800\,\mathrm{ms}$ were taken into account (Eq. 3.7). The obtained filters in the x- and y-direction were independent of each other. Then, a stimulus reconstruction was calculated from the population responses to the last $12\,\mathrm{min}$ of the stimulus by using the linear filters obtained from the first $28\,\mathrm{min}$ of the stimulus. This aimed at cross-validating the fidelity of the linear readout.

The reconstruction from the correlated responses of 25 DS cells using the linear multi-cell decoder, showed much higher correlations between stimulus and reconstruction than for a single standard DS cell (Fig. 5.2a-b). The DS cell population could encode several high- and low-frequency features of the trajectory which a

single cell could not. Furthermore, the population showed highly correlated responses to certain stimulus features which might lead to a better reconstruction of these stimulus segments with higher precision.

To estimate how much information the linear readout of the population responses provided about the motion trajectory of the stimulus, I calculated the mutual information between stimulus and reconstruction (see Sect. 3.5.3 for details). Then, I compared the obtained information estimate with the total information one would obtain by assuming all cells were independent motion encoders.

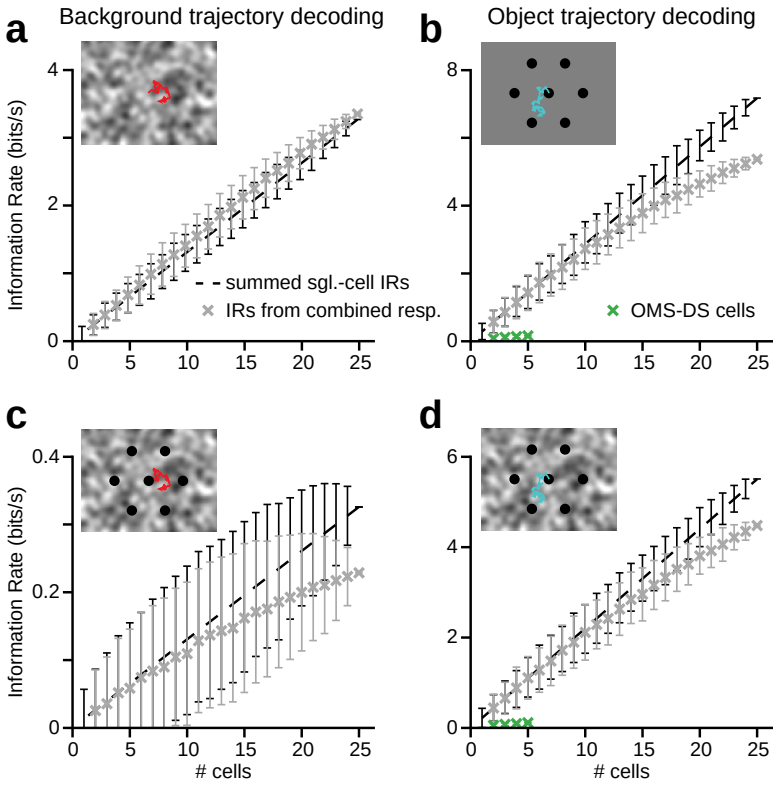

Figure 5.3 Background and object trajectory decoding of a population of direction-selective cells. Information rates of linear decoding from combined responses of n DS cells (gray crosses) compared to the summed information rates from individual cell responses (dashed lines). Error bars indicate standard deviation over all possible cell combinations. **a-b** Linear trajectory decoding of pure background motion (a) or pure object motion (b). Background trajectory decoding shows weak synergy while object trajectory decoding is redundant for larger numbers of cells, i.e., information rates from combined responses are higher or lower than summed single-cell information rates, respectively. **c-d** Linear decoding of background (c) and object motion trajectories (d) from the responses to the moving object superimposed on the moving background (inset). Both show redundancy for larger number of cells. Green crosses in (b) and (d) show information rates from OMS-DS cell populations.

For a population of 25 DS cells, I calculated the information rates for different

population sizes starting with subpopulations containing one cell, up to the full population of 25 DS cells. For each population size, I averaged over all possible subpopulations (Fig. 5.3a). Then, I compared the mutual information between stimulus and reconstruction from the correlated cell responses (gray crosses) with the summed information from the single-cell reconstructions (black dashed lines). The summed information from the single-cell reconstructions corresponds to the information that would be obtained from independent encoders.
For larger population sizes, the information rates were slightly higher when response correlations within the DS cell population were taken into account than if the cell responses were assumed independent of each other. This means that the response correlations within the DS cell population allowed a better reconstruction of the motion trajectory. The effect that the cooperative spiking of a population of neurons provided more information than the sum of information rates obtained from independently spiking neurons, is called synergy. Hence, response correlations seem to be important for the encoding of the motion trajectory.
OMS-DS cells did not contribute much to the population trajectory decoding of the jittering background motion since they did not respond well to the global stimulation. Therefore, I also applied local motion and differential motion stimuli. The local motion stimulus was used to investigate if DS cell populations, in particular OMS-DS cells, encoded jittering object motion. Another stimulus, featuring differential motion of object and background, was applied to observe if the trajectory of a moving object and the background could be independently extracted.

5.2.1 Object versus background motion decoding

Apart from the moving noise background (Fig. 5.3a, inset), I used an object composed of seven dark spots in an hexagonal arrangement moving on a mean luminance background (Fig. 5.3b, inset). This stimulus aimed at investigating the decoding of object motion trajectories from the responses of standard DS and OMS-DS cells. I also used a stimulus with the object moving on top of the moving background (Fig. 5.3c-d, inset) to investigate if background and object motion were encoded at the same time and if information about either motion trajectory could be extracted from the population code. The trajectories of object and background were independent of each other. They both followed a 2-dimensional random walk while for the object motion a small reset force was implemented in order to keep the object in the region of the recording area (see Eq. 3.5 in Sect. 3.5).
Figure 5.3b shows the average mutual information between the object motion

trajectory and its reconstruction from DS cell population responses (gray crosses) and the summed information rates of reconstructions from the single-cell responses (black dashed line). The information rates obtained from the decoding of independent DS cells were higher than the information rates obtained from the decoding of the correlated population responses. This means that the response correlations which were induced by the object motion led to redundancies in the linear decoding of the population code. Interestingly, the object trajectory could not be well reconstructed from OMS-DS cell responses (Fig. 5.3b and d, green crosses). The OMS-DS cells did in general not respond well to the random background or object motion.

Although the object motion decoding from the entire DS cell population responses showed redundancies, the linear reconstruction of the object motion trajectory was in general better than the reconstruction of the background motion trajectory (Fig. 5.3a-b). Especially, when object and background were presented at the same time, the motion trajectory of the object was much better decoded than the trajectory of the background, e.i., the mutual information between stimulus and reconstruction was higher for the object motion (Fig. 5.3c-d). The trajectory of the background motion could not be well reconstructed when the object was moving on top. Since firing rates in response to the jittering background were in general quite low, the high contrast of the dark spots compared to the background might cause the DS ganglion cells to respond better (with higher firing rates) to the object motion and reduce their responses to the background motion (maybe caused by adaptation). This would then allow a better reconstruction of the object's trajectory than of the background trajectory. Furthermore, the object's motion trajectory contained weak temporal correlations from the implemented reset force which might allow a better stimulus reconstruction.

Nevertheless, the reconstruction of the object motion trajectory was also affected by the background motion. Without background motion, the mutual information between object trajectory and its reconstruction was much higher than when object and background were both moving (cf. Fig. 5.3b and d). This means that the decoding of the object motion trajectory was more faithful when the background was static.

Synergy was only observed in the linear population decoding of the background motion trajectory when no object was present (Fig. 5.3a). But the effect was very weak and not significant when all DS cells were taken into account. The benefits of response correlations for the trajectory decoding might be washed out by averaging information rates from the whole DS cell population where cells which did not respond well to the stimulus, like OMS-DS cells, were also taken into account.

In the following, I will further examine the synergy in the decoding of background motion and focus on different subpopulations of standard DS and OMS-DS cells with either same or different preferred directions.

5.2.2 Background motion encoding of subpopulations with similar and different preferred directions

In the salamander retina, I found two types of direction-selective ganglion cells, standard DS and OMS-DS cells. Standard DS cells responded well to global coherent motion while OMS-DS cells did not. Therefore, I first separated the standard DS and OMS-DS cells into different subpopulations. Standard DS cells split up into three subtypes where each subtype had a different preferred direction. I further divided the standard DS cell subpopulation into three groups according to their directional preferences. Each of the four subpopulations showed an independent tiling of their receptive fields (Fig. 5.4c).
The OMS-DS cells provided very little information about the background motion trajectory (Fig. 5.4a, green circles) since they only responded weakly to the global motion stimulus. The subpopulations of standard DS cells with either temporal or nasal-dorsal preferred directions provided significantly more information about the background motion trajectory (Fig. 5.4a, purple and blue circles). But the summed information rates from the single-cell reconstructions (dashed lines) were much higher than the information rates from the population reconstructions (circles). This means that the background motion decoding from standard DS cells with the same preferred directions was highly redundant. This can also be well observed in figure 5.4b where I normalized the mutual information between stimulus and reconstruction from the population responses by the summed information rates from single-cell reconstructions, for every cell combination.
Since synergy could not be observed in the population decoding of OMS-DS cell responses or in subpopulations of standard DS cells with the same preferred direction, I investigated the trajectory decoding from standard DS cell subpopulations with mixed preferred directions.
For calculating the information averages for standard DS cells with mixed preferred directions (Fig. 5.4a, orange triangles), I only included cell combinations which had the least number of repeated preferred directions. For example, for stimulus reconstructions from four standard DS cells, the subpopulations contained three cells with different preferred directions plus one cell with a repeated preferred direction. This ensured a maximum mixture of preferred directions. For these cell combinations, the information rates from the correlated responses were significantly higher than the summed single-cell information rates, showing the synergy

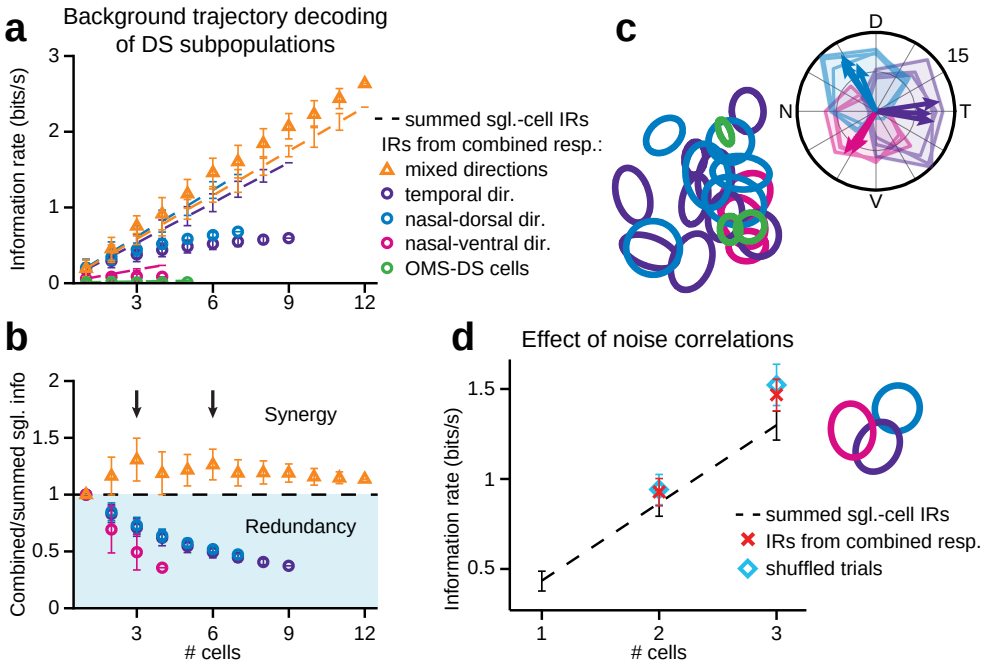

Figure 5.4 Background trajectory decoding of subpopulations of direction-selective cells. **a-b** Linear trajectory decoding of pure background motion by different subpopulations of DS cells. Standard DS cells were grouped by temporal (violet), nasal-dorsal (blue) and nasal-ventral (magenta) preferred direction. Group with mixed directions (orange triangles) included the four cells of each group with highest single-cell information rates. Information rates were only calculated for combinations with largest diversity of preferred directions. Group of OMS-DS cells does not contribute much information. Error bars indicate standard deviation over all possible cell combinations. **a** Total information rates (IRs) of combined responses (symbols) and summed single-cell IRs (dashed lines). Only for mixed directions, **b** Ratios between IRs from combined responses and summed single-cell IRs. Arrows point to combinations with highest diversity of preferred directions. **c** Receptive fields of the observed DS cell population and directional tunings of cells with best trajectory decoding. **d** Linear decoding of three cells with mixed preferred directions and proximal receptive fields (inset). Experiment with 10 repeated trials of 15 min. Summed single-cell information rates (dashed line) are compared with information rates from combined responses (crosses) and information rates from combined responses where the response of each cell was from a different trial (diamonds). Error bars indicate standard deviation over all trial combinations.

of the response correlations for the linear trajectory decoding. Especially, the normalized information rates in figure 5.4b show pronounced peaks for combinations of three and six standard DS cells with mixed preferred directions, indicating that synergy was highest when all three directions were equally represented.
But where does the synergy in the pairwise response correlations of standard DS cells with mixed preferred directions come from? Often, response correlations in the form of synchronized activity between cells are considered to provide additional information about a spatio-temporally shifting stimulus (Greschner et al., 2002). For instance, highly synchronized activity of retinal ganglion cells in response to a drifting object is thought to signal a motion reversal of the object (Schwartz et al., 2007; Chen et al., 2013). Synchrony within a short time window usually arises from shared input noise from upstream neurons, called noise correlations.
To investigate whether the synergy observed in the motion decoding from cells with mixed preferred directions was actually caused by noise correlations, I recorded the cell responses to 10 repeated trials of $15\,\mathrm{min}$ of jittering background motion. Then, I calculated the information rates from the combined and independent responses of three closely located standard DS cells preferring different motion directions and took the average over the 10 trials (Fig. 5.4d). To estimate the effect of noise correlations, I calculated the information rates from the combined responses where the responses of each cell were taken from a different trial. This shuffling would remove the correlations from a shared input noise (Averbeck et al., 2006). In this example, the decoding from the shuffled responses, i.e., without noise correlations, was slightly better than when the responses were taken from the same trials. Hence, response correlations due to shared input noise from upstream neurons seem not to be important for the observed synergy here. The crucial correlations are presumably stimulus driven.
In the following, I will outline possible reasons and coding mechanisms leading to the strong synergy I observed in the linear decoding of random background motion from the responses of standard DS cells with different preferred directions.

5.3 Role of motion encoding nonlinearities

To find out what could cause the synergy in the linear trajectory decoding of the population responses, I examined the nonlinearities within the motion encoding of individual standard DS cells. For a single DS cell, the convolution of the stimulus trajectory with the cell's motion STA (Fig. 5.5a) yields a linear estimate of the cell's expected firing rate in response to a given stimulus segment (see Sect. 3.5.1

for details). Those linear estimates correspond to a linear projection of the stimulus onto the STA vector. Hence, the linearly estimated firing rate is positive when the stimulus was similar to the STA and negative when the stimulus was highly dissimilar to the motion STA. The relation between linearly estimated firing rates and actually measured firing rates in response to the stimulus, is the motion encoding nonlinearity. Since a neuron can not have negative firing rates, these nonlinearity functions are usually rectifying, mapping negative linear firing rate estimates to positive values.

The nonlinearity functions were estimated by dividing the pairs of sorted linear estimates and measured firing rates into eight bins with the same amount of data points, starting at the lowest linear estimate. Then, the linear estimates and measured firing rates in each bin were averaged which yielded an estimate of the motion encoding nonlinearity function (similar to Fig. 5.5b). Although motion in x- and y-direction were independent of each other, responses to a certain motion trajectory in y-direction could affect the estimated mean firing rate for a certain motion trajectory in x-direction. To resolve these dependencies, I calculated the *conditional nonlinearities* for motion into x- and y-direction for pairs of linear estimate and observed firing rate when the stimulus projections into y- and x-direction, respectively, were small (≈ 0).

The obtained conditional nonlinearities were extremely *non-monotonic* (Fig. 5.5b). They showed that a standard DS cell responded strongly to motion trajectories which were similar to their motion STAs (filtered stimulus ~ 1). But they also strongly responded to motion which was highly dissimilar to the motion STAs (filtered stimulus ~ -1). This means that standard DS cells did not only strongly respond to motion into their preferred direction but also to motion into their null direction. Though, for motion into the null direction the response rates were slightly lower. This means that the motion trajectory encoding of individual standard DS cells is highly ambiguous. DS cell responses to the null direction will thereby lower the performance of the linear trajectory decoding.

The ambiguities in a DS cell's motion encoding may arise from the cell's responses to contrast changes. As shown previously, standard DS cells are OFF cells. Therefore, they might respond to image shifts which bring dark regions within the background pattern into the cell's receptive field. When the excitation by contrast changes is strong enough, the DS cell might even respond to motion into its null direction.

Here, the responses of a second DS cell with opposite preferred direction could help to correct for the responses of the first cell to motion into the non-preferred direction. Hence, the population responses of standard DS cells with different pre-

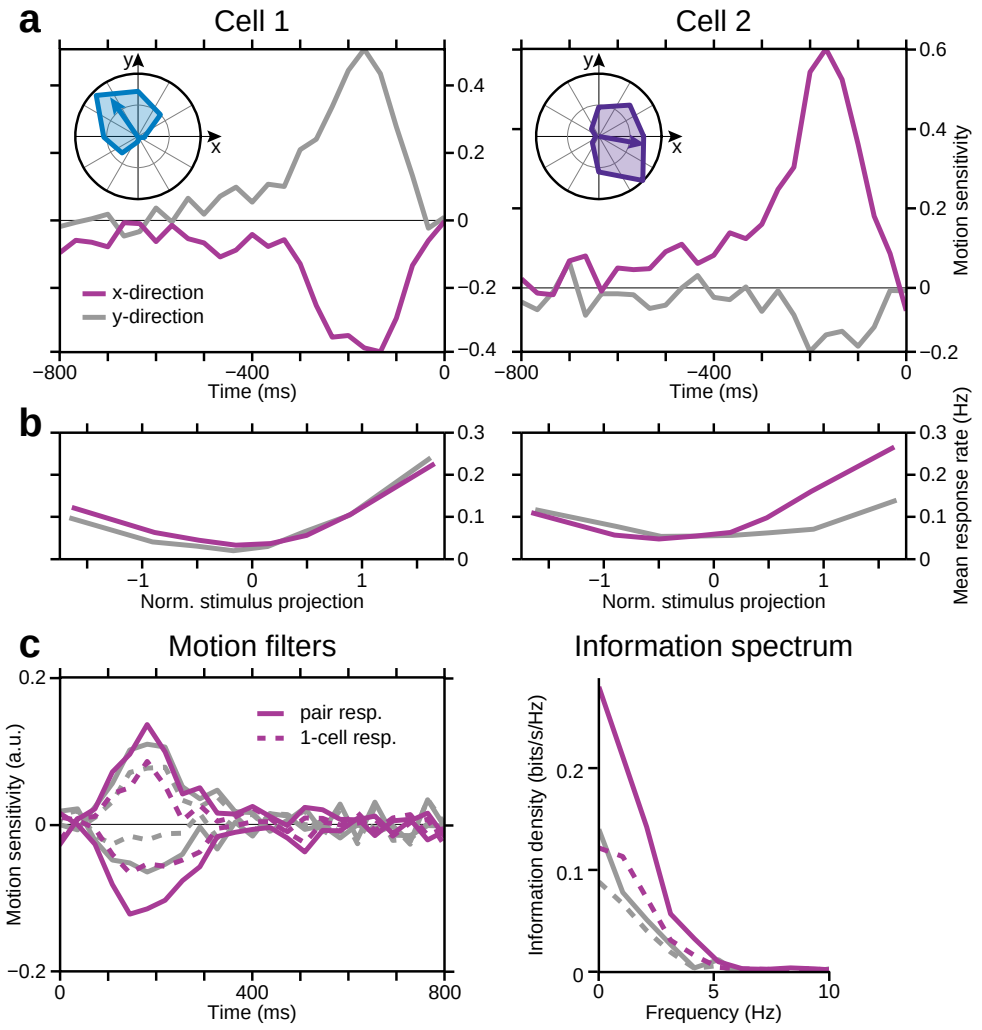

Figure 5.5 **DS cells show strongly non-monotonic nonlinearities in their motion trajectory encoding.** **a** STAs of x- and y-direction from the responses to the jittering background motion of two standard DS cells. Insets show the directional tunings of the cells from the responses to drifting gratings. **b** Non-monotonic conditional nonlinearities of x- and y-direction, obtained when the stimulus projections $f_{x/y}(s)$ in y- and x-direction, respectively, were close to zero ($|f(s)| < 0.1$). U-shapes indicate strong responses to preferred stimuli ($f(s) > 0$) as well as highly non-preferred stimuli ($f(s) < -1$). **c** Filters and information spectra obtained from the pair (solid line) and single-cell responses (dashed) of above cells from the linear multi-cell decoder. Linear decoding of pair response shows larger filter peaks than for single-cell responses, corresponding to a better directional encoding. Information spectra of the pair response show strong synergy.

ferred directions might rectify the non-monotonic nonlinearities of a single cell's motion encoding.
In figure 5.5c, the effects of the concerted firing of a DS cell pair with different preferred directions can be observed. The linear filters obtained from the pair responses have a higher amplitude than the filters obtained from the independently encoding cells. This means that the motion trajectory can be better decoded from the pair responses than from the single-cell responses. This is also reflected in the higher amplitudes of the information densities from the pair decoding (Fig. 5.5c, right, solid line).

5.3.1 Testing different nonlinearities

To observe if indeed the non-monotonic nonlinearities were the reason for the observed synergy in random motion decoding, I modeled pairs of independent DS cells using the LN-model (Sect. 3.5.1). The cells were modeled independently of each other since noise correlations were not found to contribute to the observed synergy (Fig. 5.4d). Cell responses were generated by using the experimentally obtained linear filters of standard DS cells and nonlinearities that were either fitted with an exponential or non-monotonic function (Fig. 5.6a). The stimulus was filtered and the nonlinearity functions applied to calculate the mean response rates (Fig. 5.6a). Spike rates were then generated by Poisson processes with means and standard deviations taken from the prior calculated mean response rates.
For modeled DS cell pairs with opposing preferred directions and exponential nonlinearities, the linear decoding of the pair responses did not show any synergy, i.e., the amplitudes of the linear filters and information densities from the pair responses were smaller than the amplitudes of the linear filters and summed information spectra from the single-cell responses (Fig. 5.6b).
In contrast, the decoding from cell pairs modeled with non-monotonic nonlinearities was highly synergistic for cells with opposing preferred directions (Fig. 5.6c). This is in accordance with what I observed in the experimental data (Fig. 5.5c). Furthermore, this indirectly shows that the non-monotonic nonlinearities could cause the synergy observed in the linear readouts of pair responses of standard DS cells with different preferred directions.
The decoding from cell pairs with same preferred directions was always redundant, though, the peak difference of the information spectra from pair and single-cell responses was less pronounced for DS cells modeled with exponential nonlinearities (Fig. 5.6d-e).

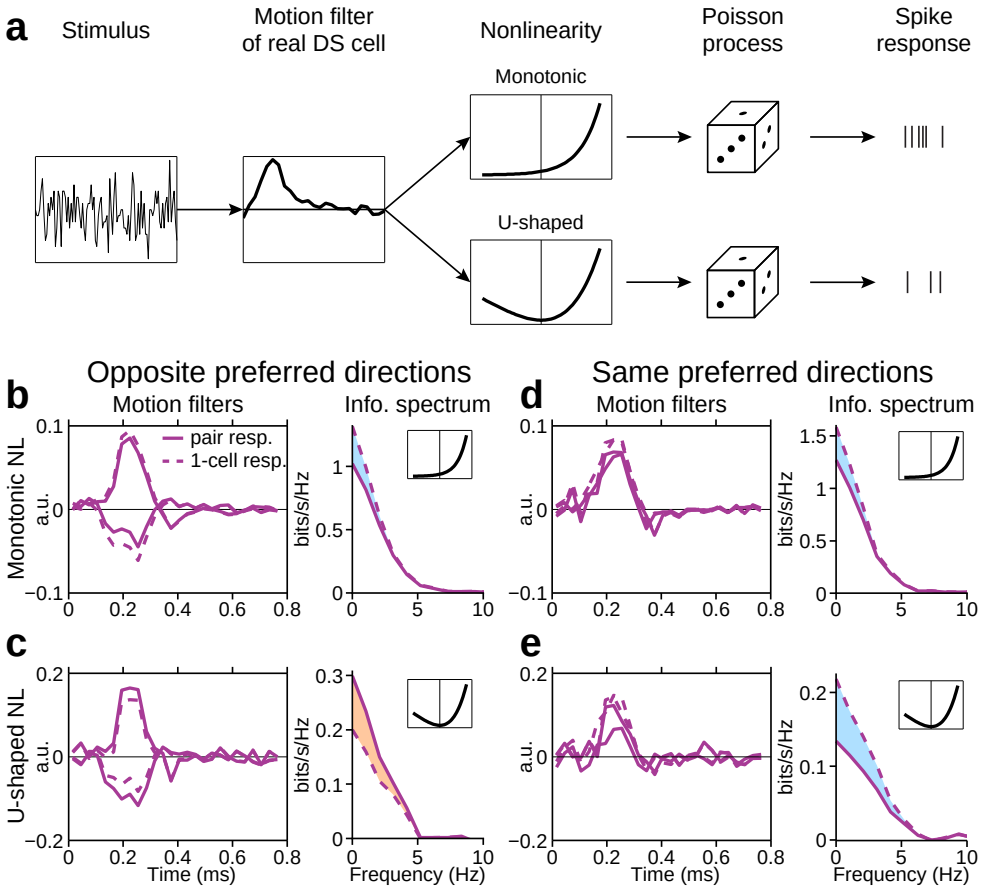

Figure 5.6 **Influence of monotonic and non-monotonic nonlinearities on linear motion decoding from DS cell pairs. a** Schematics of the two applied LN-models with different fits of the DS cell nonlinearities. **b-e** Linear filters and information densities from pairs of independently modeled DS cells with either monotonic (b, d) or u-shaped nonlinearities (c, e), $N_x^m = A \exp(Bx)$ and $N_x^u = A\, x^2 \exp(Bx)$, respectively. Solid lines correspond to linear filters and information densities from pair responses. Dashed lines correspond to linear filters and summed information spectra from single-cell responses. For simplicity, filters and information densities are only shown for motion in x-direction. Effect was compared for DS cells with opposite (b-c) and same preferred directions (d-e).

5.4 Structure of concerted activity of DS cell pairs

The non-monotonic nonlinearities of the individual DS cells had a strong influence on the synergy and redundancy observed in the linear motion decoding from DS cell pairs. One could ask, how the concerted firing of these cell pairs influences the linear readout. Or in other words, how does the spiking activity of one cell counteract the ambiguities in the motion encoding of the other cell? Here, I tried to get some insights by applying a more advanced reverse-correlation method, called canonical correlation analysis (Zeck et al., 2008; Hotelling, 1936), and a population vector-like approach (Georgopoulos et al., 1986) using relative spike codes.

5.4.1 Canonical correlation analysis

The *canonical correlation analysis* (CCA) is a reverse-correlation method which is used in neuroscience to find the modes of a given stimulus that are maximally correlated with the activity of a neural population (Zeck et al., 2008). Here, I investigated the activity patterns of DS cell pairs with similar and different preferred directions in response to the random motion trajectory. The study of these activity patterns might provide information about how synergy in the trajectory decoding could arise from the correlated pair responses.
In figure 5.7a, high- and low-frequency components from the CCA of a cell pair with different preferred directions are shown. The first components of the CCA have the highest correlations between stimulus and responses. Here, they captured the low frequencies of the stimulus and response. The frequency of the pair activity matched the frequency of the stimulus. Furthermore, the CCA components showed an anti-phasic activity of the two DS cells with different preferred directions, i.e., when one cell was active, the other was silent.
For cell pairs with similar preferred directions, the picture was slightly different (Fig. 5.7b). There, the frequencies of stimulus and neural activity also matched but the cells responded in-phase, although, small shifts can be observed. The observed stimulus components show that correlations between stimulus and response were strongest, when the stimulus was moving into the preferred or null direction of the two DS cells with the same preferred direction.

5.4.2 Additive and subtractive coding strategies

The in-phase and anti-phasic responses of DS cell pairs with similar and opposite preferred directions, respectively, promote the idea that the linear decoding simply

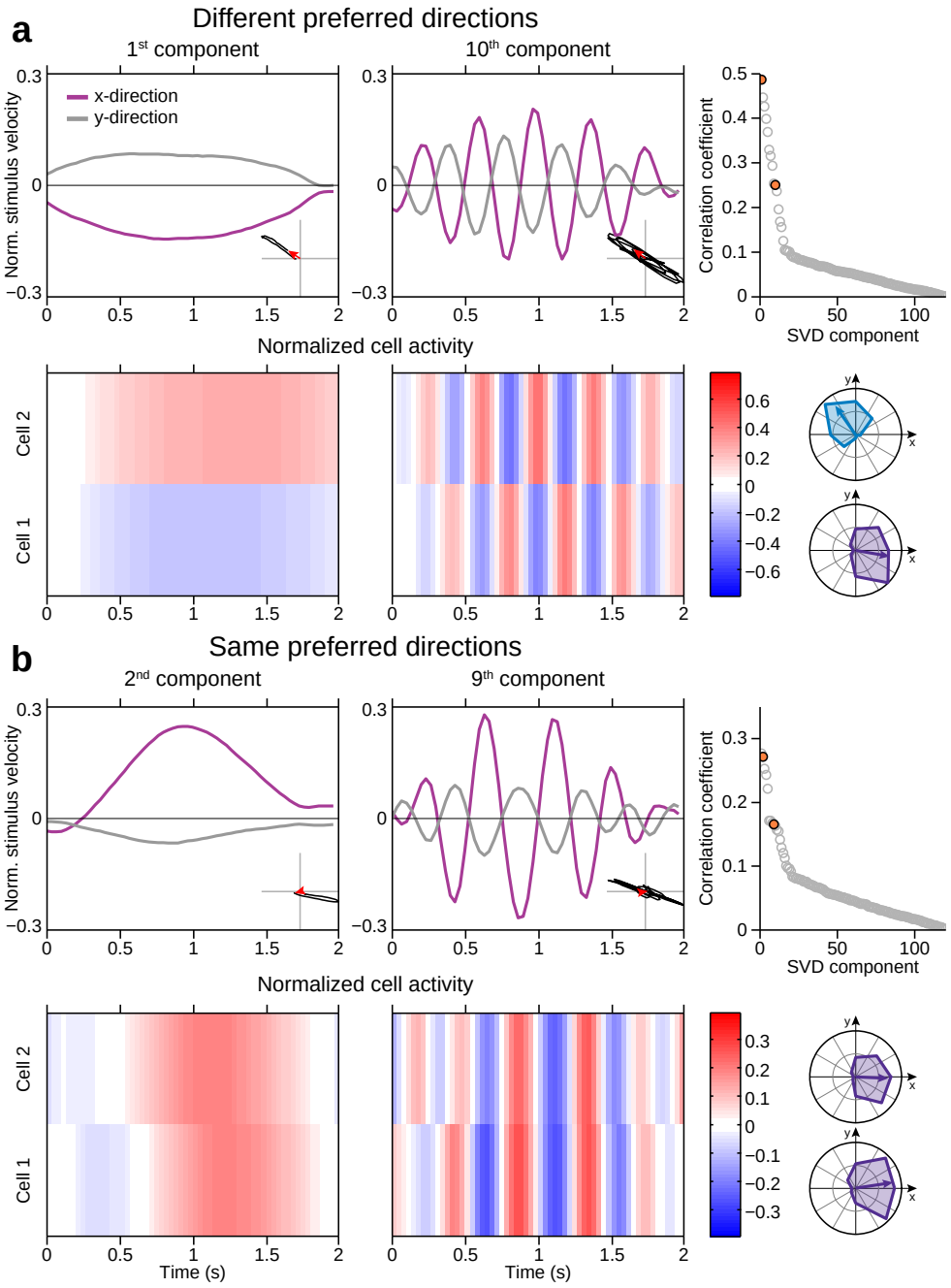

Figure 5.7 **Correlated stimulus-response structure obtained from canonical correlation analysis (CCA) of pairs of DS cells with either different (a) or same preferred directions (b). a-b left** CCA components capturing slowest frequencies, with upper panels showing average motion in x- and y-direction (violet and gray, respectively) and lower panels showing average activity of DS cells correlated to the stimulus. Inset shows average stimulus in 2-dimensional velocity space, red arrow marking the starting point. **middle** Higher CCA components capturing higher motion frequencies. **right** Upper panels show correlation coefficients between average stimulus and activity, orange circles mark example components. Lower panels show directional tuning of DS cells to drifting gratings.

depends on the weighted sum of the different directional inputs. The preferred direction of each DS cell can be represented by a vector and the weighted sum of these vectors, the *population vector*, could encode the actual motion direction (Georgopoulos et al., 1986). Population vectors were originally used to relate population responses in the primate motor cortex with a certain movement direction of the animal's arm. Spike rate-based tunings of the neurons were measured to determine the preferred direction of each cell, similar to the tunings that I obtained from the drifting gratings. Then the movement of the arm could be predicted by the sum of each direction vector, weighted by each cell's response rate.

For responses to a random motion trajectory, one can not simply apply rate-based tunings because direction and velocity of the stimulus change perpetually. Therefore, instead of calculating vector sums, I either added or subtracted the pair responses from each other and calculated the linear filters and stimulus reconstructions based on these additive and subtractive codes.

In figure 5.8a, the motion filters and information spectra from the pair responses of standard DS cells with different directional preferences are shown. One cell encoded motion into the nasal-dorsal direction and the other cell encoded motion into the temporal direction. The decoding of the pair response contained more information about the stimulus trajectory than the summed information from the single-cell response decoding, indicating a synergistic decoding of the pair response.

The additive code of this cell pair contained almost no information about the stimulus motion and the obtained linear filters were completely flat (Fig. 5.8c). The additive code showed high activity to large motion steps independent of the motion direction which is reflected by the almost symmetric conditional nonlinearities (Fig. 5.8c, lower).

On the other hand, when subtracting the spike counts of one cell from the other cell's response, the obtained information about the stimulus motion was about the same as the information obtained from the decoding of the full pair response (Fig. 5.8e). Hence, the subtractive code seems to capture the pair response correlations which are necessary for the synergistic motion decoding. The conditional nonlinearities of the subtractive code were monotonic and almost linear (Fig. 5.8e, lower). The nonlinearities show that the subtractive code responded strongly to preferred stimuli and had "negative firing rates" in response to non-preferred stimuli, resolving the ambiguities in the motion encoding of individual DS cells.

For a pair where both DS cells had similar directional preferences, the linear decoding of the pair response was largely redundant (Fig. 5.8b). In this case, the information that could be extracted from the additive code of the cell pair was

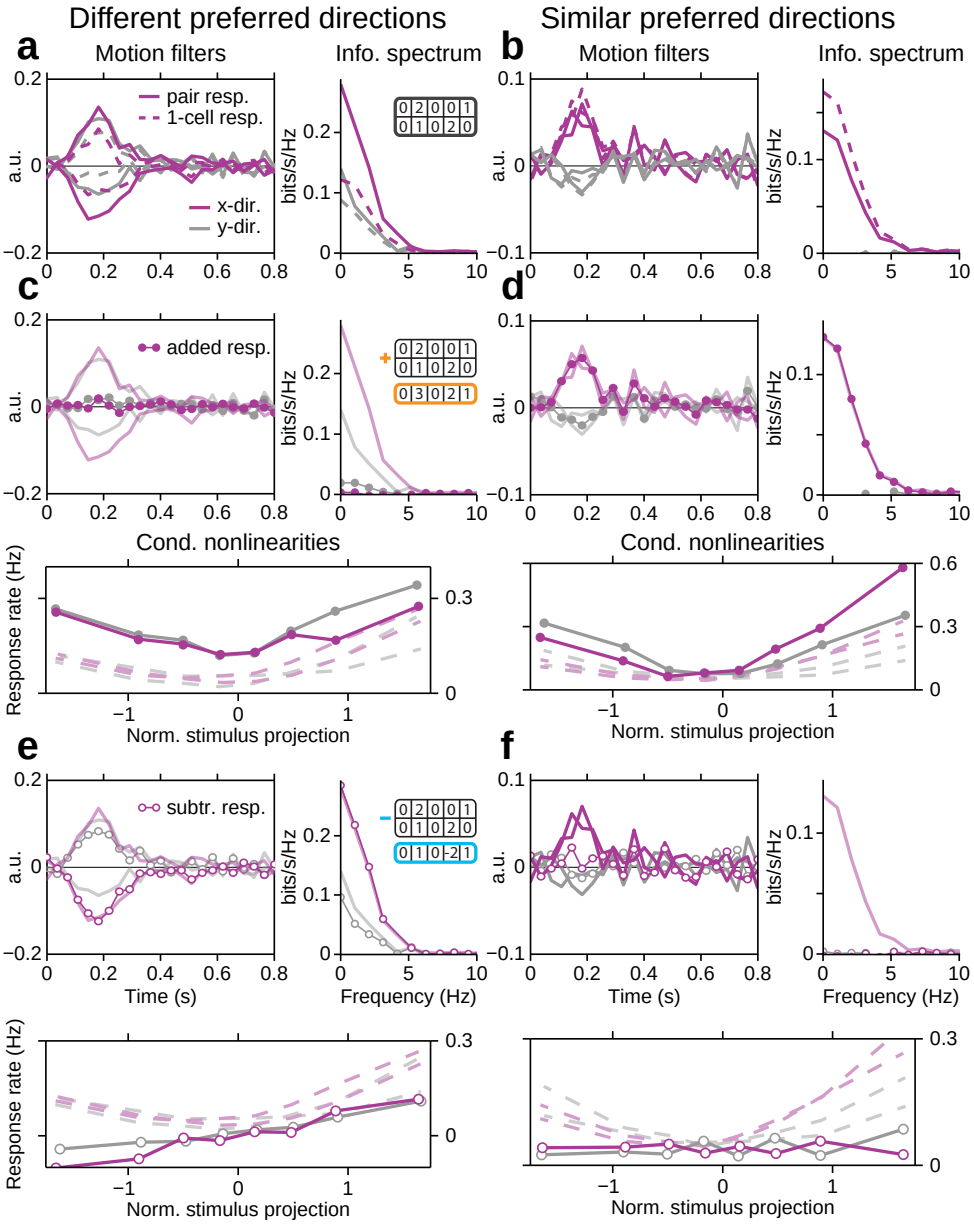

Figure 5.8 **Linear filters and information densities of relative spike codes compared with the complete pair response code for cell pairs with different (a, c, e) and similar preferred directions (b, d, f).** **a-b** For comparison: Linear filters (left) and information densities (right) from pair responses (solid line) and single cell responses (dashed). Information density of individual cells has been summed. **c-f** Linear filters (left), information densities (right) and conditional nonlinearities (below) when adding (c-d, solid bullets) or subtracting pair spikes within the same time bin (e-f, open bullets). Spike subtraction straightened the nonlinearities while spike summation led to a stronger curvature.

equal to the information obtained from the full pair response (Fig. 5.8d). The conditional nonlinearities were strongly non-monotonic, hence, the linear decoding of the additive code would still suffer from responses to strongly non-preferred motion stimuli, similar to what has been observed for the single-cell encoding.
For the subtractive code of two DS cells with similar preferred directions, the linear filters and conditional nonlinearities were completely flat (Fig. 5.8f), hence, the responses to preferred and non-preferred motion stimuli of one cell canceled out with the responses of the other cell and no motion specific response remained. Accordingly, no information about the motion trajectory could be decoded from the subtractive code of cells with similar preferred directions.

The additive and subtractive codes of DS cell pairs with similar and different preferred directions, respectively, seemed to capture the most important correlations within the pair responses for describing the motion trajectory. This was shown in the above examples. Is this true for all DS cell pairs within a population? I calculated the information ratios of the information obtained from pair responses, added and subtracted pair responses and divided them by the summed information from the single-cell responses for every DS cell pair in one experiment. In figure 5.9a, left, it can be observed that for DS cells with different preferred directions the decoding of the pair responses was synergistic for more than 75% of the pairs while only about 50% of the subtractive codes showed synergy. Accordingly, the subtractive code could capture most but not all the correlations within the pair responses that were important for the synergistic motion decoding.
For cells with similar preferred directions, the decoded information from the pair response almost matched the information from the additive code (Fig. 5.9a, right). Contributions of the subtractive code were negligible.

Standard DS cells do not only encode the direction of a moving stimulus but they also respond to contrast changes. As shortly discussed in section 5.3, the simultaneous encoding of motion direction and contrast may lead to the observed non-monotonic nonlinearities in a DS cell's motion encoding. Two DS cells which share spatial inputs due to overlapping receptive fields, would be similarly driven by contrast changes. When these two cells have different directional preferences, the response of each cell to the contrast change would be increased or reduced, depending on the motion direction which implied the contrast change and the directional preference of each cell. The response correlations from the shared spatial inputs could then either improve or corrupt the motion decoding.
In figure 5.9b, I plotted the averaged information ratios of each cell pair in relation to their receptive field distances. For cells with different preferred directions, the information ratios from pair responses and subtracted pair responses strongly

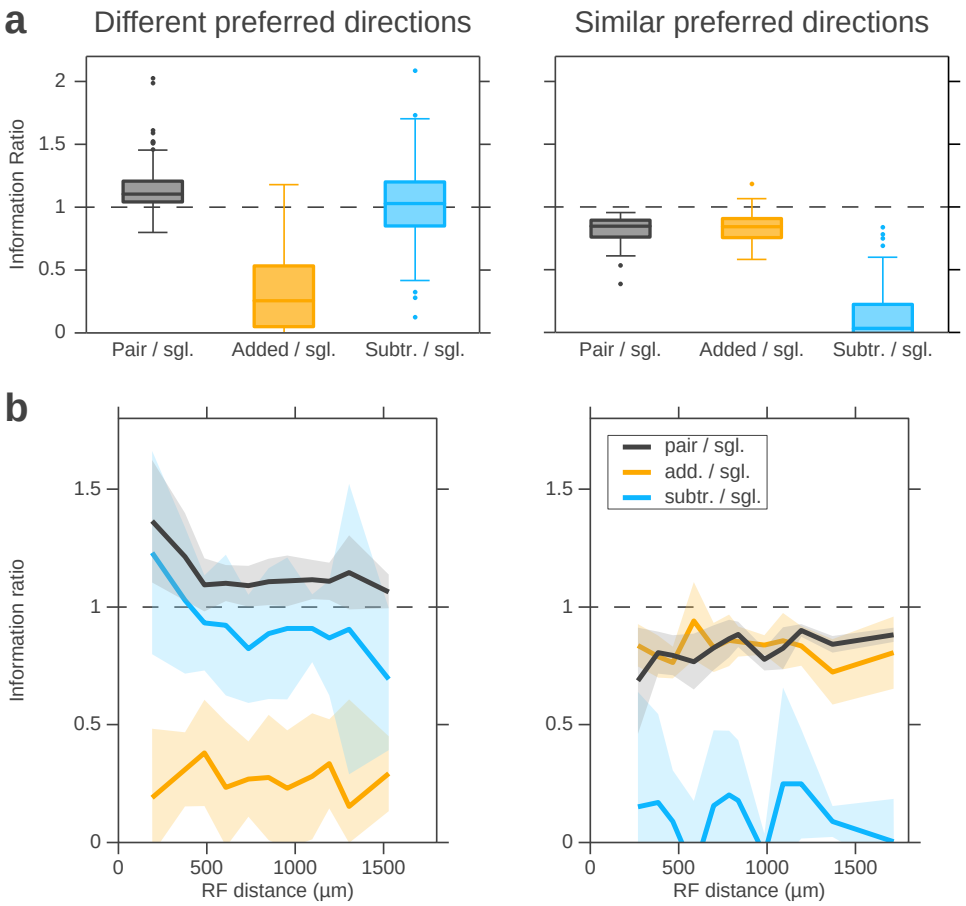

Figure 5.9 **Most information about motion trajectories can be extracted from the subtractive and additive codes of pairs containing different (left) or similar preferred directions (right), respectively. a** Information ratios of information from pair responses (black), added (orange) and subtracted pair responses (cyan) divided by the summed single-cell information. Dashed line shows the border between synergy (above) and redundancy (below). **b** Above information ratios plotted versus receptive field distances between cells. Lines and shaded regions show averages and standard deviations of 12 cells per bin. **Abbr.:** Pair: Information from pair responses, Added: Information from added pair responses, Subtr.: Information from subtracted pair responses, Sgl.: Summed information from single-cell responses.

increased for small receptive field distances (Fig. 5.9b, left). Hence, the shared spatial contrast might have synergistic effects for the linear motion decoding from DS cells with different directional preferences. For cells with similar preferred directions, the information ratios from the pair responses and added pair responses were slightly smaller for close-by DS cells than for DS cells which were further apart from each other.

Due to the tiling of the receptive fields of standard DS cells with similar preferred directions, cells with different preferred directions had stronger receptive field overlaps than cells with similar preferred directions. Therefore, the observed effect of a shared spatial input might be stronger for cells with different preferred directions.

6 — Discussion and Outlook

Motion is an essential part of our everyday visual experience. The detection of moving objects and their pursuit is not only important for catching a ball during a game but also in situations of traffic to avoid approaching cars. Yet, it is not well understood how moving objects are detected and tracked and to which extent retinal pre-processing is important. Furthermore, eye, head and body movements shift the image that is projected onto our retinas. Even when fixating our gaze, there are small tremor-like eye movements which induce global shifts of the projected image and are superimposed onto the object motion trajectory.

I tried to answer the question how the output from retinal ganglion cells could assist in the detection and tracking of moving objects and, furthermore, how object motion and other image features could be decorrelated from the global image shifts induced by eye and head movements. I approached these questions on the single-cell and population encoding level. First, I analyzed the motion-specific responses of individual retinal ganglion cells. Second, I investigated the encoding of random background motion by certain subpopulations of motion-sensitive retinal ganglion cells.

I have shown that there are two putative types of direction-selective ganglion cells in the salamander retina, standard DS and OMS-DS cells. They are suitable for processing the motion direction of background and object motion, respectively, and presumably send their outputs to different downstream brain areas. Receptive field properties, organization of preferred directions and responses to more complex motion stimuli hint to their prospective purpose in initiating different oculomotor responses. It is however interesting that I found OMS-DS cells which selectively respond to certain directions of object motion and standard OMS cells which are sensitive to local differential motion of an object irrespective of its direction. I will discuss possible advantages of such a pathway splitting below.

As the standard DS cells might be responsible for processing the motion direction of the retinal slip, I used populations of standard DS cells to study their capabilities in encoding random motion trajectories, similar to those induced by fixational eye movements. Using a linear multi-cell decoder, I compared the mutual information

between the stimulus and its linear reconstruction from either independent or correlated DS cell responses. There, I found that for a population of standard DS cells with different directional preferences, the stimulus reconstruction was better when including response correlation then without them. This synergy in the population decoding of the trajectory was not caused by noise-correlations, as induced by shared input noise from upstream neurons, but rather by the stimulus-driven response correlations between standard DS cells with different preferred directions. These correlations possibly counteract the low fidelity of random motion decoding from individual DS cell responses.

6.1 Two types of direction-selective ganglion cells

Direction-selectivity can be found in retinal ganglion cells across vertebrates as frogs, turtles, birds, rabbits and mice (Lettvin et al., 1959; Ariel and Adolph, 1985; Maturana and Frenk, 1963; Barlow and Hill, 1963; Weng et al., 2005; Sun et al., 2006). However, the existence of direction-selective ganglion cells in the salamander retina is still a matter of debate. While former studies reported direction-selective retinal ganglion cells in mudpuppy (*Necturus maculosus*) and tiger salamander (*Ambystoma tigrinum*) (Werblin, 1970; Pan and Slaughter, 1991), a more recent study could not find significant direction-selectivity in the tiger salamander retina (Segev et al., 2006). There might however be differences in the developmental stage of the retina, since Segev et al. (2006) used larval tiger salamander. There, direction-selectivity might not have fully developed yet.
In the retina of adult axolotl salamanders (*Ambystoma mexicanum*), I found two types of direction-selective cells, standard DS and OMS-DS cells, which preferably responded to certain directions of drifting motion, the preferred direction, but not to motion into the opposite direction, the null direction. Standard DS and OMS-DS cells however differed in their responses to differential and coherent global motion. While standard DS cells responded well to both, local and global motion, the responses of OMS-DS cells to global coherent motion were strongly reduced. Standard DS and OMS-DS cells also had different receptive field sizes and systems of preferred directions. These properties could be indicators for their functional roles. Furthermore, they indicate that standard DS and OMS-DS cells could be different cell types, of distinct morphology and genetics, each type extracting different features of the visual scene.
Standard DS cells had large receptive fields which would enable them to integrate motion over an extended area. Since they also responded well to global coherent motion, they might encode the motion direction of the whole scene as induced by

head and eye movements and play an important role in the correction of the retinal slip. This is further substantiated by the alignment of their preferred directions. Standard DS cells could be divided into three subtypes, each subtype having a different preferred direction which was 120° apart from the preferred directions of the other subtypes. The preferred directions could be roughly aligned with the orientations of the three semicircular canals in the vestibular system of the axolotl (Maddin and Sherratt, 2014).

OMS-DS cells might be important for encoding the motion direction of small moving objects which would require a high spatial resolution. This is given by the cells' small receptive fields which were among the smallest within the recorded cell population together with standard OMS cells. Furthermore, OMS-DS cells were well directionally tuned to small drifting spots. Their preferred directions were oriented along the four cardinal directions coinciding with the horizontal and vertical rotational axes of the four external recti eye muscles (Hilton, 1956). Despite their small receptive fields, OMS-DS cells were quite sparse in my recordings and had very low coverage of the visual field. Therefore, usually only two or three directions were observed within a single recording.

The sparseness of OMS-DS cells could have two obvious reasons, either the group of OMS-DS cells consists mainly of displaced ganglion cells, situated in the inner nuclear layer of the retina (Li et al., 1990; Montgomery et al., 1981) where their signals could not be recorded by planar multielectrode arrays, or the stimulus which I used for spike sorting did not drive the cells sufficiently to fire enough action potentials for being detected in the analysis.

To further substantiate the hypothesis that standard DS and OMS-DS cells might have two different purposes in the processing of motion, i.e., the encoding of the motion direction of global background motion and small moving objects, respectively, I applied a more complex motion stimulus. It consisted of individual components drifting into two different directions which resulted in a third motion direction of the global pattern. With this plaid stimulus, I analyzed whether DS cells (standard DS and OMS-DS cells) were more strongly driven by the global motion of the pattern or the local motion of the individual components. The analysis revealed that the significantly component-sensitive DS cells also showed a strong object-motion-sensitivity while significantly pattern-sensitive DS cells had a more intermediate object-motion-sensitivity. Hence, standard DS cells seem to better integrate global motion over their large receptive fields and OMS-DS cells rather integrate local motion within a small area, being suppressed by global motion.

The different properties of standard DS and OMS-DS cells observed here, indicate

that standard DS and OMS-DS cells could be two different cell types, processing different views of the visual world. This is also indicated by the clear tiling of the receptive fields of standard DS and OMS-DS directional subtypes. The receptive fields of standard DS cells with the same preferred direction covered the visual field like a mosaic with only minor overlaps and some gaps where cell were probably not recorded because of low signal-to-noise ratio. On the other hand, standard DS cells with different preferred directions were strongly overlapping. The tiling of directional subtypes has been first observed in the ON-OFF direction-selective cells of the rabbit retina (Amthor and Oyster, 1995; DeVries and Baylor, 1997; Vaney, 1994). More recently, it could be shown that the directional subtypes of ON and ON-OFF DS cells in mouse have different molecular markers (Kay et al., 2011; Yonehara et al., 2009). Hence, the directional subtypes of DS ganglion cells in mouse are genetically different and therefore show independent receptive field tilings. OMS-DS cells, which usually were much sparser in my recordings, had no overlaps among each other but strong overlaps with the receptive fields of standard DS cells of either preferred direction.
Although molecular markers are at present one of the leading criteria for identifying different cell types (Sanes and Masland, 2014), the strongly differing functional outputs and receptive field properties shown here support the hypothesis that standard DS and OMS-DS cells are distinct cell types probably processing in parallel the direction of global and local motion, respectively.

6.1.1 Analogies to the mammalian retina

The two different organizations of preferred directions of standard DS and OMS-DS cells are very similar to the preferred directions of ON and ON-OFF DS cells in mammals, respectively. The ON DS cells have also three subtypes, one with preferred direction along the nasal-temporal axis and the other two with preferred directions 120° apart (Oyster and Barlow, 1967; Sun et al., 2006). Due to their tuning to slow velocities (Oyster, 1968; Sivyer et al., 2010; Wyatt and Daw, 1975) and their projections to the accessory optic system (AOS) (Simpson, 1984), ON DS cells are thought to be important for image-stabilization by encoding the direction of slow full-field motion (Dhande et al., 2013; Vaney et al., 2001). The standard DS cells in the salamander retina could have similar functions since they respond well to global coherent motion. In frogs, direction-selective cells have also been observed which project to the nucleus of the basal optic tract (Cook and Podugolnikova, 2001; Bastakov et al., 2015) which is the amphibian analog of the medial terminal nucleus of the AOS in mammals (Fritzsch, 1980).
OMS-DS cells might be the analogous of the ON-OFF DS cells in mouse and

rabbit which have four subtypes with preferred directions separated by 90° (Oyster and Barlow, 1967; Weng et al., 2005; Briggman et al., 2011). The ON-OFF DS cells in rabbit also show a strong surround suppression by coherent motion (Chiao and Masland, 2003; ÖLveczky et al., 2003) and their receptive fields are smaller than the receptive fields of the ON DS cells (Barlow and Hill, 1963; Barlow et al., 1964; Weng et al., 2005; Rivlin-Etzion et al., 2011). However, although the preferred directions of OMS-DS cells were separated by 90°, I could only identify three directional subtypes. In the turtle retina, a similar distribution was found (Bowling, 1980).

Unlike ON and ON-OFF DS cells in mammals, standard DS and OMS-DS cells are both OFF type, as most ganglion cells in the axolotl retina. Also both types responded to a wide range of velocities (data was not shown) similar to the DS cell types in turtle (Ariel and Adolph, 1985).

Although many of the recorded OMS-DS cells preferred motion into the ventral direction, they are most probably not related to the OFF DS cells (or JAM-B cells) in mouse which exclusively prefer upward motion (Kim et al., 2008). Unlike ON and ON-OFF DS cells, JAM-B cells are only direction-selective at mesopic light levels (Joesch and Meister, 2016). I usually recorded at photopic light levels. In the few experiments where I recorded under mesopic conditions the fraction of OMS-DS cells and their direction-selectivity index did not change compared to higher light levels.

Apart from functional analogies, direction selectivity in the salamander and mammalian retina might also be computed via similar mechanisms. In rabbit and mouse, the direction selectivity of ON and ON-OFF DS cells is mediated by gabaergic inhibition from starburst amacrine cells (Briggman et al., 2011; Taylor and Vaney, 2003; Weng et al., 2005; Wyatt and Daw, 1976). Starburst amacrine cells are the only acetylcholine releasing cells in the mammalian retina and can be identified in a choline acetyltransferase (ChAT) staining. Acetylcholine releasing amacrine cells were also found in the inner nuclear layer and ganglion cell layer of the salamander retina at similar depths as in the mammalian retina (Zhang and Wu, 2001). I have shown that the GABA antagonists picrotoxin and gabazine (SR-95531) significantly reduced the direction selectivity of standard DS and OMS-DS cells in the retina of the axolotl salamander.

More similarities can be observed in the reactions to strychnine. In both, mammals and axolotl, the response to the drifting gratings was reduced during strychnine application (Wyatt and Daw, 1976). Usually, the activity of retinal ganglion cells increases when inhibition is blocked. Nevertheless, reduced firing rates of DS ganglion cells during strychnine application were also observed in the turtle retina

(Ariel and Adolph, 1985). There, further experiments indicated that glycine might regulate the presynaptic excitatory inputs to the DS cells.
The compelling analogies between the standard DS and OMS-DS cells in salamander and the ON and ON-OFF DS cells in mouse and rabbit suggest that the parallel processing of global and local motion direction could be fairly universal across species.

6.2 Object-motion sensitivity of retinal ganglion cells

Most retinal ganglion cells seem to have some degree of object-motion sensitivity. While the majority of cells showed low to intermediate object-motion sensitivity, about 28% of the recorded cells were strongly object-motion sensitive. Although there was no clear gap in the distribution of the object-motion-sensitivity index, I estimated a threshold for separating the two populations by visual inspection and using a Gaussian mixture model.
While several cell types in rabbit were shown to be object-motion sensitive, e. g., ON brisk transient cells and ON-OFF direction-selective cells, in tiger salamander, only fast OFF cells were mentioned in the literature (ÖLveczky et al., 2003). Here, I showed that also in the salamander retina there are direction-selective OMS cells, the OMS-DS cells, and non-direction-selective OMS cells, which I called standard OMS cells but which might also divide into further subtypes. The OMS cells in this study were mainly slow OFF cells. This is contradictory to earlier observations in the tiger salamander (ÖLveczky et al., 2003).
More recent studies of the analog of the OMS cells in mouse, the W3B cells, showed that these cells have comparably slow response kinetics (Zhang et al., 2012). Apparently, their object-motion-sensitivity relies on unusual excitatory input from amacrine cells that express vesicular glutamate transporter 3 (VG3s) (Kim et al., 2015; Krishnaswamy et al., 2015; Zhang et al., 2012). These VG3s are object-motion-sensitive themselves due to their strong surround suppression from spiking wide-field amacrine cells (Kim et al., 2015). This adds another processing step into the signaling pathway for object-motion-sensitivity. VG3s have also strong projections onto other ganglion cell types, e.g., ON-OFF direction-selective cells and W3D cells (Krishnaswamy et al., 2015; Lee et al., 2014).
In previous studies in the tiger salamander, a polyaxonal wide-field amacrine cell was proposed to mediate object-motion sensitivity via glycinergic inhibition onto bipolar cells projecting to OMS cells. When object and background motion are in-phase during global coherent motion, the bipolar cell excitatory signal onto OMS cells is suppressed by the glycinergic amacrine cells (Baccus et al., 2008). Interest-

ingly, in axolotl not only glycine antagonists affected the object-motion sensitivity of standard OMS and OMS-DS cells, but also GABA antagonists diminished the cells' object-motion sensitivity significantly. This suggests that gabaergic inhibition might be required for balancing the excitatory inputs to OMS cells and that the circuitry for generating object-motion sensitivity in salamander retina might be more complex than currently assumed.
Regardless of whether there are excitatory amacrine cells in the axolotl retina, OMS cells probably receive object-motion-sensitive input from excitatory upstream neurons. A ganglion cell type which is at the same time object-motion-sensitive and direction-selective could then arise from receiving excitatory input from object-motion-sensitive interneurons (Baccus et al., 2008) and inhibitory input from acetylcholine-releasing amacrine cells (Euler et al., 2002).

6.2.1 Simultaneous processing of position and direction of a moving object

Why does the salamander retina have two types of object-motion-sensitive cells? Or more precisely, what information can be gained from the output of direction-selective OMS cells when standard OMS cells already encode object motion? When pursuing a moving object with our eyes, one has to extrapolate the object's motion trajectory in order to be able to catch the it. The future position of an object can be extrapolated from its previous positions. But since the estimates of the previous positions are not precise, knowledge about the object's current speed and direction could improve the extrapolation of the future position (Kalman, 1960; Faisal et al., 2008).
Standard OMS cells respond to local motion irrespective of its direction (ÖLveczky et al., 2003; Baccus et al., 2008) while OMS-DS cells preferentially respond to certain directions of a moving object. These two signals might serve as location and direction estimates of a moving object. Especially when the object is occluded for a short time period, information about its previous direction could improve the estimate of the future position (Kristan et al., 2009). Computational frameworks which combine information about object position and direction are able to explain various effects in human motion perception, as the slowing of motion shown in the visual periphery or the curveball illusion (Kwon et al., 2015).
Experimentally it has been shown that flies have two different motion processing pathways, one for encoding the position of a moving object and the other encoding the object's motion direction (Bahl et al., 2013). When blocking the motion encoding pathway, flies could not pursue global motion any longer, they lost their oculomotor response. On the other hand, they were still able to track or fixate

on an object but with lower precision (fixation response) (Bahl et al., 2013; Virsik and Reichardt, 1976; Wehrhahn and Hausen, 1980).
Hence, the simultaneous processing of a moving object's position and direction by standard OMS and OMS-DS cells, respectively, in the salamander retina could aid the tracking of prey and predators and would therefore be crucial for the salamander's survival.

6.3 Advantages of DS directional subtypes for random motion encoding

Populations of direction-selective ganglion cells are known to faithfully encode the motion direction of a drifting grating (Amthor et al., 2005; Fiscella et al., 2015; Franke et al., 2016; Zylberberg et al., 2016) but were never shown to encode tremor-like motion as induced by fixational eye movements. Some studies show the encoding of 1-dimensional random motion of a sinusoidal grating by direction-selective neurons in monkey visual cortex (Bair and Movshon, 2004; McLelland et al., 2015). Others focus on the predictive coding of correlated random bar motion by arbitrary populations of retinal ganglion cells (Marre et al., 2015; Palmer et al., 2015).
Since I hypothesize standard DS cells to provide important information for correcting for the retinal slip, I investigated if a hypothetical downstream neuron could use the responses of a population of standard DS cells to reconstruct a two-dimensional random motion trajectory as induced by fixational eye movements (Manteuffel et al., 1977; Engbert and Kliegl, 2004). I explicitly asked how much information about the random motion trajectory a linear downstream decoder could obtain from the population responses of the standard DS cells.
I compared the information from the population responses to the summed information from single-cell responses and expected that stimulus-driven correlations in the population code would induce lots of redundancy. The linear decoding of population responses of DS cells with similar preferred directions was indeed worse than what one would expect from the independent single-cell responses. But the encoding of standard DS cells with different preferred directions led to synergy in the decoded information. The information obtained from standard DS cell populations with different preferred directions was significantly higher than the summed information obtained from the single-cell responses.
Information of the linear decoding of OMS-DS cell responses was in general very low, even for stimuli with random object motion. A possible reason could be that OMS-DS cells might respond better to more continuous motion, similar to the

trajectories of potential prey or predators.
The observed synergy in the population responses of standard DS cells, was not caused by noise correlations, i.e., correlations that are induced by noise from shared upstream neurons which might result in strong synchrony or asynchrony of the ganglion cells' activity. There is an ongoing debate whether noise-correlations are of importance for retinal spike coding (Nirenberg et al., 2001; Franke et al., 2016; Zylberberg et al., 2016). For the decoding of the direction of a drifting grating from the responses of ON-OFF DS cells in the mouse, stimulus-dependent noise-correlations seem to be of a particular importance (Franke et al., 2016; Zylberberg et al., 2016). For the synergy in the linear decoding of random motion trajectories from standard DS cell responses, noise correlations were not important. Noise-correlations even slightly diminished the performance of the linear decoder.
Therefore, I investigated what happened on the single-cell level, i.e., how do the linear filters change when correlations are removed and more importantly, to which features of the motion trajectory does a cell respond? For pairs of DS cells with different preferred directions, I noticed that the linear filters had reduced peaks when removing their pair correlations. Since the linear filters are optimized to have maximal correlation between stimulus and response, a reduced peak of the linear filter is directly related to a lower performance of the linear encoding of the preferred direction and, hence, the information that can be read out.
The reduced peak in the linear filters of the single-cell responses originated from a non-monotonic input-output relationship between stimulus and response. For example, when an OFF cell encodes a temporal contrast flicker, its contrast-encoding nonlinearity is usually monotonic which means low responses to brightening and strong responses to darkening temporal contrast. The non-monotonic nonlinearities in the motion encoding of standard DS cells imply that they do not only respond to motion into their preferred direction but that they also show strong responses to motion into their null direction which will corrupt the linear readout. I hypothesized that the non-monotonic nonlinearities lead to the observed synergy in the linear readout of standard DS cells with different preferred directions. To test this hypothesis, I modeled pairs of independent direction-selective neurons with either monotonic or non-monotonic nonlinearities where the generated spikes only depended on the motion trajectory and not on any other spatial stimulus information. For these simulated pairs of neurons, synergy in the linear readout was only observed for non-monotonic nonlinearities. This indicates that the non-monotonic nonlinearities cause the observed synergy.

6.3.1 Competition between motion and contrast encoding

It still has to be illuminated what causes the non-monotonic nonlinearities. A plausible explanation could be that the encoding of contrast influences the encoding of the motion direction. For example, by global image shifts, the pattern that is projected onto a DS cell's will change with every shift. For large shifts, the pattern will change more strongly. The sudden contrast changes might evoke strong responses even though the contrast change might be caused by motion into the cell's null direction.

Motion detection and contrast changes are inseparably entangled. Without spatial structure, the detection of motion would not be possible. On the other hand, contrast changes as occur when an object is shortly flashed in a cell's receptive field, do not necessarily imply motion. Here, I investigated the encoding of motion mostly independently from the spatial pattern. But the encoding of motion is probably highly correlated with the emergence of certain image features in the DS cell's receptive field. A next step would now be to investigate the encoding of the correlations between image features and motion trajectories. The usual reverse correlation methods are not applicable here since the spatial component of the stimulus is highly correlated in time. Nevertheless, the STAs obtained from the responses to spatio-temporal white noise might allow a first estimate.

A possible experiment to test the influence of the DS cells' contrast sensitivity on their motion encoding would be to have repeated trials of the same trajectory with different offsets of the pattern's position. There, cells with responses from different trials could either have a stronger or weaker correlation in their motion responses. This would depend on whether the contrast encoding is corrupting or improving the joint motion decoding from DS cell population responses, respectively.

What could now be the mechanisms for a more faithful linear decoding of the random motion trajectory by standard DS cells with different preferred directions? I used canonical correlation analysis (CCA) (Zeck et al., 2008) and a population vector-like analysis (Georgopoulos et al., 1988) to investigate the activity patterns of DS cell pairs. I found that the stimulus-induced anti-phasic spiking of DS cell pairs with different preferred directions provided the major contribution to the observed synergy in the population decoding.

For example, if the simultaneous contrast encoding of the cells shapes the non-monotonic nonlinearities, a large motion step into one cell's null direction could still evoke a significant response due to the induced strong contrast change. If a downstream neuron only receives input from this one cell, its linearly assumed decoding would interpret this as motion into the preferred direction of the cell.

However, if there is additional input from a DS cell with different preferred direction, this cell would give an even stronger response. Hence, the difference between the two cell responses would then indicate that the motion was not into the first cell's preferred direction but into the preferred direction of the second cell. Here, the cooperative spiking of standard DS cells with different directional preferences reduces the uncertainties about the motion trajectory.
The corrective mechanisms outlined here, are very similar to what has been proposed to explain the sharp directional tunings of direction-selective neurons in the rabbit LGN (Levick et al., 1969). These might receive inputs from ON-OFF DS cells with opposite preferred directions, with one providing excitatory input and the other inhibitory input. This would result in a subtractive code for decoding the motion trajectory.

6.4 Conclusion

The processing of motion in visual scenes is essential for navigating through our environment. Here, I showed in the axolotl salamander that the retina already processes different motion features in parallel. For example, two types of direction-selective ganglion cells are dedicated to process motion direction. One type is sensitive to certain directions of local object motion and might contribute crucial information for prey capture. The output of the other direction-selective cell type might assist in correcting for the retinal slip by detecting the direction of global image shifts, as induced by self-motion.
For the latter type, I investigated the decoding of global motion trajectories from population responses and which information a downstream neuron might be able to retrieve. The decoding of direction and velocity from individual cell responses was thereby strongly affected by the cell's responses to strong contrast changes as induced by large motion steps in either direction. Since motion can not be detected without changes in spatial contrast, the encoding of motion direction and contrast changes are highly correlated, leading to ambiguities in the decoding of motion direction. These ambiguities could be partially resolved by combining responses from direction-selective cells with different directional preferences which manifested in a synergistic population readout.
Stimulus-driven response correlations could thereby help to better decorrelate information about motion direction and spatial contrast changes. For example, while strong contrast changes, that are induced by large motion steps in either direction, will lead to correlated activity of the entire cell population, motion direction could be detected by the relative spiking difference between cells with different di-

rectional preferences. For pairs of direction-selective cells with different preferred directions this would result in an additive pair code for extracting general contrast changes while a subtractive code could account for the direction of motion. Hence, the readout strongly depends on how the inputs from direction-selective ganglion cells are combined by downstream neurons. This further serves as an example for the great potential of neural population codes.

Bibliography

Adelson, E. H. and Movshon, J. A. (1982), Phenomenal coherence of moving visual patterns, *Nature*, 300, 523–525.

Amthor, F. R. and Oyster, C. W. (1995), Spatial organization of retinal information about the direction of image motion, *PNAS*, 92, 4002–4005.

Amthor, F. R., Tootle, J. S., and Grzywacz, N. M. (2005), Stimulus-dependent correlated firing in directionally selective retinal ganglion cells, *Vis. Neurosci.*, 22, 769–787. doi: 10.1017/S0952523805226081.

Ariel, M. and Adolph, A. R. (1985), Neurotransmitter inputs to directionally sensitive turtle retinal ganglion cells., *J. Neurophysiol.*, 54, 1123–43.

Averbeck, B. B., Latham, P. E., and Pouget, A. (2006), Neural correlations, population coding and computation., *Nat. Rev. Neurosci.*, 7, 358–366. doi: 10.1038/nrn1888.

Baccus, S. A., Oelveczky, B. P., Manu, M., and Meister, M. (2008), A retinal circuit that computes object motion., *J. Neurosci.*, 28, 6807–17. doi: 10.1523/JNEUROSCI.4206-07.2008.

Bahl, A., Ammer, G., Schilling, T., and Borst, A. (2013), Object tracking in motion-blind flies, *Nat. Neurosci.*, 16, 1–11. doi: 10.1038/nn.3386.

Bair, W. and Movshon, J. A. (2004), Adaptive Temporal Integration of Motion in Direction-Selective Neurons in Macaque Visual Cortex, *J. Neurosci.*, 24, 9305–9323. doi: 10.1523/JNEUROSCI.0554-04.2004.

Barlow, H. B. (1953), Summation and inhibition in the frog's retina., *J. Physiol.*, 119, 69–88. doi: 10.1113/jphysiol.1953.sp004829.

Barlow, H. B. and Hill, R. M. (1963), Selective sensitivity to direction of movement in ganglion cells of the rabbit retina, *Science*, 139, 412–414.

Barlow, H. B. and Levick, W. R. (1965), The mechanism of directionally selective units in rabbit's retina, *J. Physiol.*, 178, 477–504.

Barlow, H. B., Hill, R. M., and Levick, W. R. (1964), Retinal ganglion cells responding selectively to direction and speed of image motion in the rabbit, *J. Physiol.*, 173, 377–407.

Bastakov, V. A., Kiseleva, E., and Orlov, O. Y. (2015), Direction-selective units in the frog's basal optic root nucleus, *J. Integr. Neurosci.*, 14, 491–501.

Berry II, M. J., Brivanlou, I. H., Jordan, T. A., and Meister, M. (1999), Anticipation of moving stimuli by the retina, *Nature*, 398, 334–338.

Borg-Graham, L. J. and Grzywacz, N. M. (1992). A model of the directional selectivity circuit in retina: transformations by neurons singly and in concert. In McKenna, T., Zornetzer, S. F., and Davis, J. L., editors, *Single neuron Comput.*, chapter 13, pages 347–375. Academic Press, St. Louis, Missouri. ISBN 0-12-484815-X.

Borghuis, B. G. and Leonardo, A. (2015), The role of motion extrapolation in amphibian prey capture, *J. Neurosci.*, 35, 15430–15441. doi: 10.1523/JNEUROSCI.3189-15.2015.

Borst, A. and Euler, T. (2011), Seeing things in motion: models, circuits, and mechanisms., *Neuron*, 71, 974–994. doi: 10.1016/j.neuron.2011.08.031.

Bowling, D. B. (1980), Light responses of ganglion cells in the retina of the turtle, *J. Physiol.*, 299, 173–196.

Branco, T., Clark, B. A., and Häusser, M. (2010), Dendritic Discrimination of Temporal, *Science*, 329, 1671–1675.

Briggman, K. L., Helmstaedter, M., and Denk, W. (2011), Wiring specificity in the direction-selectivity circuit of the retina., *Nature*, 471, 183–8. doi: 10.1038/nature09818.

Brivanlou, I. H., Warland, D. K., and Meister, M. (1998), Mechanisms of concerted firing among retinal ganglion cells., *Neuron*, 20, 527–39.

Cafaro, J. and Rieke, F. (2010), Noise correlations improve response fidelity and stimulus encoding, *Nature*, 468, 964–967. doi: 10.1038/nature09570.

Caldwell, J. H. and Daw, N. W. (1978), New properties of rabbit retinal ganglion cells, *J. Physiol.*, 276, 257–276.

Caldwell, J. H., Daw, N. W., and Wyatt, H. J. (1978), Effects of picrotoxin and strychnine on rabbit retinal ganglion cells: Lateral interactions for cells with more complex receptive fields, *J. Physiol.*, 276, 277–298.

Castelo-Branco, M., Formisano, E., Backes, W., Zanella, F., Neuenschwander, S., Singer, W., and Goebel, R. (2002), Activity patterns in human motion-sensitive areas depend on the interpretation of global motion., *PNAS*, 99, 13914–9. doi: 10.1073/pnas.202049999.

Chen, E. Y., Marre, O., Fisher, C., Schwartz, G., Levy, J., Silviera, R. A. D., and Berry II, M. J. (2013), Alert Response to Motion Onset in the Retina, *J. Neurosci.*, 33, 120–132. doi: 10.1523/JNEUROSCI.3749-12.2013.

Chen, H., Liu, X., and Tian, N. (2014), Subtype-Dependent Postnatal Development of Direction- and Orientation-Selective Retinal Ganglion Cells in Mice., *J. Neurophysiol.*, 112, 2092–2101. doi: 10.1152/jn.00320.2014.

Chiao, C.-C. and Masland, R. H. (2003), Contextual tuning of direction-selective retinal ganglion cells., *Nat. Neurosci.*, 6, 1251–1252. doi: 10.1038/nn1147.

Chichilnisky, E. J. (2001), A simple white noise analysis of neuronal light responses., *Netw. Comput. Neural Syst.*, 12, 199–213.

Cimini, B. A., Strang, C. E., Wotring, V. E., Keyser, K. T., and Eldred, W. D. (2008), Role of acetylcholine in nitric oxide production in the salamander retina., *J. Comp. Neurol.*, 507, 1952–63. doi: 10.1002/cne.21655.

Cleland, B. G. and Levick, W. R. (1974a), Properties of rarely encountered types of ganglion cells in the cat's retina and an overall classification, *J. Physiol.*, 240, 457–492.

Cleland, B. G. and Levick, W. R. (1974b), Brisk and sluggish concentrically organized ganglion cells in the cat's retina, *J. Physiol.*, 240, 421–456.

Cochran, S. L., Dieringer, N., and Precht, W. (1984), Basic optokinetic-ocular reflex pathways in the frog., *J. Neurosci.*, 4, 43–57.

Collewijn, H. (1975), Direction-selective units in the rabbit's nucleus of the optic tract, *Brain Res.*, 100, 489–508. doi: 10.1016/0006-8993(75)90154-7.

Collewijn, H. and Kowler, E. (2008), The significance of microsaccades for vision and oculomotor control, *J. Vis.*, 820, 1–21. doi: 10.1167/8.14.20.

Contini, M. and Raviola, E. (2003), GABAergic synapses made by a retinal dopaminergic neuron, *PNAS*, 100, 1358–1363. doi: 10.1073/pnas.0337681100.

Cook, J. E. and Podugolnikova, T. A. (2001), Evidence for spatial regularity among retinal ganglion cells that project to the accessory optic system in a frog, a reptile, a bird, and a mammal., *Vis. Neurosci.*, 18, 289–297. doi: 10.1017/S0952523801182131.

Corbetta, M. and Shulman, G. L. (2002), Control of goal-directed and stimulus-driven attention in the brain, *Nat. Rev. Neurosci.*, 3, 215–229. doi: 10.1038/nrn755.

Cover, T. M. and Thomas, J. A. (1991). *Elements of information theory*. John Wiley & Sons, Inc., 2nd edition. ISBN 0070050236.

Dacey, D. M. (1989), Axon-bearing amacrine cells of the macaque monkey retina, *J. Comp. Neurol.*, 284, 275–293. doi: 10.1002/cne.902840210.

Dacheux, R. F., Chimento, M. F., and Amthor, F. R. (2003), Synaptic input to the on-off directionally selective ganglion cell in the rabbit retina, *J. Comp. Neurol.*, 456, 267–278. doi: 10.1002/cne.10521.

Davenport, C. M., Detwiler, P. B., and Dacey, D. M. (2007), Functional polarity of dendrites and axons of primate A1 amacrine cells, *Vis. Neurosci.*, 24, 449–457. doi: 10.1017/S0952523807070010.

Valois, R. L.d, Cottaris, N. P., Mahon, L. E., Elfar, S. D., and Wilson, J. A. (2000), Spatial and temporal receptive fields of geniculate and cortical cells and directional selectivity., *Vision Res.*, 40, 3685–3702. doi: 10.1016/S0042-6989(00)00210-8.

DeVries, S. H. and Baylor, D. A. (1997), Mosaic Arrangement of Ganglion Cell Receptive Fields in Rabbit Retina, *J. Neurophysiol.*, 78, 2048–2060.

Dhande, O. S., Estevez, M. E., Quattrochi, L. E., El-Danaf, R. N., Nguyen, P. L., Berson, D. M., and Huberman, A. D. (2013), Genetic dissection of retinal inputs to brainstem nuclei controlling image stabilization., *J. Neurosci.*, 33, 17797–17813. doi: 10.1523/JNEUROSCI.2778-13.2013.

Ebbesson, S. O. E. (1972), A Proposal for a Common Nomenclature for some Optic Nuclei in Vertebrates and the Evidence for a Common Origin of Two such Cell Groups, *Brain. Behav. Evol.*, 6, 75–91.

Engbert, R. and Kliegl, R. (2004), Microsaccades keep the eyes' balance during fixation, *Psychol. Sci.*, 15, 431–436. doi: 10.1111/j.0956-7976.2004.00697.x.

Engbert, R. and Mergenthaler, K. (2006), Microsaccades are triggered by low retinal image slip., *PNAS*, 103, 7192–7. doi: 10.1073/pnas.0509557103.

Euler, T., Detwiler, P. B., and Denk, W. (2002), Directionally selective calcium signals in dendrites of starburst amacrine cells., *Nature*, 418, 845–852. doi: 10.1038/nature00931.

Euler, T., Haverkamp, S., Schubert, T., and Baden, T. (2014), Retinal bipolar cells: elementary building blocks of vision, *Nat. Rev. Neurosci.*, 15, 507–519. doi: 10.1038/nrn3783.

Faisal, A. A., Selen, L. P. J., and Wolpert, D. M. (2008), Noise in the nervous system., *Nat. Rev. Neurosci.*, 9, 292–303. doi: 10.1038/nrn2258.

Farmer, S. G. and Rodieck, R. W. (1982), Ganglion cells of the cat accessory optic system: Morphology and retinal topography, *J. Comp. Neurol.*, 205, 190–198.

Farrow, K., Teixeira, M., Szikra, T., Viney, T. J., Balint, K., Yonehara, K., and Roska, B. (2013), Ambient illumination toggles a neuronal circuit switch in the retina and visual perception at cone threshold, *Neuron*, 78, 325–338. doi: 10.1016/j.neuron.2013.02.014.

Fiscella, M., Franke, F., Farrow, K., Müller, J., Roska, B., Azeredo da Silveira, R., and Hierlemann, A. (2015), Visual Coding with a Population of Direction-Selective Neurons, *J. Neurophysiol.*, page jn.00919.2014. doi: 10.1152/jn.00919.2014.

Fisher, R. A. (1915), Frequency distribution of the values of the correlation coefficient in samples from an indefinitely large population, *Biometrika*, 10, 507–521.

Franconeri, S. L. and Simons, D. J. (2003), Moving and looming stimuli capture attention, *Percept. Psychophys.*, 65, 999–1010. doi: 10.3758/BF03194829.

Franke, F., Fiscella, M., Sevelev, M., Roska, B., Hierlemann, A., and Silveira, R. A.d (2016), Structures of Neural Correlation and How They Favor Coding, *Neuron*, 89, 409–422. doi: 10.1016/j.neuron.2015.12.037.

Fritzsch, B. (1980), Retinal projections in European Salamandridae, *Cell Tissue Res.*, 213, 325–341.

Georgopoulos, A. P., Schwartz, A. B., and Kettner, R. E. (1986), Neuronal population coding of movement direction, *Science*, 233, 1416–1419. doi: 10.1126/science.3749885.

Georgopoulos, A. P., Kettner, R. E., and Schwartz, A. B. (1988), Primate motor cortex and free arm movements to visual targets in three-dimensional space. II. Coding of the direction of movement by a neuronal population, *J. Neurosci.*, 8, 2928–2937. doi: 10.1089/scd.2011.0674.

Gjorgjieva, J., Sompolinsky, H., and Meister, M. (2014), Benefits of pathway splitting in sensory coding., *J. Neurosci.*, 34, 12127–44. doi: 10.1523/JNEUROSCI.1032-14.2014.

Greschner, M., Bongard, M., Ruján, P., and Ammermüller, J. (2002), Retinal ganglion cell synchronization by fixational eye movements improves feature estimation., *Nat. Neurosci.*, 5, 341–7. doi: 10.1038/nn821.

Hassenstein, B. and Reichardt, W. (1956), Systemtheoretische Analyse der Zeit, Reihenfolgen und Vorzeichenauswertung Bei der Bewegungsperzeption des Rüsselkafers Chlorophanus, *Zeitschrift für Naturforsch.*, 11, 513–524.

Hattar, S., Liao, H. W., Takao, M., Berson, D. M., and Yau, K.-W. (2002), Melanopsin-containing retinal ganglion cells: architecture, projections, and intrinsic photosensitivity., *Science*, 295, 1065–70. doi: 10.1126/science.1069609.

Hattar, S., Kumar, M., Park, A., Tong, P., Tung, J., Yau, K.-W., and Berson, D. M. (2006), Central Projections of Melanopsin- Expressing Retinal Ganglion Cells in the Mouse, *J. Comp. Neurol.*, 497, 326–349. doi: 10.1002/cne.

Hausselt, S. E., Euler, T., Detwiler, P. B., and Denk, W. (2007), A dendrite-autonomous mechanism for direction selectivity in retinal starburst amacrine cells., *PLoS Biol.*, 5, e185. doi: 10.1371/journal.pbio.0050185.

Haverkamp, S., Grünert, U., and Wässle, H. (2001a), Localization of kainate receptors at the cone pedicles of the primate retina, *J. Comp. Neurol.*, 436, 471–486. doi: 10.1002/cne.1081.

Haverkamp, S., Grünert, U., and Wässle, H. (2001b), The synaptic architecture of AMPA receptors at the cone pedicle of the primate retina., *J. Neurosci.*, 21, 2488–2500. doi: 21/7/2488 [pii].

Heflin, S. J. and Cook, P. B. (2007), Narrow and wide field amacrine cells fire action potentials in response to depolarization and light stimulation, *Vis. Neurosci.*, 24, 197–206. doi: 10.1017/S095252380707040X.

Herrick, C. J. (1925), The amphibian forebrain III. The optic tracts and centers of amblystoma and the frog, *J. Comp. Neurol.*, 39, 433–489. doi: 10.1002/cne.900390304.

Hilton, W. A. (1956), Eye muscles of salamanders, *Herpetologica*, 12, 273–276. doi: 10.2307/3889834.

Hood, D. C. and Finkelstein, M. A. (1986). Sensitivity to light. In Boff, K., Kaufmann, L., and Thomas, J., editors, *Handb. Percept. Hum. Perform. (Vol. 1 Sens. Process. Perseption)*. John Wiley & Sons, New York.

Hotelling, H. (1936), Relations between two sets of variates, *Biometrika*, 28, 321–377.

Jensen, R. J. and DeVoe, R. D. (1983), Comparison of directionally selective with other ganglion cells in the turtle retina: Intracellular recording and staining, *J. Comp. Neurol.*, 217, 271–287.

Joesch, M. and Meister, M. (2016), A neuronal circuit for colour vision based on rod–cone opponency, *Nature*, pages 1–15. doi: 10.1038/nature17158.

Kalman, R. E. (1960), A new approach to linear filtering and prediction problems, *J. Basic Eng.*, 82, 35–45. doi: 10.1115/1.3662552.

Kanjhan, R. and Sivyer, B. (2010), Two types of ON direction-selective ganglion cells in rabbit retina, *Neurosci. Lett.*, 483, 105–109. doi: 10.1016/j.neulet.2010.07.071.

Kay, J. N., De la Huerta, I., Kim, I.-J., Zhang, Y., Yamagata, M., Chu, M. W., Meister, M., and Sanes, J. R. (2011), Retinal ganglion cells with distinct directional preferences differ in molecular identity, structure, and central projections., *J. Neurosci.*, 31, 7753–62. doi: 10.1523/JNEUROSCI.0907-11.2011.

Kim, I.-J., Zhang, Y., Yamagata, M., Meister, M., and Sanes, J. R. (2008), Molecular identification of a retinal cell type that responds to upward motion, *Nature*, 452, 478–482. doi: 10.1038/nature06739.

Kim, I.-J., Zhang, Y., Meister, M., and Sanes, J. R. (2010), Laminar restriction of retinal ganglion cell dendrites and axons: Subtype-specific developmental patterns revealed with transgenic markers, *J. Neurosci.*, 30, 1452–1462. doi: 10.1523/JNEUROSCI.4779-09.2010.

Kim, J. S., Greene, M. J., Zlateski, A., Lee, K., Richardson, M., Turaga, S. C., Purcaro, M., Balkam, M., Robinson, A., Behabadi, B. F., Campos, M., Denk,

W., and Seung, H. S. (2014), Space-time wiring specificity supports direction selectivity in the retina., *Nature*, 509, 331–336. doi: 10.1038/nature13240.

Kim, T., Soto, F., and Kerschensteiner, D. (2015), An excitatory amacrine cell detects object motion and provides feature-selective input to ganglion cells in the mouse retina., *Elife*, 4. doi: 10.7554/eLife.08025.

Kittila, C. a. and Massey, S. C. (1997), Pharmacology of directionally selective ganglion cells in the rabbit retina., *J. Neurophysiol.*, 77, 675–89.

Klein, D. C., Moore, R. Y., and Reppert, S. M. (1991). *Suprachiasmatic Nucleus: The Mind's Clock*. Oxford University Press.

Ko, H.-K., Poletti, M., and Rucci, M. (2010), Microsaccades precisely relocate gaze in a high visual acuity task., *Nat. Neurosci.*, 13, 1549–53. doi: 10.1038/nn.2663.

Krishnaswamy, A., Yamagata, M., Duan, X., Hong, Y. K., and Sanes, J. R. (2015), Sidekick 2 directs formation of a retinal circuit that detects differential motion, *Nature*. doi: 10.1038/nature14682.

Kristan, M., Perš, J., Kovačič, S., and Leonardis, a. (2009), A local-motion-based probabilistic model for visual tracking, *Pattern Recognit.*, 42, 2160–2168. doi: 10.1016/j.patcog.2009.01.002.

Kuffler, S. W. (1953), Discharge Patterns and Functional Organization of Mammalian Retina, *J. Neurophysiol.*, 16, 37–68.

Kwon, O.-S., Tadin, D., and Knill, D. C. (2015), Unifying account of visual motion and position perception, *PNAS*, 112, 8142–8147. doi: 10.1073/pnas.1500361112.

Land, M. F. and McLeod, P. (2000), From eye movements to actions: how batsmen hit the ball., *Nat. Neurosci.*, 3, 1340–5. doi: 10.1038/81887.

Lee, S., Kim, K., and Zhou, Z. J. (2010), Role of ACh-GABA cotransmission in detecting image motion and motion direction, *Neuron*, 68, 1159–1172. doi: 10.1016/j.neuron.2010.11.031.

Lee, S., Chen, L., Chen, M., Ye, M., Seal, R. P., and Zhou, Z. J. (2014), An unconventional glutamatergic circuit in the retina formed by vGluT3 amacrine cells, *Neuron*, 84, 708–715. doi: 10.1016/j.neuron.2014.10.021.

Leonardo, A. and Meister, M. (2013), Nonlinear dynamics support a linear population code in a retinal target-tracking circuit., *J. Neurosci.*, 33, 16971–82. doi: 10.1523/JNEUROSCI.2257-13.2013.

Lettvin, J. Y., Maturana, H. R., McCulloch, W. S., and Pitts, W. H. (1959), What the frog's eye tells the frog's brain, *Proc. IEEE*, 47, 1940–1951.

Levick, W. R., Oyster, C. W., and Takahashi, E. S. (1969), Rabbit lateral geniculate nucleus: Sharpener of directional information, *Science*, 165, 712–714.

Li, T., Wu, S. M., Lam, D. M.-K., and Watt, C. B. (1990), Localization of classical neurotransmitters in interneurons of the larval tiger salamander retina., *Invest. Ophthalmol. Vis. Sci.*, 31, 262–271.

Lisberger, S. G., Morris, E. J., and Tychsen, L. (1987), Visual motion processing and sensory-motor integration for smooth pursuit eye movements, *Annu. Rev. Neurosci.*, 10, 97–1292.

Maddin, H. C. and Sherratt, E. (2014), Influence of fossoriality on inner ear morphology: insights from caecilian amphibians., *J. Anat.* doi: 10.1111/joa.12190.

Maekawa, K. and Simpson, J. I. (1973), Climbing fiber responses evoked in vestibulocerebellum of rabbit from visual system., *J. Neurophysiol.*, 36, 649–666.

Manteuffel, G., Plasa, L., Sommer, T. J., and Wess, O. (1977), Involuntary eye movements in salamanders, *Naturwiss.*, 64, 533–534.

Marre, O., Amodei, D., Deshmukh, N., Sadeghi, K., Soo, F., Holy, T. E., and Berry II, M. J. (2012), Mapping a complete neural population in the retina, *J. Neurosci.*, 32, 14859–14873. doi: 10.1523/JNEUROSCI.0723-12.2012.

Marre, O., Botella-Soler, V., Simmons, K. D., Mora, T., Tkačik, G., and Berry II, M. J. (2015), High accuracy decoding of dynamical motion from a large retinal population, *PLoS Comput. Biol.*, 11, e1004304. doi: 10.1371/journal.pcbi.1004304.

Martinez-Conde, S. and Macknik, S. L. (2008), Fixational eye movements across vertebrates : Comparative dynamics, physiology and perception, *J. Vis.*, 8, 1–16. doi: 10.1167/8.14.28.Introduction.

Masland, R. H. (2012a), The Neuronal Organization of the Retina, *Neuron*, 76, 266–280. doi: 10.1016/j.neuron.2012.10.002.The.

Masland, R. H. (2012b), The tasks of amacrine cells, *Vis. Neurosci.*, 29, 3–9. doi: 10.1016/j.surg.2006.10.010.Use.

Masland, R. H. and Mills, J. W. (1979), Autoradiographic identification of ACh in the rabbit retina, *J. Cell Biol.*, 83, 159–178.

Maturana, H. R. and Frenk, S. (1963), Directional movement and horizontal edge detectors in the pigeon retina, *Science*, 142, 977–979.

Maturana, H. R., Lettvin, J. Y., McCulloch, W. S., and Pitts, W. H. (1960), Anatomy and physiology of vision in the frog (Rana pipiens), *J. Gen. Physiol.*, 43, 129–175.

Maximov, V., Maximova, E., and Maximov, P. (2005), Direction selectivity in the goldfish tectum revisited, *Ann. N. Y. Acad. Sci.*, 1048, 198–205. doi: 10.1196/annals.1342.018.

May, P. J. (2005), The mammalian superior colliculus: Laminar structure and connections, *Prog. Brain Res.*, 151, 321–378. doi: 10.1016/S0079-6123(05)51011-2.

Mazurek, M., Kager, M., and Van Hooser, S. D. (2014), Robust quantification of orientation selectivity and direction selectivity, *Front. Neural Circuits*, 8, 1–17. doi: 10.3389/fncir.2014.00092.

McLelland, D., Baker, P. M., Ahmed, B., Kohn, A., and Bair, W. (2015), Mechanisms for rapid adaptive control of motion processing in macaque visual cortex, *J. Neurosci.*, 35, 10268–10280. doi: 10.1523/JNEUROSCI.1418-11.2015.

Meister, M. (1996), Multineuronal codes in retinal signaling, *PNAS*, 93, 609–614.

Meister, M., Lagnado, L., and Baylor, D. A. (1995), Concerted signaling by retinal ganglion cells., *Science*, 270, 1207–1210.

Menger, N., Pow, D. V., and Wässle, H. (1998), Glycinergic amacrine cells of the rat retina, *J. Comp. Neurol.*, 401, 34–46.

Montgomery, N., Fite, K. V., and Bengston, L. (1981), The accessory optic system of Rana pipiens: Neuroanatomical connections and intrinsic organization, *J. Comp. Neurol.*, 203, 595–612. doi: 10.1146/annurev.ne.07.030184.000305.

Movshon, J. A., Adelson, E. H., Gizzi, M. S., and Newsome, W. T. (1985). The analysis of moving visual patterns. In Chagas, C., Gattass, R., and Gross, C., editors, *Pattern Recognit. Mech.*, pages 117–151, Rome. Vatican Press.

Nirenberg, S., Carcieri, S. M., Jacobs, A. L., and Latham, P. E. (2001), Retinal ganglion cells act largely as independent encoders, *Nature*, 411, 698–701. doi: 10.1038/35079612.

Nomura, A., Shigemoto, R., Nakamura, Y., Okamoto, N., Mizuno, N., and Nakanishi, S. (1994), Developmentally regulated postsynaptic localization of a metabotropic glutamate receptor in rat rod bipolar cells, *Cell*, 77, 361–369. doi: 10.1016/0092-8674(94)90151-1.

Ölveczky, B. P., Baccus, S. A., and Meister, M. (2003), Segregation of object and background motion in the retina., *Nature*, 423, 401–8. doi: 10.1038/nature01652.

Oyster, C. W. (1968), The analysis of image motion by the rabbit retina, *J. Physiol.*, 199, 613–635.

Oyster, C. W. and Barlow, H. B. (1967), Direction-selective units in rabbit retina: distribution of preferred directions, *Science*, 155, 841–842. doi: 10.1126/science.155.3764.841.

Oyster, C. W., Simpson, J. I., Takahashi, E. S., and Soodak, R. E. (1980), Retinal ganglion cells projecting to the rabbit accessory optic system, *J. Comp. Neurol.*, 190, 49–61. doi: 10.1002/cne.901900105.

Palmer, S. E., Marre, O., Berry II, M. J., and Bialek, W. (2015), Predictive information in a sensory population, *PNAS*, 112, 6908–6913. doi: 10.1073/pnas.0709640104.

Pan, Z.-H. and Slaughter, M. M. (1991), Control of Retinal Information Coding by GABAb Receptors, *J. Neurosci.*, 11, 1810–1821.

Panzeri, S., Schultz, S. R., Treves, A., and Rolls, E. T. (1999), Correlations and the encoding of information in the nervous system, *Proc. R. Soc. London. B*, 266, 1001–1012. doi: 10.1098/rspb.1999.0736.

Perkel, D. H., Gerstein, G. L., and Moore, G. P. (1967), Neuronal Spike Trains and Stochastic Point Processes .2. Simultaneous Spike Trains, *Biophys. J.*, 7, 419–440. doi: 10.1016/S0006-3495(67)86596-2.

Pouzat, C., Mazor, O., and Laurent, G. (2002), Using noise signature to optimize spike-sorting and to assess neuronal classification quality, *J. Neurosci. Methods*, 122, 43–57. doi: 10.1016/S0165-0270(02)00276-5.

Rivlin-Etzion, M., Zhou, K., Wei, W., Elstrott, J., Nguyen, P. L., Barres, B. A., Huberman, A. D., and Feller, M. B. (2011), Transgenic mice reveal unexpected diversity of on-off direction-selective retinal ganglion cell subtypes and brain structures involved in motion processing., *J. Neurosci.*, 31, 8760–8769. doi: 10.1523/JNEUROSCI.0564-11.2011.

Sanes, J. R. and Masland, R. H. (2014), The types of retinal ganglion cells: Current status and implications for neuronal classification, *Annu. Rev. Neurosci.*, 38, 221–246. doi: 10.1146/annurev-neuro-071714-034120.

Schneidman, E., Bialek, W., and Berry II, M. J. (2003), Synergy, redundancy, and independence in population codes, *J. Neurosci.*, 23, 11529–11553. doi: 10.1523/JNEUROSCI.5319-04.2005.

Schwartz, G., Taylor, S., Fisher, C., Harris, R., and Berry II, M. J. (2007), Synchronized firing among retinal ganglion cells signals motion reversal, *Neuron*, 55, 958–969. doi: 10.1016/j.neuron.2007.07.042.

Segev, R., Puchalla, J., and Berry II, M. J. (2006), Functional organization of ganglion cells in the salamander retina., *J. Neurophysiol.*, 95, 2277–2292. doi: 10.1152/jn.00928.2005.

Shannon, C. E. (1948), A mathematical theory of communication, *Bell Syst. Tech. J.*, 27, 379–423. doi: 10.1145/584091.584093.

Sharpe, L. T. and Stockman, A. (1999), Rod pathways : the importance of seeing nothing, *Trends Neurosci.*, 22, 497–504.

Simpson, J. I. (1984), The accessory optic system, *Annu. Rev. Neurosci.*, 7, 13–41.

Simpson, J. I., Leonard, C. S., and Soodak, R. E. (1988), The accessory optic system of rabbit. II. Spatial organization of direction selectivity., *J. Neurophysiol.*, 60, 2055–2072.

Sivyer, B., Wyk, M.v, Vaney, D. I., and Taylor, W. R. (2010), Synaptic inputs and timing underlying the velocity tuning of direction-selective ganglion cells in rabbit retina., *J. Physiol.*, 588, 3243–53. doi: 10.1113/jphysiol.2010.192716.

Soodak, R. E. and Simpson, J. I. (1988), The accessory optic system of rabbit. I. Basic visual response properties., *J. Neurophysiol.*, 60, 2037–2054.

Stafford, D. K. and Dacey, D. M. (1997), Physiology of the A1 amacrine: a spiking, axon-bearing interneuron of the macaque monkey retina, *Vis. Neurosci.*, 14, 507–522.

Stanley, G. B., Jin, J., Wang, Y., Desbordes, G., Wang, Q., Black, M. J., and Alonso, J.-M. (2012), Visual Orientation and Directional Selectivity through Thalamic Synchrony., *J. Neurosci.*, 32, 9073–88. doi: 10.1523/JNEUROSCI.4968-11.2012.

Stockman, A. and Sharpe, L. T. (2006), Into the twilight zone: The complexities of mesopic vision and luminous efficiency, *Ophthalmic Physiol. Opt.*, 26, 225–239. doi: 10.1111/j.1475-1313.2006.00325.x.

Stoner, G. R. and Albright, T. D. (1993), Image segmentation cues in motion processing: Implications for modularity in vision, *J. Cogn. Neurosci.*, pages 129–149.

Sun, W., Deng, Q., Levick, W. R., and He, S. (2006), ON direction-selective ganglion cells in the mouse retina., *J. Physiol.*, 576, 197–202. doi: 10.1113/jphysiol.2006.115857.

Taylor, W. R. and Vaney, D. I. (2003), New directions in retinal research, *Trends Neurosci.*, 26, 379–385. doi: 10.1016/S0166-2236(03)00167-X.

Tukker, J. J., Taylor, W. R., and Smith, R. G. (2004), Direction selectivity in a model of the starburst amacrine cell., *Vis. Neurosci.*, 21, 611–625. doi: 10.1017/S0952523804214109.

Uhlenbeck, G. E. and Ornstein, L. S. (1930), On the theory of the Brownian motion, *Phys. Rev.*, 36, 823–841. doi: 10.1103/PhysRev.36.823.

Vaney, D. I. (1994), Territorial organization of direction-selective ganglion cells in rabbit retina, *J. Neurosci.*, 14, 6301–6316.

Vaney, D. I., He, S., Taylor, W. R., and Levick, W. R. (2001), Direction-selective ganglion cells in the retina, *Motion Vis.*, pages 13–56.

Vaney, D. I., Sivyer, B., and Taylor, W. R. (2012), Direction selectivity in the retina: symmetry and asymmetry in structure and function., *Nat. Rev. Neurosci.*, 13, 194–208. doi: 10.1038/nrn3165.

Vardi, N., Duvoisin, R., Wu, G., and Sterling, P. (2000), Localization of mGluR6 to dendrites of ON bipolar cells in primate retina, *J. Comp. Neurol.*, 423, 402–412. doi: 10.1002/1096-9861(20000731)423:3¡402::AID-CNE4¿3.0.CO;2-E.

Virsik, R. P. and Reichardt, W. (1976), Detection and tracking of moving objects by the fly Musca domestica*, *Biol. Cybern.*, 98, 83–98. doi: 10.1016/j.evalprogplan.2009.12.007.

Vlasits, A. L., Morrie, R. D., Tran-Van-Minh, A., Bleckert, A., Gainer, C. F., DiGregorio, D. A., and Feller, M. B. (2016), A role for synaptic input distribution in a dendritic computation of motion direction in the retina, *Neuron*, 89, 1317–1330. doi: 10.1016/j.neuron.2016.02.020.

Warland, D. K., Reinagel, P., and Meister, M. (1997), Decoding visual information from a population of retinal ganglion cells., *J. Neurophysiol.*, 78, 2336–2350.

Wässle, H. (2004), Parallel processing in the mammalian retina., *Nat. Rev. Neurosci.*, 5, 747–57. doi: 10.1038/nrn1497.

Wehrhahn, C. and Hausen, K. (1980), How is tracking and fixation accomplished in the nervous system of the fly?, *Biol. Cybern.*, 38, 179–186. doi: 10.1007/BF00337407.

Weng, S., Sun, W., and He, S. (2005), Identification of ON-OFF direction-selective ganglion cells in the mouse retina., *J. Physiol.*, 562, 915–923. doi: 10.1113/jphysiol.2004.076695.

Werblin, F. S. (1970), Response of retinal cells to moving spots: intracellular recording in Necturus maculosus., *J. Neurophysiol.*, 33, 342–350.

Werblin, F. S. (1991), Synaptic connections, receptive fields and patterns of activity in the tiger salamander retina, *Investig. Ophthalmol. Vis. Sci.*, 32, 459–483.

Wyatt, H. J. and Daw, N. W. (1975), Directionally Sensitive Ganglion Cells in the Rabbit Retina : Specificity for Stimulus Direction, Size and Speed, *J. Neurophysiol.*, 38, 613–626.

Wyatt, H. J. and Daw, N. W. (1976), Specific effects of neurotransmitter antagonists on ganglion cells in rabbit retina, *Science*, 191, 204–205.

Yang, C.-Y., Lukasiewicz, P. D., Maguire, G., Werblin, F. S., and Yazulla, S. (1991), Amacrine cells in the tiger salamander retina: morphology, physiology, and neurotransmitter identification., *J. Comp. Neurol.*, 312, 19–32. doi: 10.1002/cne.903120103.

Yang, G. and Masland, R. H. (1994), Receptive fields and dendritic structure of directionally selective retinal ganglion cells, *J. Neurosci.*, 14, 5267–5280.

Yonehara, K., Shintani, T., Suzuki, R., Sakuta, H., Takeuchi, Y., Nakamura-Yonehara, K., and Noda, M. (2008), Expression of SPIG1 reveals development of a retinal ganglion cell subtype projecting to the medial terminal nucleus in the mouse, *PLoS One*, 3, e1533. doi: 10.1371/journal.pone.0001533.

Yonehara, K., Ishikane, H., Sakuta, H., Shintani, T., Nakamura-Yonehara, K., Kamiji, N. L., Usui, S., and Noda, M. (2009), Identification of retinal ganglion cells and their projections Involved in central transmission of information about upward and downward image motion, *PLoS One*, 4, e4320. doi: 10.1371/journal.pone.0004320.

Yonehara, K., Farrow, K., Ghanem, A., Hillier, D., Balint, K., Teixeira, M., Jüttner, J., Noda, M., Neve, R. L., Conzelmann, K.-K., and Roska, B. (2013), The first stage of cardinal direction selectivity is localized to the dendrites of retinal ganglion cells., *Neuron*, 79, 1078–85. doi: 10.1016/j.neuron.2013.08.005.

Yu, Y. Y. Y., Mann, G., and Gosine, R. (2007). Task-driven moving object detection for robots using visual attention. In *7th IEEE-RAS Int. Conf. Humanoid Robot.*, pages 428–433. IEEE. ISBN 978-1-4244-1861-9. doi: 10.1109/ICHR.2007.4813905.

Zago, M., Iosa, M., Maffei, V., and Lacquaniti, F. (2010), Extrapolation of vertical target motion through a brief visual occlusion, *Exp. Brain Res.*, 201, 365–384. doi: 10.1007/s00221-009-2041-9.

Zeck, G., Bethge, M., and Macke, J. H. (2008). Receptive Fields without Spike-Triggering. In Platt, J. C., Koller, D., Singer, Y., and Roweis, S. T., editors, *Adv. Neural Inf. Process. Syst. 20*, pages 969–976. Curran Associates, Inc. ISBN 978-1-605-60352-0.

Zelinsky, G., Sherman, A., and Yago, T. (2015), Simulating multiple object tracking performance using a Kalman filter model, *J. Vis.*, 15, 465. doi: 10.1167/15.12.465.

Zhang, J. and Wu, S. M. (2001), Immunocytochemical analysis of cholinergic amacrine cells in the tiger salamander retina., *Neuroreport*, 12, 1371–1375.

Zhang, Y., Kim, I.-J., Sanes, J. R., and Meister, M. (2012), The most numerous ganglion cell type of the mouse retina is a selective feature detector, *PNAS*, 109, E2391–8. doi: 10.1073/pnas.1211547109.

Zylberberg, J., Cafaro, J., Turner, M. H., Shea-Brown, E., and Rieke, F. (2016), Direction-Selective Circuits Shape Noise to Ensure a Precise Population Code, *Neuron*, 89, 369–383. doi: 10.1016/j.neuron.2015.11.019.

Curriculum Vitae

Personal Details

Norma Krystyna Kühn
born April 21, 1986 in Rostock, Germany

Education

2011 – 2016 **PhD Student in the Sensory and Motor Neuroscience Program**, Göttingen Graduate School for Neurosciences, Biophysics, and Molecular Biosciences (GGNB), Georg-August-Universität Göttingen, Germany, Supervisor: Prof. Dr. Tim Gollisch

2005 – 2011 **Diploma in Physics**, Universität Leipzig, Germany
Dissertation: *Fluctuation theorems in systems of globally coupled Stratonovich models*, Supervisor: Prof. Dr. Ulrich Behn

2008 – 2009 **Erasmus Exchange**, Universidad de Granada, Spain

Awards and Honors

Since 2012 **Dorothea-Schlözer Fellowship**,
Georg-August-Universität Göttingen, Germany

Summer Schools and Workshops

2013 **5th G-Node Winter Course in Neural Data Analysis**,
Munich, Germany

2012 **Okinawa Computational Neuroscience Course 2012**,
Okinawa, Japan

Teaching

SS 2016	Supervising laboratory rotation of Neuroscience-MSc student
SS 2015	Course on multielectrode array recordings from the retina
SS 2015	Python programming introductory course
SS 2013	Python Programming Course for Neuroscience-MSc Program
SS 2013	Python programming introductory course
SS 2013	Course on multielectrode array recordings from the retina

Professional Service

2012 – 2014 **Student representative of the Sensory and Motor Neuroscience Program** of the Göttingen Graduate School for Neurosciences, Biophysics, and Molecular Biosciences (GGNB), Georg-August-Universität Göttingen, Germany

2012 **Co-organizer of the 3rd jDPG Theoretikerworkshop** (sponsored by Deutsche Physikalische Gesellschaft e.V.), Burg Breuberg, Germany, Topic: *Simulationen in der Physik*

2011 **Co-organizer of the 2nd jDPG Theoretikerworkshop** (sponsored by Deutsche Physikalische Gesellschaft e.V.), Böhlen, Germany, Topic: *Zukunftstechnologien*

Abstracts and Conference Proceedings

Computational and Systems Neuroscience (Cosyne) 2016,
Salt Lake City, USA (25-28 February, 2016)
Synergy in motion trajectory encoding of direction-selective ganglion cells in the salamander retina, Norma Kühn and Tim Gollisch

European Retina Meeting 2015, Brighton, UK (1-3 October, 2015)
Encoding of object and background motion in the salamander retina,
Norma Kühn and Tim Gollisch

Bernstein Conference 2015, Göttingen, Germany (15-17 September, 2015)
Encoding of object and background motion trajectories in the salamander retina,
Norma Kühn and Tim Gollisch

11th Göttingen Meeting of the German Neuroscience Society,
Göttingen, Germany (18-21 March, 2015)
Motion encoding in the salamander retina, Norma Kühn and Tim Gollisch

Bernstein Conference 2014, Göttingen, Germany (2-5 September, 2014)
Motion Encoding in the Salamander Retina, Norma Kühn and Tim Gollisch

European Retina Meeting 2013, Alicante, Spain (2-5 October, 2013)
Oral presentation: *Motion Encoding in the Salamander Retina*,
Norma Kühn and Tim Gollisch

10th Göttingen Meeting of the German Neuroscience Society,
Göttingen, Germany (13-16 March, 2013)
How retinal ganglion cells encode object motion and motion direction,
Norma Kühn and Tim Gollisch

Bernstein Conference 2012, Munich, Germany (12-14 September, 2012)
The Encoding of Object Motion and Motion Direction in the Retina,
Norma Kühn and Tim Gollisch

14th Deutsche Physikerinnentagung, Munich, Germany (4-7 November, 2010)
Oral presentation: *Fluctuation theorems in systems driven by multiplicative noise*,
Norma Kühn and Ulrich Behn